

# Unconventional superconductivity within the single-orbital Hubbard model beyond the Random Phase Approximation

Karim Zantout

September 17, 2016

Goethe Universität Frankfurt am Main  
Institut für Theoretische Physik

**Supervisor and first referee:**

Prof. Maria-Roser Valentí

**Second referee:**

Prof. Claudius Gros

---

**Erklärung** nach § 28 (12) Ordnung für den Bachelor- und dem Masterstudiengang

Hiermit erkläre ich, dass ich die Arbeit selbstständig und ohne Benutzung anderer als der angegebenen Quellen und Hilfsmittel verfasst habe. Alle Stellen der Arbeit, die wörtlich oder sinngemäß aus Veröffentlichungen oder aus anderen fremden Texten entnommen wurden, sind von mir als solche kenntlich gemacht worden. Ferner erkläre ich, dass die Arbeit nicht - auch nicht auszugsweise - für eine andere Prüfung verwendet wurde.

Frankfurt, den

---

## **Acknowledgement**

I would like to thank Prof. Maria-Roser Valentí for having entrusted me with this work and her guidance throughout the whole work.

My thanks also go to the whole research group of Prof. Valentí whose members were always willing for discussion; especially to Steffen Backes who was an important support regarding the numerical implementation and the physical interpretation of the results and to Michaela Altmeyer for discussions concerning superconductivity and the controlling of this work. Finally, I express gratitude to my family and friends who were a personal support; among those my father was a great help to check the spelling of this work.

---

**Contents**

<b>1. Overview</b>	<b>1</b>
<b>2. Introduction</b>	<b>3</b>
2.1. The Hubbard model . . . . .	3
2.2. Cuprates and organic charge transfer salts . . . . .	4
<b>3. Green's functions and Susceptibilities</b>	<b>8</b>
3.1. Overview of Correlation functions . . . . .	8
3.1.1. Motivation from experiments . . . . .	8
3.1.2. Susceptibilities and Linear-Response Theory . . . . .	9
3.1.3. Definition of the single-particle Green's function . . . . .	10
3.2. Properties of correlation functions . . . . .	12
3.2.1. Time translational invariance . . . . .	12
3.2.2. Space translational invariance . . . . .	12
3.3. Single-particle Green's function . . . . .	14
3.3.1. Spectral weight . . . . .	14
3.3.2. Non-interacting Green's function . . . . .	16
3.4. Matsubara Green's function . . . . .	17
3.4.1. Definition . . . . .	18
3.4.2. Anti-periodicity and Fourier expansion . . . . .	18
3.4.3. Relation between the retarded Green's function $G^R$ and the Matsubara Green's function $G$ . . . . .	20
3.4.4. Analytical continuation . . . . .	22
3.5. Interacting Green's function and self-energy . . . . .	23
3.5.1. The functional derivative formalism . . . . .	23
3.5.2. Spin and charge susceptibilities . . . . .	26
<b>4. Two-Particle Self-Consistent approach and Random Phase Approximation</b>	<b>29</b>
4.1. Sum rules . . . . .	29
4.2. The Random Phase Approximation (RPA) . . . . .	29
4.2.1. Disadvantages of RPA . . . . .	30
4.2.2. Starting point: $\text{tr}(\Sigma G)$ . . . . .	31
4.2.3. Correlation lengths . . . . .	33
4.3. Two-particle properties and self-consistency equations . . . . .	34
4.3.1. Internal checks . . . . .	39
4.4. The Fluctuation Exchange approximation (FLEX) . . . . .	39
<b>5. Superconductivity</b>	<b>40</b>
5.1. The linearized Eliashberg equation . . . . .	40
5.2. Symmetry of the gap function . . . . .	41
<b>6. Numerical results for the square and triangular lattice</b>	<b>42</b>
6.1. Square lattice - Cuprates . . . . .	42
6.1.1. Pseudogap and crossover temperature $T_x$ . . . . .	42
6.1.2. Superconductivity . . . . .	43
6.2. Triangular lattice - Organic charge transfer salts . . . . .	47
6.2.1. Pseudogap and superconductivity . . . . .	48
6.2.2. Comparisons to other theories . . . . .	49

<b>7. Summary and Outlook</b>	<b>51</b>
<b>A. Numerical issues</b>	<b>53</b>
A.1. High-frequency behaviour of $G$ and $\Sigma$ . . . . .	53
A.2. Calculation of the filling $n$ / adjusting the chemical potential $\mu$ . . . . .	53
A.3. Matsubara sums of the form $\sum_n f(n) * g(n + m)$ . . . . .	54
<b>B. <math>\vec{k}</math>-integration</b>	<b>57</b>
B.1. Calculation of the Lindhard function $\chi_0(\vec{q}, iq_n)$ . . . . .	60

## 1. Overview

In 1986 Georg Bednorz and Alex Müller published their experimental observation of a superconducting critical temperature  $T_c = 35K$  in a sample of  $(La, Ba)_2CuO_4$ . The following year it was found that  $YBa_2Cu_3O_7$  has a critical temperature of  $T_c \approx 90K$  that can not be described within BCS theory any more since the weak electron-phonon coupling that drives the superconductivity in so-called conventional superconductors limits the critical temperature to a value of about 40 K.

Another important point is the symmetry of the superconducting gap function that shows no sign changes in the conventional superconducting compounds but was observed to bear sign changes of different kinds in the unconventional superconductors (Sec. 5.2).

Moreover, the phase diagram of unconventional superconductors often shows a pseudogap regime and/or antiferromagnetic ordering in the vicinity of the superconducting domain. Unconventional superconductivity is one of the remaining mysteries in solid state theory since the pairing mechanism for the electrons is not known yet. Unlike the conventional superconductors that reveal mainly phonon driven Cooper pairs in unconventional superconductors many physicists believe that spin and charge fluctuations are the prevailing pairing mechanisms that can be described within the Hubbard model.

This work is also inclined towards this explanation and deals therefore with the numerically approximative solution of the Hubbard model.

Long established methods like the Random Phase Approximation (RPA) or Fluctuation Exchange Approximation (FLEX) for solving the single-orbital Hubbard model are violating conservation laws, sum rules concerning spin and charge, the Mermin-Wagner-theorem and/or the Pauli principle, e.g. calculations that are based on RPA show a finite temperature phase transition to antiferromagnetism which is prohibited by the Mermin-Wagner-theorem (continuous symmetries can not be spontaneously broken at finite temperatures in dimensions  $d \leq 2$  if a sufficiently strong short-range interaction is present) and violate the Pauli principle (Sec. 4.2.1).

The Two Particle Self-Consistent Theory (TPSC) that was developed by Y. M. Vilk and A.-M. Tremblay [1] expresses the spin and the charge susceptibilities as functions of two irreducible vertices  $U_{sp}$  and  $U_{ch}$  in a way that the theory obeys conservation laws and the Pauli principle.

By this ansatz one is not bound to physically adjustable parameters or the applicability of Migdal's theorem (vertex corrections for the electron-phonon interaction are  $O(\frac{\lambda\omega_D}{E_F})$ ,  $\omega_D$  is the Debye frequency and  $E_F$  the Fermi energy, and can be therefore neglected in the Migdal-Eliashberg theory for conventional superconductors).

TPSC provides accurate results in the domain of weak to intermediate coupling ( $U/t \ll 8$  to  $U/t \lesssim 8$ ). Unfortunately, it is not applicable to dimensions  $d \leq 1$ , too deep inside the renormalized classical regime and for strong coupling except for very high temperatures (see 4.3.1).

In this work we will start with a presentation of all needed formalisms to be able to derive and physically motivate TPSC and compare it then to other theories. The main parts are based on the first complete paper about TPSC [1] and the lecture notes of A.M.-S. Tremblay [2].

The next part is dedicated to some numerical case studies where we will take a close look at antiferromagnetic correlations, the pseudogap regime and superconductivity studied within the linearized Eliashberg equation for square and triangular lattices.

---

Finally, we present an outlook to extensions and open problems of TPSC.

Throughout the whole work we use the following units and definitions:

$$\begin{aligned}k_B &\equiv \hbar \equiv a \equiv 1 \quad ; \quad a : \text{lattice spacing} \\ \beta &\equiv 1/T \\ \langle \cdot \rangle &\equiv \frac{\text{tr}(e^{-\beta H} \cdot)}{\text{tr}(e^{-\beta H})} \\ \xi_{\vec{k}} &\equiv \epsilon_{\vec{k}} - \mu \\ f(1, 1') &\equiv f(\vec{r}, t; \vec{r}', t') \\ f(1, \bar{1})g(\bar{1}, 1') &\equiv \int d^3r_1 \int dt_1 f(1; \vec{r}_1, t_1)g(\vec{r}_1, t_1; 1') \\ \delta(t - t')\delta(\vec{r} - \vec{r}') &\equiv \delta(1 - 1') \\ f(\xi_{\vec{k}}) &\equiv \frac{1}{e^{\beta \xi_{\vec{k}}} + 1}\end{aligned}$$

## 2. Introduction

### 2.1. The Hubbard model

Although it is rather easy to write down the full Hamiltonian for a many-body system it is nearly impossible to solve it.

Firstly, one is confronted with a differential equation that contains a huge amount of variables ( $\sim 10^{23}$ ) and many interactions that make even numerical attempts useless. Secondly, even if it would be possible to solve this problem one will end up with a lot of data that will not show any physical effect without arranging the vast set of solutions in an appropriate manner.

Solid state theory has therefore developed a lot of techniques to tackle this problem by defining new spaces, making use of elegant formalisms and projecting on models that are more convenient.

A long established and famous model is the Hubbard model that was proposed by John Hubbard in 1963 [3].

In the case of one orbital it can be written as

$$H = - \sum_{\langle ij \rangle \sigma} t_{ij} (c_{i\sigma}^\dagger c_{j\sigma} + c_{j\sigma}^\dagger c_{i\sigma}) + U \sum_i n_{i\uparrow} n_{i\downarrow} - \mu \sum_i n_i, \quad (2.1)$$

where  $c_{i\sigma}$  destroys an electron of spin  $\sigma$  at site  $i$ ,  $c_{i\sigma}^\dagger$  creates an electron of spin  $\sigma$  at site  $i$  and  $n_{i\sigma}$  is the number operator. The brackets  $\langle, \rangle$  signal that only nearest neighbors have to be counted.

The Coulomb interaction  $U$  is constant and only taken into account for electrons on the same site. Moreover, the kinetic energy is encoded in the hopping integrals  $t_{ij}$  and the underlying lattice of ions is static. The first sum is carried out for a small number of neighbors, e.g. next nearest and second nearest neighbors (Fig. 2.1).

The chemical potential  $\mu$  is introduced as an Lagrange parameter to guarantee the right filling.

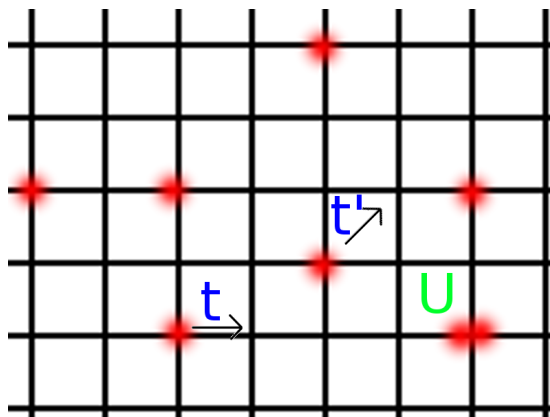


Figure 2.1: An illustration of the Hubbard model for a square lattice where electrons are depicted as red dots. The Coulomb interaction is reduced to a constant on-site term  $U$ . The arrows show hopping elements  $t$  and  $t'$  to the first nearest neighbor and second nearest neighbor, respectively.

Even if this model has an appealing and simple form, no general solution was found but for the one dimensional and the infinite dimensional case.

Nevertheless many approaches have been proposed to find approximate solutions that were proven to be good descriptions of real materials, e.g. Mott-Metal-Insulator transition in several strongly correlated systems.

The kinetic part is in general obtained by performing a Density Functional Theory (DFT) calculation that provides a band structure. By using the projective Wannier function method we determine the tight binding parameters that reflect the underlying lattice geometry. In the simple case of a  $d$ -dimensional cube, where one can assume that only next nearest neighbor hoppings are important, the calculation takes the following form:

$$\begin{aligned}
 H &\xrightarrow{\text{Fourier}} -t \sum_{\langle ij \rangle} \sum_{\vec{k}\sigma, \vec{k}'\sigma} (c_{\vec{k}\sigma}^\dagger c_{\vec{k}'\sigma} e^{i(\vec{k}\vec{r}_i - \vec{k}'\vec{r}_j)} + h.c.) \\
 &= -t \sum_{\nu=\pm 1} \sum_{l=1}^d \sum_{\vec{k}\sigma, \vec{k}'\sigma} c_{\vec{k}\sigma}^\dagger c_{\vec{k}'\sigma} \sum_i e^{i[\vec{k}\vec{r}_i - \vec{k}'(\vec{r}_i + \nu a \vec{e}_l)]} \\
 &= -t \sum_{\nu=\pm 1} \sum_{l=1}^d \sum_{\vec{k}\sigma, \vec{k}'\sigma} c_{\vec{k}\sigma}^\dagger c_{\vec{k}'\sigma} e^{-i\vec{k}'\nu a \vec{e}_l} \sum_i e^{i(\vec{k} - \vec{k}')\vec{r}_i} \\
 &= -t \sum_{\nu=\pm 1} \sum_{l=1}^d \sum_{\vec{k}\sigma, \vec{k}'\sigma} c_{\vec{k}\sigma}^\dagger c_{\vec{k}'\sigma} e^{-i\vec{k}'\nu a \vec{e}_l} \delta_{\vec{k}, \vec{k}'} \\
 &= -t \sum_{l=1}^d \sum_{\vec{k}\sigma} c_{\vec{k}\sigma}^\dagger c_{\vec{k}\sigma} \cos(\vec{k} a \vec{e}_l) \\
 &= \sum_{\vec{k}\sigma} \left[ -2t \sum_{l=1}^d \cos(k_l) \right] c_{\vec{k}\sigma}^\dagger c_{\vec{k}\sigma} \tag{2.2}
 \end{aligned}$$

$$\Rightarrow \epsilon_{\vec{k}} = -2t \sum_{l=1}^d \cos(k_l). \tag{2.3}$$

Including hoppings to the second and third nearest neighbours ( $t'$  and  $t''$ ) leads to

$$\epsilon_{\vec{k}} = -2t \sum_{l=1}^d \cos(k_l) - 4t' \prod_{m=1}^d \cos(k_m) - 2t'' \sum_{n=1}^d \cos(2k_n). \tag{2.4}$$

This dispersion relation will serve as a starting point not only for many different kinds of theories but also for TPSC.

## 2.2. Cuprates and organic charge transfer salts

Two groups of superconducting materials are supposed to be adaptable to the single-orbital Hubbard model and therefore we are going to present them in this section.

### Cuprates

A typical representative of the cuprates is  $\text{YBa}_2\text{Cu}_3\text{O}_7$  (see Fig.2.2) but all systems have cuprate ( $\text{CuO}_2^-$ )-layers in their unit cells in common that are divided by blocks of molecules that serve as a charge reservoir. Effectively, one can describe the systems as

quasi-2D where the blocks between the  $\text{CuO}_2$ -planes change only the filling and have no other influence.

Further approximations like the neglect of the oxygen  $2p_{x,y}$ -orbitals and only taking into account of the copper  $3d_{x^2-y^2}$ -orbitals, the reduction of the Coulomb interaction to an on-site Hubbard interaction  $U$  and restricting the kinetic term to effective nearest-neighbor hoppings  $t(t' \dots)$  lead to a description of cuprates by the single-orbital Hubbard model. Naturally, this can be extended to a many-orbital Hubbard model where one includes the effect of the oxygen  $2p_{x,y}$ -orbitals [4].

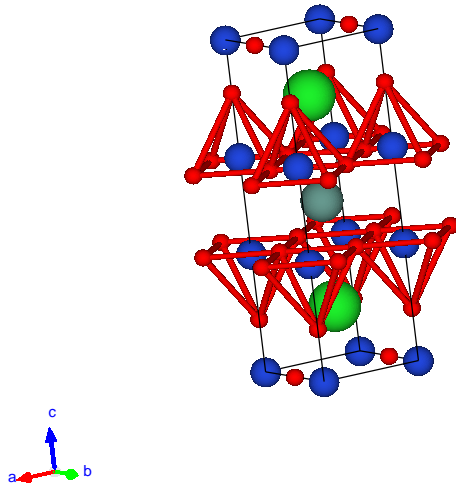


Figure 2.2: Unit cell of  $\text{YBa}_2\text{Cu}_3\text{O}_7$  where one finds Yttrium (grey) between two  $\text{CuO}_2$ -planes (red and blue). The remaining blocks above and below the planes can be very different. In this case it is Barium (green) and  $\text{CuO}$ -chains that serve as a charge reservoir.

Various experimental techniques like NMR, ARPES, resistivity and susceptibility measurements have clarified the phase diagram of cuprates and give a benchmark for theoretical models (Fig. 2.3).

In this work we concentrate on the pseudogap and superconductivity and therefore Fig. 2.3 shows only those two phases that are characterized by the crossover temperature  $T_x$  and the superconducting critical temperature  $T_c$ . Increasing antiferromagnetic correlations within the pseudogap phase are expected to be important for the understanding of the superconducting dome below.

#### Organic charge transfer salts

At first glance, it seems impossible to model organic charge transfer salts by a simple single-orbital Hubbard model because the unit cell consists of many complex structured molecules (see Fig. 2.4). But measurements have shown that the anion-planes separating the ET layers serve as insulating barriers and therefore one might approximate the physics by only taking the conducting ET layers into account. Viewing along the molecule axis of the ET molecules allows us to identify a very appealing structure since we can summarize the molecules to dimers (red and blue ellipses in Fig. 2.4) that form a triangular lattice.

Again one can reduce the Coulomb interaction to an on-site Hubbard interaction  $U$

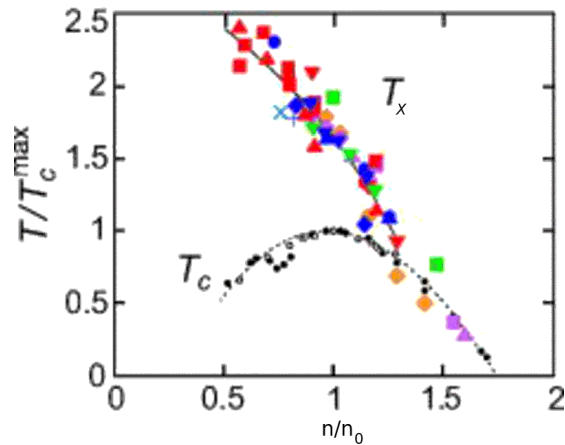


Figure 2.3: Segment of the phase diagram of various cuprate systems studied with different techniques by T. Nakano *et al.* (see key in [5]). The studied systems reveal a dome-like shape for the superconducting critical temperature  $T_c$  that reaches its maximum value  $T_c^{max}$  at some optimal filling  $n = n_0$ . Above the superconducting dome we find the pseudogap region that sets in below  $T_x$ .

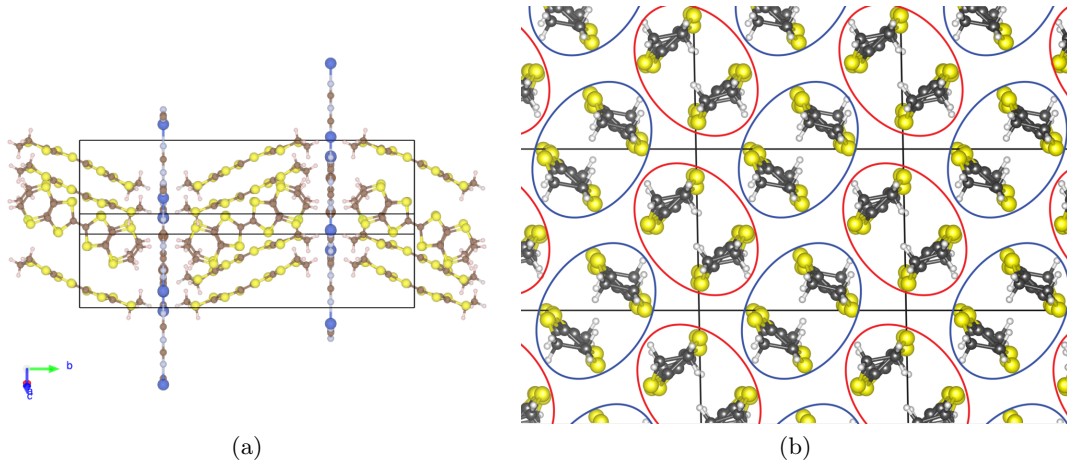


Figure 2.4: (a) The unit cell of  $\kappa$ -(ET) $_2$ -Cu[N(CN) $_2$ ]Br consists of conducting extended ET layers and narrow Cu[N(CN) $_2$ ]Br-blocks that allow electric current parallel to the ET layers. (b) Viewing along the long ET molecule axis gives a structure that allows the regrouping of molecules into dimers (red and blue ellipses). This model for the organic charge transfer salts is called dimer model.

and confine the kinetic term to the nearest neighbors and find thus the single-orbital Hubbard model. The same calculations as for the square lattice (see 2.4) lead to an energy dispersion of the form

$$\epsilon_{\vec{k}} = -2t(\cos(k_x) + \cos(k_y)) - 2t'\cos(k_x + k_y). \quad (2.5)$$

In contrast to the cuprates the next step of improvement is the extension to a multi-site model that takes care of the inner structure of each dimer. It has been shown that this advanced model gives a different symmetry of the gap function and might therefore also have an effect on the calculation of the critical temperature  $T_c$  [6].

The next part of this work will introduce Green's functions and susceptibilities that are crucial ingredients for the formalism that leads to TPSC.

---

### 3. Green's functions and Susceptibilities

Green's functions and susceptibilities are special types of correlation functions, so the first step of this chapter is to introduce correlation functions. Afterwards it will be easy to use these general results for those representatives. In the end, a connection between Green's functions and susceptibilities will be drawn.

#### 3.1. Overview of Correlation functions

##### 3.1.1. Motivation from experiments

Physics is founded on the grounds of experiments and the aim of theoretical physics is to build a mathematical model that fits to the observations and gives a widely applicable understanding of the involved mechanisms that allows further predictions.

Assuming that during an experiment the interaction between the system and the probe can be described via a coupling constant  $g$  one can write the Hamiltonian

$$H_{system-probe} \approx g(O_{system} \otimes 1_{probe})(1_{system} \otimes O_{probe}), \quad (3.1)$$

where  $O_{system}$  and  $O_{probe}$  are some operators acting on the system and the probe, respectively. This form of the Hamiltonian is indeed a very good model for a big range of experimental techniques. In general, experimentalists measure not only one final state of the probe but a continuum, so we have to make use of Fermi's Golden rule

$$p_{i \rightarrow f} = 2\pi |\langle f | H_{system-probe} | i \rangle|^2 \delta(E_f - E_i - \omega), \quad (3.2)$$

which tells us that the transition probability  $p_{i \rightarrow f}$  from some initial state  $i$  to a final state  $f$  is given by the squared absolute value of the transition matrix element  $\langle f | H_{system-probe} | i \rangle$ . In addition, the  $\delta$ -function  $\delta(E_f - E_i - \omega)$  guarantees that the energy difference between the initial and the final state  $E_f - E_i$  is compensated by the energy change of the probe  $\omega$ , i.e. energy conservation. During an experiment one detects the changes in the probe and performs no measurements of the system directly. Therefore, to get the transition probability for the probe it is necessary to sum over all possible final states (selection rules are included in the matrix elements).

In order to do calculations at finite temperatures one has to perform the thermal average over all initial states of the system. Using the form of the Hamiltonian (Eq. 3.1) one gets the transition probability

$$\begin{aligned} P &= \sum_{f_{system}} p_{i \rightarrow f} \\ &= 2\pi g^2 |\langle i_{probe} | O_{probe} | f_{probe} \rangle|^2 \sum_{f_{system}} |\langle i_{system} | O_{system} | f_{system} \rangle|^2 \delta(E_f - E_i - \omega) \\ &= g^2 |\langle i_{probe} | O_{probe} | f_{probe} \rangle|^2 \sum_{f_{system}} |\langle i_{system} | O_{system} | f_{system} \rangle|^2 \int_{-\infty}^{\infty} dt e^{-i(E_f - E_i - \omega)t} \\ &= g^2 |\langle i_{probe} | O_{probe} | f_{probe} \rangle|^2 \int_{-\infty}^{\infty} dt e^{i\omega t} \times \\ &\quad \times \sum_{f_{system}} \langle i_{system} | e^{iH_{system}t} O_{system} e^{-iH_{system}t} | f_{system} \rangle \langle f_{system} | O_{system} | i_{system} \rangle \\ &= g^2 |\langle i_{probe} | O_{probe} | f_{probe} \rangle|^2 \int_{-\infty}^{\infty} dt e^{i\omega t} \langle i_{system} | O_{system}(t) O_{system} | i_{system} \rangle \end{aligned}$$

$$\xrightarrow{\text{thermal avg.}} g^2 |\langle i_{probe} | O_{probe} | f_{probe} \rangle|^2 \int_{-\infty}^{\infty} dt e^{i\omega t} \langle O_{system}(t) O_{system} \rangle, \quad (3.3)$$

where  $\langle \cdot \rangle$  denotes the ensemble average as mentioned in section 1.

This last equation can be decoupled in two parts:

The first part contains information about the probe that is usually easy to evaluate, e.g. free electrons, electro-magnetic waves etc.

In the second part one is confronted with a Fourier transform of an object that is called

$$\boxed{\begin{array}{c} \text{correlation function} \\ \langle O(x) O'(y) \rangle. \end{array}} \quad (3.4)$$

$x$  and  $y$  summarize all kinds of variables whereupon the arbitrary operators  $O$  and  $O'$  depend.

To summarize: In a large range of experiments correlation functions play a key role to interpret experimental data or model certain physical effects.

### 3.1.2. Susceptibilities and Linear-Response Theory

In many cases of models one can decompose the full Hamiltonian  $H_{full}(t)$  into a sum

$$H_{full}(t) = H_0 + H_1(t), \quad (3.5)$$

where  $H_0$  might be related to the unperturbed system and  $H_1(t)$  to a perturbation generated by a probe or  $H_0$  is the kinetic part of a Hamiltonian and  $H_1(t)$  the interacting part. Recalling the form of interactions between system and probe (Eq. 3.1) one can reformulate the perturbation

$$H_1(t) = \int d^3r O_{system}(\vec{r}, t) \phi(\vec{r}, t) \quad (3.6)$$

and sum up the effects of the probe to an effective field  $\phi(\vec{r}, t)$ .

These are the foundations of Linear-Response theory and the rest will be mere algebra and first order perturbation theory that leads to the definition of susceptibilities.

The central question is how does the expectation value  $\langle A(\vec{r}, t) \rangle$  of an observable  $A(\vec{r})$  evolve if the system is at some initial time  $t_0$  in thermal equilibrium and evolves afterwards under the given perturbation. In the Dirac interaction picture this reads

$$\langle A(\vec{r}, t) \rangle = \langle U_I^\dagger(t, t_0) A_H(\vec{r}, t) U_I(t, t_0) \rangle \quad (3.7)$$

$$A_H(\vec{r}, t) = e^{iH_0 t} A(\vec{r}) e^{-iH_0 t}, \quad (3.8)$$

while  $A_H(\vec{r}, t)$  is the time-evolved operator without the perturbation. In order to take into account that the perturbation is only weak, one neglects higher order contributions from  $\phi(\vec{r}, t)$ , i.e. one takes the functional derivative at  $\phi = 0$ ,

$$\begin{aligned} \left. \frac{\delta \langle A(\vec{r}, t) \rangle}{\delta \phi(\vec{r}', t')} \right|_{\phi=0} &= \left\langle \left[ 1 + i \int_{t_0}^t dt' \int d^3r' O_{system}(\vec{r}', t') \phi(\vec{r}', t') + O((H_1)^2) \right] A_H(\vec{r}, t) \times \right. \\ &\quad \times \left. \left[ 1 - i \int_{t_0}^t dt' \int d^3r' O_{system}(\vec{r}', t') \phi(\vec{r}', t') + O((H_1)^2) \right] \right\rangle / \\ &\quad \left. \left. \delta \phi(\vec{r}', t') \right|_{\phi=0} \right. \end{aligned}$$

### 3.1 Overview of Correlation functions

---

$$= i\langle [O_{system}(\vec{r}', t'), A_H(\vec{r}, t)] \rangle. \quad (3.9)$$

In general, one is interested in causality and the change of the expectation value can only occur after the perturbation, so we insert  $\Theta(t - t')$  to assure this.

This leads to the definition of the

retarded susceptibility  
 $\chi_{O_{system}A}^R(\vec{r}, t; \vec{r}', t') \equiv i\langle [O_{system}(\vec{r}', t'), A_H(\vec{r}, t)] \Theta(t - t') \rangle.$

(3.10)

The change in the expectation value of an observable is therefore described by the susceptibility if one can assume that the perturbation is weak and it is allowed to treat it within first order perturbation theory.

#### 3.1.3. Definition of the single-particle Green's function

From the electrodynamics course one might remember that Green's functions have been introduced as solutions of the Poisson equation with boundary conditions.

Due to the fact that the general Schrödinger equation is a linear partial differential equation one should not be surprised to find it also in solid state physics.

Starting point of this chapter is a general Hamiltonian  $H$  and two states  $\Psi_0(\vec{r}, t)$  and  $\Psi(\vec{r}, t)$  where the second state is obtained by time-evolution of the first, i.e.

$$\Psi(\vec{r}, t) = \int d^3r' \langle \vec{r} | e^{-iH(t-t')} | \vec{r}' \rangle \Psi_0(\vec{r}', t'). \quad (3.11)$$

Since we have chosen  $\Psi_0$  to be the initial state one is obliged to put  $\Theta(t - t')$  to preserve causality,

$$\begin{aligned} \Psi(\vec{r}, t) \Theta(t - t') &= \int d^3r' \langle \vec{r} | e^{-iH(t-t')} | \vec{r}' \rangle \Psi_0(\vec{r}', t') \Theta(t - t') \\ &\equiv i \int d^3r' G_s^R(\vec{r}, t; \vec{r}', t') \Psi_0(\vec{r}', t'), \end{aligned} \quad (3.12)$$

where we have used the definition of the

one-body retarded Green's function  
 $G_s^R(\vec{r}, t; \vec{r}', t') \equiv -i \langle \vec{r} | e^{-iH(t-t')} | \vec{r}' \rangle \Theta(t - t').$

(3.13)

Later, we will see that these functions are all we need for calculations and it is the first step away from wave functions and towards Feynman diagrams.

So far, this is the definition for single-particle problems but how do we deal with many-body systems?

One might be tempted to translate the definition the one-body retarded Green's function (Def. 3.13) to many-body systems by taking the average over the ground-state  $|0\rangle$  and work with creation  $\Psi^\dagger(\vec{r})$  and annihilation operators  $\Psi(\vec{r})$  that create and destroy at electrons at position  $\vec{r}$ , respectively:

$$\begin{aligned} -i \langle \vec{r} | e^{-iH(t-t')} | \vec{r}' \rangle \Theta(t - t') &= -i \langle 0 | \Psi(\vec{r}) e^{-iHt} e^{iHt'} \Psi^\dagger(\vec{r}') | 0 \rangle \Theta(t - t') \quad | H|0\rangle = 0|0\rangle \\ &= -i \langle 0 | e^{iHt} \Psi(\vec{r}) e^{-iHt} e^{iHt'} \Psi^\dagger(\vec{r}') e^{-iHt'} | 0 \rangle \Theta(t - t') \\ &= -i \langle 0 | \Psi(\vec{r}, t) \Psi^\dagger(\vec{r}', t') | 0 \rangle \Theta(t - t') \end{aligned}$$

$$\xrightarrow{T>0} -i\langle\Psi(\vec{r}, t)\Psi^\dagger(\vec{r}', t')\rangle\Theta(t-t'). \quad (3.14)$$

This first attempt shows two important disadvantages:

1) The condition

$$\lim_{t\rightarrow t'+0} G^R(\vec{r}, t; \vec{r}', t') \sim \delta(\vec{r}-\vec{r}') \quad (3.15)$$

reflecting that a particle does not change its position when the regarded time scale goes to zero will in general not be satisfied since the ground-state is a linear combination of product-states (namely Slater determinants).

2) The propagation of holes is not explicitly taken into account.

The least invasive change of the last equation would be the following:

$$-i\langle\{\Psi(\vec{r}, t), \Psi^\dagger(\vec{r}', t')\}\rangle\Theta(t-t') \quad (3.16)$$

and indeed it obviously mends 2) and a few lines show also the improvement concerning 1):

$$\begin{aligned} \lim_{t\rightarrow t'+0} \left[ -i\langle\{\Psi(\vec{r}, t), \Psi^\dagger(\vec{r}', t')\}\rangle\Theta(t-t') \right] &= \lim_{t\rightarrow t'+0} \left[ -i\langle\Psi(\vec{r}, t)\Psi^\dagger(\vec{r}', t') \right. \\ &\quad \left. + \Psi^\dagger(\vec{r}', t')\Psi(\vec{r}, t)\rangle \right] \\ &= \lim_{t\rightarrow t'+0} \left[ -i\langle\Psi(\vec{r}, t)\Psi^\dagger(\vec{r}', t') \right. \\ &\quad \left. + \delta(\vec{r}-\vec{r}') - \Psi(\vec{r}, t)\Psi^\dagger(\vec{r}', t')\rangle \right] \\ &= -i\delta(\vec{r}-\vec{r}'). \end{aligned} \quad (3.17)$$

Hence, the final definition of the single-particle Green's function of a many-body state is

$$\boxed{G^R(\vec{r}, t; \vec{r}', t') \equiv -i\langle\{\Psi(\vec{r}, t), \Psi^\dagger(\vec{r}', t')\}\rangle\Theta(t-t')} \quad (3.18)$$

In this form we can recognize that we are dealing with a correlation function. It is the correlation of the state  $\Psi$  with itself at different times and positions.

Before we continue with Green's functions (Sec. 3.3) we will show basic properties of correlation functions that will be needed later.

### 3.2. Properties of correlation functions

#### 3.2.1. Time translational invariance

Assuming that the system is initially prepared in a thermal equilibrium state one can conclude that an arbitrary correlation function  $C(\vec{r}, t; \vec{r}', t')$  exhibits time translational invariance,

$$C(\vec{r}, t; \vec{r}', t') \equiv \langle O(\vec{r}, t) O'(\vec{r}', t') \rangle = C(\vec{r}, \vec{r}'; t - t'). \quad (3.19)$$

Proof:

Starting from a thermal equilibrium means that we can take the thermal average as usual:

$$\begin{aligned} C(\vec{r}, t; \vec{r}', t') &= \frac{\text{tr} \left[ e^{-\beta H} e^{iHt} O(\vec{r}) e^{-iHt} e^{iHt'} O'(\vec{r}') e^{-iHt'} \right]}{\text{tr}(e^{-\beta H})} \\ &= \frac{\text{tr} \left[ e^{-\beta H} e^{iH(t-t')} O(\vec{r}) e^{-iH(t-t')} O'(\vec{r}') \right]}{\text{tr}(e^{-\beta H})} \\ &= \frac{\text{tr} \left[ e^{-\beta H} O(\vec{r}, t-t') O'(\vec{r}') \right]}{\text{tr}(e^{-\beta H})} \\ &= C(\vec{r}, \vec{r}'; t - t'). \end{aligned} \quad (3.20)$$

□

#### 3.2.2. Space translational invariance

The definition of space translational invariance is the following:

$$[T_{\vec{R}}, H] = 0, \quad (3.21)$$

where  $T_{\vec{R}}$  is the space translation operator that moves a state by some vector  $\vec{R} \in S$ ,  $S$  is a set of lattice vectors and  $H$  is the Hamiltonian of the system. From this we also know

$$[T_{\vec{R}}, e^{-\beta H}] = 0 \quad (3.22)$$

and therefore

$$\begin{aligned} C(\vec{r}, t; \vec{r}', t') &= \text{tr} \left[ e^{-\beta H} O(\vec{r}, t) O'(\vec{r}', t') \right] / \text{tr}(e^{-\beta H}) \\ &= \text{tr} \left[ e^{-\beta H} T_{\vec{R}} T_{-\vec{R}} O(\vec{r}, t) T_{\vec{R}} T_{-\vec{R}} O'(\vec{r}', t') \right] / \text{tr}(e^{-\beta H}) \\ &= \text{tr} \left[ e^{-\beta H} T_{-\vec{R}} O(\vec{r}, t) T_{\vec{R}} T_{-\vec{R}} O'(\vec{r}', t') T_{\vec{R}} \right] / \text{tr}(e^{-\beta H}) \\ &= \text{tr} \left[ e^{-\beta H} O(\vec{r} + \vec{R}, t) O'(\vec{r}' + \vec{R}, t') \right] / \text{tr}(e^{-\beta H}) \\ &= C(\vec{r} + \vec{R}, t; \vec{r}' + \vec{R}, t'). \end{aligned} \quad (3.23)$$

Starting from a translational invariant system one can calculate

$$C(\vec{r}, t; \vec{r}', t') = \langle O(\vec{r}, t) O'(\vec{r}', t') \rangle$$

$$\begin{aligned}
 &= \frac{1}{V} \left\langle \sum_{\vec{k}'\vec{k}} O_{\vec{k}}(t) e^{i(\vec{k}\vec{r}+\vec{k}'\vec{r}')} O'_{\vec{k}'}(t') \right\rangle \\
 &= \frac{1}{V} \left\langle \sum_{\vec{k}'\vec{k}} O_{\vec{k}}(t) e^{i\left[(\vec{k}+\vec{k}')\frac{\vec{r}'+\vec{r}}{2} + \frac{\vec{k}-\vec{k}'}{2}(\vec{r}-\vec{r}')\right]} O'_{\vec{k}'}(t') \right\rangle. \quad (3.24)
 \end{aligned}$$

So far, nothing special happened but now one uses the translational invariance (Eq. 3.23), i.e.

$$\frac{1}{V} \int_V d\left(\frac{\vec{r}'+\vec{r}}{2}\right) [C(\vec{r}, t; \vec{r}', t')] = \frac{1}{V} \int_V d\left(\frac{\vec{r}'+\vec{r}}{2}\right) [C(\vec{r}+\vec{R}, t; \vec{r}'+\vec{R}, t')] \quad (3.25)$$

and therefore the integral does not depend on the integrand and gives just 1.

$$\begin{aligned}
 1 \cdot C(\vec{r}, t; \vec{r}', t') &= 1 \cdot \frac{1}{N_{\vec{k}}} \left\langle \sum_{\vec{k}'\vec{k}} O_{\vec{k}}(t) e^{i\left[(\vec{k}+\vec{k}')\frac{\vec{r}'+\vec{r}}{2} + \frac{\vec{k}-\vec{k}'}{2}(\vec{r}-\vec{r}')\right]} O'_{\vec{k}'}(t') \right\rangle \\
 &= \frac{1}{N_{\vec{k}}} \left\langle \sum_{\vec{k}'\vec{k}} O_{\vec{k}}(t) \frac{1}{V} \int_V d\left(\frac{\vec{r}'+\vec{r}}{2}\right) \left( e^{i(\vec{k}+\vec{k}')\frac{\vec{r}'+\vec{r}}{2}} e^{i\frac{\vec{k}-\vec{k}'}{2}(\vec{r}-\vec{r}')} O'_{\vec{k}'}(t') \right) \right\rangle \\
 &= \frac{1}{N_{\vec{k}}} \left\langle \sum_{\vec{k}'\vec{k}} O_{\vec{k}}(t) \delta_{\vec{k}, -\vec{k}'} e^{i\frac{\vec{k}-\vec{k}'}{2}(\vec{r}-\vec{r}')} O'_{\vec{k}'}(t') \right\rangle \\
 &= \frac{1}{N_{\vec{k}}} \left\langle \sum_{\vec{k}} O_{\vec{k}}(t) e^{i\vec{k}(\vec{r}-\vec{r}')} O'_{-\vec{k}}(t') \right\rangle \\
 &= C(\vec{r}-\vec{r}'; t, t'). \quad (3.26)
 \end{aligned}$$

Note:

In the case where one of the operators is a hermitian conjugate the  $-\vec{k}$  becomes a  $\vec{k}$  as follows from the Fourier transformation.

This is the case for Green's functions and in the following we will use the Fourier transform that follows from Eq. 3.26.

### 3.3. Single-particle Green's function

#### 3.3.1. Spectral weight

The first application of the single-particle Green's function (Def. 3.18) is the calculation of the spectral weight.

To do this it is helpful to perform a Fourier transform to move from time to frequency space,

$$\begin{aligned} G^R(\vec{r}, \vec{r}'; \omega) &= \int_{-\infty}^{\infty} d(t-t') e^{i\omega(t-t')} G^R(\vec{r}, \vec{r}'; t-t') \\ &= -i \lim_{\eta \rightarrow 0^+} \int_0^{\infty} d(t-t') e^{i\omega(t-t')} \langle \{ \Psi(\vec{r}, t-t'), \Psi^\dagger(\vec{r}') \} \rangle e^{-\eta(t-t')}. \end{aligned} \quad (3.27)$$

We manipulate now the anti-commutator in the last expression by using a complete set of eigenvectors  $\{|n\rangle\}$  properly taking into account the creation and annihilation operators:

$$\begin{aligned} &\langle \{ \Psi(\vec{r}, t-t'), \Psi^\dagger(\vec{r}') \} \rangle \\ &= \sum_{m,n} \left[ \langle n | e^{-\beta H} e^{iH(t-t')} \Psi(\vec{r}) e^{-iH(t-t')} | m \rangle \langle m | \Psi^\dagger(\vec{r}') | n \rangle \right. \\ &\quad \left. + \langle n | e^{-\beta H} \Psi^\dagger(\vec{r}') | m \rangle \langle m | e^{iH(t-t')} \Psi(\vec{r}) e^{-iH(t-t')} | n \rangle \right] / \text{tr}(e^{-\beta H}) \\ &= \sum_{m,n} \left[ e^{-\beta(E_n - \mu N_n)} \left( e^{-i(t-t')(E_m - (N_n+1)\mu - (E_n - N_n\mu))} \langle n | \Psi(\vec{r}) | m \rangle \langle m | \Psi^\dagger(\vec{r}') | n \rangle \right. \right. \\ &\quad \left. \left. + e^{-i(t-t')(E_n - N_n\mu - (E_m - (N_n-1)\mu))} \langle n | \Psi^\dagger(\vec{r}') | m \rangle \langle m | \Psi(\vec{r}) | n \rangle \right) \right] / \text{tr}(e^{-\beta H}). \end{aligned} \quad (3.28)$$

where  $N_n$  is the number of particles in the state  $|n\rangle$ .

Having separated the  $(t-t')$ -dependency it is now easy to perform the integral and we get therefore

$$\begin{aligned} G^R(\vec{r}, \vec{r}'; \omega) &= \lim_{\eta \rightarrow 0^+} \sum_{m,n} \left[ e^{-\beta(E_n - \mu N_n)} \left( \frac{1}{\omega + i\eta - (E_m - E_n - \mu)} \langle n | \Psi(\vec{r}) | m \rangle \langle m | \Psi^\dagger(\vec{r}') | n \rangle \right. \right. \\ &\quad \left. \left. + \frac{1}{\omega + i\eta - (E_n - E_m - \mu)} \langle n | \Psi^\dagger(\vec{r}') | m \rangle \langle m | \Psi(\vec{r}) | n \rangle \right) \right] / \\ &\quad / \text{tr}(e^{-\beta H}). \end{aligned} \quad (3.29)$$

Changing in the second line the summation indices  $m \leftrightarrow n$  we get

$$\begin{aligned} G^R(\vec{r}, \vec{r}'; \omega) &= \lim_{\eta \rightarrow 0^+} \sum_{m,n} \left( e^{-\beta(E_n - \mu N_n)} + e^{-\beta(E_m - \mu N_m)} \right) \times \\ &\quad \times \left( \frac{\langle n | \Psi(\vec{r}) | m \rangle \langle m | \Psi^\dagger(\vec{r}') | n \rangle}{\omega + i\eta - (E_m - E_n - \mu)} \right) / \text{tr}(e^{-\beta H}). \end{aligned} \quad (3.30)$$

Let us now have a look at the imaginary part of the retarded Green's function 3.30

$$\text{Im}(G^R(\vec{r}, \vec{r}'; \omega)) = \lim_{\eta \rightarrow 0^+} \sum_{m,n} \left( e^{-\beta(E_n - \mu N_n)} + e^{-\beta(E_m - \mu N_m)} \right) \times$$

$$\times \left( -\frac{\eta \langle n | \Psi(\vec{r}) | m \rangle \langle m | \Psi^\dagger(\vec{r}') | n \rangle}{(\omega - (E_m - E_n - \mu))^2 + \eta^2} \right) / \text{tr}(e^{-\beta H}) \quad (3.31)$$

Remembering the identity

$$\frac{1}{\pi} \lim_{\eta \rightarrow 0^+} \frac{\eta}{x^2 + \eta^2} = \delta(x) \quad (3.32)$$

leads to

$$\begin{aligned} \text{Im}(G^R(\vec{r}, \vec{r}'; \omega)) &= -\pi \sum_{m,n} \left( e^{-\beta(E_n - \mu N_n)} + e^{-\beta(E_m - \mu N_m)} \right) \langle n | \Psi(\vec{r}) | m \rangle \langle m | \Psi^\dagger(\vec{r}') | n \rangle \times \\ &\times (\delta(\omega - (E_m - E_n - \mu))) / \text{tr}(e^{-\beta H}) \end{aligned} \quad (3.33)$$

Due to the  $\delta$ -function and the matrix elements one knows that

$$\begin{aligned} N_m &= N_n + 1 \\ \omega &= E_m - E_n - \mu \end{aligned} \quad (3.34)$$

and therefore

$$\begin{aligned} \text{Im}(G^R(\vec{r}, \vec{r}'; \omega)) &= -\pi \sum_{m,n} (1 + e^{-\beta\omega}) e^{-\beta(E_n - \mu N_n)} \langle n | \Psi(\vec{r}) | m \rangle \langle m | \Psi^\dagger(\vec{r}') | n \rangle \times \\ &\times (\delta(\omega - (E_m - E_n - \mu))) / \text{tr}(e^{-\beta H}). \end{aligned} \quad (3.35)$$

From this one can now define the

spectral weight

$$\begin{aligned} A(\vec{r}, \vec{r}', \omega) &\equiv \sum_{m,n} (1 + e^{-\beta\omega}) e^{-\beta(E_n - \mu N_n)} \langle n | \Psi(\vec{r}) | m \rangle \langle m | \Psi^\dagger(\vec{r}') | n \rangle \times \\ &\times 2\pi \delta(\omega - (E_m - E_n - \mu)) / \text{tr}(e^{-\beta H}) \\ &= -2\text{Im}(G^R(\vec{r}, \vec{r}', \omega)). \end{aligned} \quad (3.36)$$

The interpretation of the spectral weight  $A(\vec{r}, \vec{r}', \omega)$  is that the first addend describes excitations with one more particle and the second addend with one more hole.

Those excitations provide an energy  $\omega$  that can be positive, negative or zero depending on whether the excitation energy  $E_m - E_n$  is bigger, smaller or equal to the chemical potential  $\mu$ . The weight of this excitation is the overlap matrix elements between the initial state and the excited one.

To relate the spectral weight  $A(\vec{r}, \vec{r}', t)$  with the retarded Green's function  $G^R(\vec{r}, \vec{r}', t)$  one has only to perform a Fourier transformation,

$$\begin{aligned} A(\vec{r}, \vec{r}', t) &= \int_{-\infty}^{\infty} \frac{d\omega}{2\pi} e^{-i\omega t} A(\vec{r}, \vec{r}', \omega) \\ &= \sum_{m,n} e^{-i(E_m - E_n - \mu)t} \left[ e^{-\beta(E_n - \mu N_n)} + e^{-\beta(E_m - \mu N_m)} \right] \langle n | \Psi(\vec{r}) | m \rangle \langle m | \Psi^\dagger(\vec{r}') | n \rangle / \\ &\quad / \text{tr}(e^{-\beta H}) \end{aligned}$$

### 3.3 Single-particle Green's function

$$\begin{aligned}
&= \sum_{m,n} \left[ e^{-\beta(E_n - \mu N_n)} + e^{-\beta(E_m - \mu N_m)} \right] \langle n | e^{iHt} \Psi(\vec{r}) e^{-iHt} | m \rangle \langle m | \Psi^\dagger(\vec{r}') | n \rangle / \\
&\quad / \text{tr}(e^{-\beta H}) \\
&= \sum_n \langle n | e^{-\beta(E_n - \mu N_n)} \{ \Psi(\vec{r}, t), \Psi^\dagger(\vec{r}') \} | n \rangle / \text{tr}(e^{-\beta H}) \\
&= \langle \{ \Psi(\vec{r}, t), \Psi^\dagger(\vec{r}') \} \rangle. \tag{3.37}
\end{aligned}$$

Another useful relation is the following which can be obtained by performing a Fourier transformation twice,

$$\begin{aligned}
G^R(\vec{r}, \vec{r}', \omega) &= \int_{-\infty}^{\infty} dt e^{i\omega t} G^R(\vec{r}, \vec{r}', t) \\
&= -i \int_0^{\infty} dt e^{i(\omega + i\eta)t} A(\vec{r}, \vec{r}', t) \\
&= -i \int_0^{\infty} dt e^{i(\omega + i\eta)t} \int_{-\infty}^{\infty} \frac{d\omega'}{2\pi} e^{-i\omega' t} A(\vec{r}, \vec{r}', \omega') \\
&= -i \int_{-\infty}^{\infty} \frac{d\omega'}{2\pi} A(\vec{r}, \vec{r}', \omega') \int_0^{\infty} dt e^{i(\omega + i\eta - \omega')t} \\
&= \int_{-\infty}^{\infty} \frac{d\omega'}{2\pi} \frac{A(\vec{r}, \vec{r}', \omega')}{\omega + i\eta - \omega'}. \tag{3.38}
\end{aligned}$$

Let us assume space translational invariance and evaluate

$$\begin{aligned}
\int_{-\infty}^{\infty} \frac{d\omega}{2\pi} A(\vec{k}, \omega) &= \sum_{m,n} \left( e^{-\beta(E_n - \mu N_n)} + e^{-\beta(E_m - \mu N_m)} \right) \langle n | c_{\vec{k}} | m \rangle \langle m | c_{\vec{k}}^\dagger | n \rangle / \text{tr}(e^{-\beta H}) \\
&= \sum_n e^{-\beta(E_n - \mu N_n)} \langle n | c_{\vec{k}} c_{\vec{k}}^\dagger | n \rangle / \text{tr}(e^{-\beta H}) \\
&\quad + \sum_m e^{-\beta(E_m - \mu N_m)} \langle m | c_{\vec{k}}^\dagger c_{\vec{k}} | m \rangle / \text{tr}(e^{-\beta H}) \\
&= \langle \{ c_{\vec{k}}, c_{\vec{k}}^\dagger \} \rangle \\
&= 1. \tag{3.39}
\end{aligned}$$

This result allows us to interpret the spectral weight  $A(\vec{k}, \omega)$  as a probability that excitations described above are true eigenstates of the many-body system.

#### 3.3.2. Non-interacting Green's function

Later, it will be shown that the full Green's function can be expanded in terms of the non-interacting Green's function  $G_0(\vec{k}, \omega)$  and therefore it will be useful to consider the calculation of the non-interacting Green's function in momentum space.

Starting from the Hamiltonian (Eq. 2.1) and transforming to momentum space (Eq. 2.4) one uses space translational invariance,

$$\begin{aligned}
G^R(\vec{k}, t) &= -i \left\langle \left\{ c_{\vec{k}}(t), c_{\vec{k}}^\dagger \right\} \right\rangle \Theta(t) \\
&= -i e^{-i\xi_{\vec{k}} t} \times 1 \times \Theta(t) \tag{3.40}
\end{aligned}$$

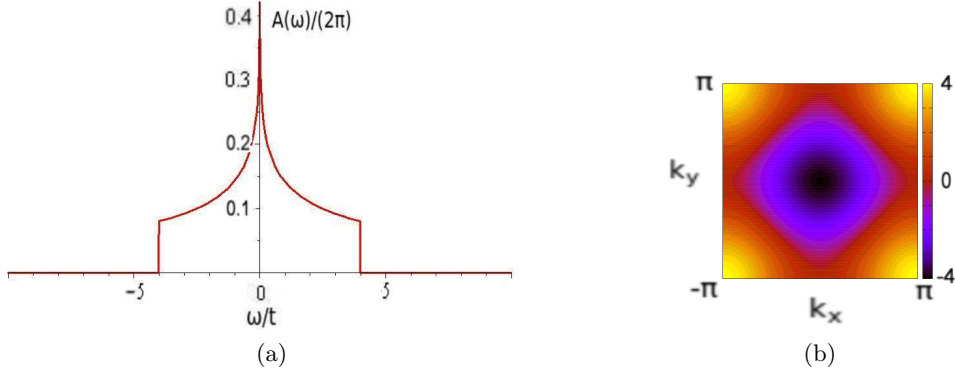


Figure 3.1: (a) The normalized spectral weight  $A(\omega)$  is symmetric due to particle-hole symmetry and half-filling. It drops at  $|\omega| > 4t$  which is the bandwidth as expected. The singularity at  $\omega/t = 0, \pm 4$  comes from a flat (b) dispersion  $\xi_{\vec{k}}/t$  since  $\int d^2k \sim \int \frac{d\xi_{\vec{k}}}{|\nabla \xi_{\vec{k}}|}$  and the number of contributing points is maximal for  $\omega = 0$ .

$$\begin{aligned} G^R(\vec{k}, \omega) &= -i \lim_{\eta \rightarrow 0^+} \int_0^\infty dt e^{i(\omega+i\eta)t} e^{-i\xi_{\vec{k}}t} \\ &= \lim_{\eta \rightarrow 0^+} \frac{1}{\omega + i\eta - \xi_{\vec{k}}}. \end{aligned} \quad (3.41)$$

From this we can also calculate the spectral weight (Def. 3.36) analytically for nearest neighbors hopping at half-filling, i.e.  $\mu = 0$ :

$$\begin{aligned} A(\vec{k}, \omega) &= -2 \lim_{\eta \rightarrow 0^+} \text{Im} \left( \frac{1}{\omega + i\eta - \xi_{\vec{k}}} \right) \\ &= \lim_{\eta \rightarrow 0^+} \frac{-1}{i} \left( \frac{1}{\omega + i\eta - \xi_{\vec{k}}} - \frac{1}{\omega - i\eta - \xi_{\vec{k}}} \right) \\ &= 2 \lim_{\eta \rightarrow 0^+} \frac{\eta}{(\omega - \xi_{\vec{k}})^2 + \eta^2} \\ &= 2\pi \delta(\omega - \xi_{\vec{k}}). \end{aligned} \quad (3.42)$$

Processing an integration in 2D over the whole Brillouin zone one gets the well-known spectral function  $A(\omega)$  - after normalizing (Eq. 3.39) -

$$\frac{1}{2\pi} A(\omega) = \frac{1}{2\pi^2 t} \int_0^{\pi/2} \frac{d\phi}{\sqrt{1 - \left[1 - \left(\frac{\omega}{4t}\right)^2\right] \sin^2 \phi}}, \quad (3.43)$$

that is shown in 3.1 and exhibits the typical divergence at  $\omega = 0$  and drops to zero at  $|\omega| = 4t$ .

### 3.4. Matsubara Green's function

To calculate expectation values in thermodynamic equilibrium perturbatively one has to evaluate the time-ordered products that appear in the time-evolution operator working in the interaction representation.

It turns out that a generalization of the Green's function to the complex time axis can

be related to the retarded Green's function and - that is the most important issue - is computationally more appealing, i.e. the complex time  $\tau$  is defined as

$$\tau \equiv it. \quad (3.44)$$

### 3.4.1. Definition

The Matsubara Green's function is defined by:

$$\begin{aligned} G(\vec{r}, \vec{r}'; \tau - \tau') &\equiv -\langle T_\tau \Psi(\vec{r}, \tau) \Psi^\dagger(\vec{r}', \tau') \rangle \\ &\equiv -\langle \Psi(\vec{r}, \tau) \Psi^\dagger(\vec{r}', \tau') \rangle \Theta(\tau - \tau') + \langle \Psi^\dagger(\vec{r}', \tau') \Psi(\vec{r}, \tau) \rangle \Theta(\tau' - \tau). \end{aligned} \quad (3.45)$$

The second equation defines the time-ordering operator (for fermions) where the commutation of the fermionic creation and annihilation operators induces a minus sign. Otherwise, the time-ordering operator only arranges the operators in a decreasing order of time starting from left.

### 3.4.2. Anti-periodicity and Fourier expansion

In this section we see how it is possible to map the information of continuous imaginary time  $\tau$  to discrete Matsubara frequencies  $ik_n$ .

Suppose  $\tau < 0$  (shifting  $\tau'$  to 0),

$$\begin{aligned} G(\vec{r}, \vec{r}'; \tau) &= \langle T_\tau \Psi^\dagger(\vec{r}', 0) \Psi(\vec{r}, \tau) \rangle \\ &= \frac{\text{tr} [e^{-\beta K} \Psi^\dagger(\vec{r}') (e^{K\tau} \Psi(\vec{r}) e^{-K\tau})]}{\text{tr}(e^{-\beta K})} \\ &= \frac{\text{tr} [(e^{K\tau} \Psi(\vec{r}) e^{-K\tau}) e^{-\beta K} \Psi^\dagger(\vec{r}')] }{\text{tr}(e^{-\beta K})} \\ &= \frac{\text{tr} [(e^{-\beta K} e^{\beta K}) (e^{K\tau} \Psi(\vec{r}) e^{-K\tau}) e^{-\beta K} \Psi^\dagger(\vec{r}')] }{\text{tr}(e^{-\beta K})} \\ &= \langle T_\tau \Psi(\vec{r}, \tau + \beta) \Psi^\dagger(\vec{r}', 0) \rangle \\ &= -G(\vec{r}, \vec{r}'; \tau + \beta). \end{aligned} \quad (3.46)$$

The same argumentation for  $\tau > 0$  leads to

$$G(\vec{r}, \vec{r}'; \tau) = -G(\vec{r}, \vec{r}'; \tau - \beta). \quad (3.47)$$

This anti-periodicity tells us that all necessary information about the Matsubara Green's function is already present in the interval  $[-\beta, \beta]$ .

Using this anti-periodicity we can expand the Matsubara Green's function  $G(\vec{r}, \vec{r}'; \tau)$  in a Fourier series,

$$G(\vec{r}, \vec{r}'; \tau) = \frac{1}{\beta} \sum_{n=-\infty}^{\infty} e^{-ik_n \tau} G(\vec{r}, \vec{r}'; ik_n) \quad (3.48)$$

$$k_n = \frac{(2n+1)\pi}{\beta} \quad (3.49)$$

$$G(\vec{r}, \vec{r}'; ik_n) = \int_0^\beta d\tau e^{ik_n \tau} G(\vec{r}, \vec{r}'; \tau). \quad (3.50)$$

As an important example we will demonstrate the calculation of the non-interacting Matsubara Green's function  $G_0(\vec{k}, ik_n)$ . The first step is calculating  $c_{\vec{k}}(\tau)$  from the Heisenberg equation of motion dropping the explicit imaginary time dependence for clarity,

$$\begin{aligned}
 \frac{\partial}{\partial \tau} c_{\vec{k}} &= [H_0, c_{\vec{k}}] \\
 &= \sum_{\vec{k}'} \xi_{\vec{k}'} [c_{\vec{k}'}^\dagger c_{\vec{k}'}, c_{\vec{k}}] \\
 &= \sum_{\vec{k}'} \xi_{\vec{k}'} c_{\vec{k}'}^\dagger \{c_{\vec{k}'}, c_{\vec{k}}\} - \{c_{\vec{k}'}^\dagger, c_{\vec{k}}\} c_{\vec{k}'} \\
 &= \sum_{\vec{k}'} \xi_{\vec{k}'} c_{\vec{k}'}^\dagger \cdot 0 - \delta_{\vec{k}\vec{k}'} c_{\vec{k}'} \\
 &= -\xi_{\vec{k}} c_{\vec{k}}.
 \end{aligned} \tag{3.51}$$

Regarding the initial condition in the Heisenberg picture, i.e.  $c_{\vec{k}}(0) = c_{\vec{k}}$  we obtain

$$c_{\vec{k}}(\tau) = e^{-\xi_{\vec{k}}\tau} c_{\vec{k}}. \tag{3.52}$$

By repeating the same steps as for the derivation of the translation invariance (Eq. 3.26) (Note that there is no minus sign because the second operator in the Matsubara Green's function (Def. 3.45) is hermitian conjugated):

$$G(\vec{k}; \tau) = -\langle T_\tau c_{\vec{k}}(\tau) c_{\vec{k}}^\dagger \rangle \tag{3.53}$$

$$\begin{aligned}
 G_0(\vec{k}; \tau) &= -e^{-\xi_{\vec{k}}\tau} [\langle c_{\vec{k}} c_{\vec{k}}^\dagger \rangle \Theta(\tau) - \langle c_{\vec{k}}^\dagger c_{\vec{k}} \rangle \Theta(-\tau)] \\
 &= -e^{-\xi_{\vec{k}}\tau} [(1 - f(\xi_{\vec{k}})) \Theta(\tau) - f(\xi_{\vec{k}}) \Theta(-\tau)].
 \end{aligned} \tag{3.54}$$

Taking the Fourier transform to Matsubara frequencies leads to

$$\begin{aligned}
 G_0(\vec{k}; ik_n) &= \int_0^\beta d\tau e^{ik_n\tau} G_0(\vec{k}; \tau) \\
 &= -(1 - f(\xi_{\vec{k}})) \int_0^\beta d\tau e^{(ik_n - \xi_{\vec{k}})\tau} \\
 &= \frac{1}{ik_n - \xi_{\vec{k}}}.
 \end{aligned} \tag{3.55}$$

From the Matsubara Green's function in momentum space  $G(\vec{k}, \tau)$  we already see that

$$\lim_{\tau \rightarrow 0^-} G(\vec{k}, \tau) = \langle c_{\vec{k}}^\dagger c_{\vec{k}} \rangle \tag{3.56}$$

and in the special case of non-interacting systems

$$\lim_{\tau \rightarrow 0^-} G_0(\vec{k}, \tau) = \langle c_{\vec{k}}^\dagger c_{\vec{k}} \rangle = f(\xi_{\vec{k}}). \tag{3.57}$$

The same result must be obtained if the calculus is carried out for the Fourier transformed (Eq. 3.55), i.e.

$$\lim_{\tau \rightarrow 0^-} \sum_n e^{ik_n\tau} G(\vec{k}, ik_n) = \langle c_{\vec{k}}^\dagger c_{\vec{k}} \rangle \tag{3.58}$$

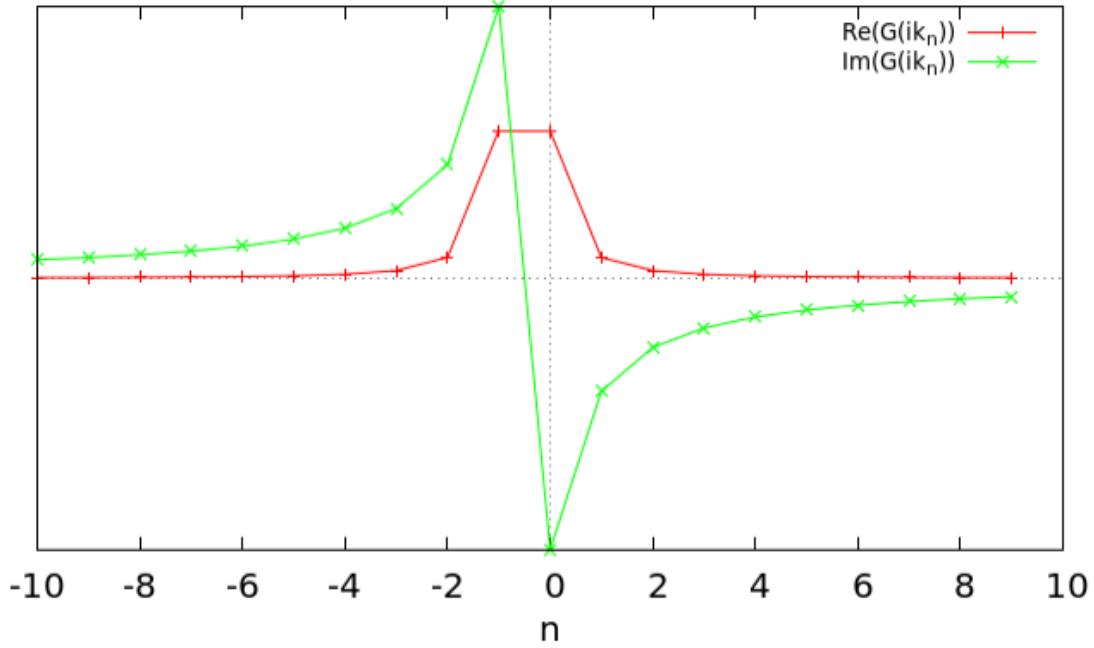


Figure 3.2: Qualitative form of an arbitrary Matsubara Green's function  $G(\vec{k}, ik_n)$  for a given  $\vec{k}$ . The red line shows the real part that is symmetric under  $n \rightarrow -n-1$  and the imaginary part (green line) that exhibits antisymmetry.

$$\lim_{\tau \rightarrow 0^-} \sum_n \frac{e^{ik_n \tau}}{ik_n - \xi_{\vec{k}}} = f(\xi_{\vec{k}}). \quad (3.59)$$

In practical (numerical) calculations one has to sum over Matsubara frequencies which is discussed in appendix A.

However, the symmetry of the Matsubara Green's functions  $G_0(\vec{k}, ik_n)$  and  $G(\vec{k}, ik_n)$  that follows directly from the definition of the Matsubara frequencies  $k_n$  is shown in Fig. 3.2:

$$G_0(\vec{k}, ik_n) = G_0^*(\vec{k}, ik_{-n-1}). \quad (3.60)$$

### 3.4.3. Relation between the retarded Green's function $G^R$ and the Matsubara Green's function $G$

We will now find the relationship between the retarded Green's function  $G^R(\vec{r}, \vec{r}'; t)$  and the Matsubara Green's function  $G(\vec{r}, \vec{r}'; \tau)$  where we will use  $\tau > 0$ ,

$$\begin{aligned} G(\vec{r}, \vec{r}'; ik_n) &= \int_0^\beta d\tau e^{ik_n \tau} G(\vec{r}, \vec{r}'; \tau) \quad |3.45 \\ &= \int_0^\beta d\tau e^{ik_n \tau} [-\langle \Psi(\vec{r}, \tau) \Psi^\dagger(\vec{r}', 0) \rangle \Theta(\tau) + \langle \Psi^\dagger(\vec{r}', 0) \Psi(\vec{r}, \tau) \rangle \Theta(-\tau)] \\ &= \int_0^\beta d\tau e^{ik_n \tau} [-\langle \Psi(\vec{r}, \tau) \Psi^\dagger(\vec{r}', 0) \rangle]. \end{aligned} \quad (3.61)$$

The integration  $\int d\tau$  is merely along the imaginary axis since  $\tau = it!$  We will assume that  $k_n > 0$  (otherwise we do the following steps in the mirrored plane). Since  $G(\vec{r}, \vec{r}'; \tau)$  is analytic in the whole semi-plane  $\text{Im}(\tau) \in (0, \beta)$  the integration can be performed over an arbitrary path as long as the end points are fixed (follows from the residual theorem). We will choose the path in the complex plane  $(\text{Re}(z), \text{Im}(z))$ :  $(0, 0) \xrightarrow{1} (\infty, 0) \xrightarrow{2} (\infty, \beta) \xrightarrow{3} (0, \beta)$ .

$$\text{path 1} = \int_{t=0}^{t=\infty} d(it) e^{ik_n it} [-\langle e^{iKt} \Psi(\vec{r}) e^{-iKt} \Psi^\dagger(\vec{r}') \rangle] \quad (3.62)$$

$$\begin{aligned} \text{path 2} &= \int_{\tau=0}^{\tau=\infty} d\tau e^{-\infty} [-\langle e^{K\tau} \Psi(\vec{r}) e^{-K\tau} \Psi^\dagger(\vec{r}') \rangle] \\ &= 0 \end{aligned} \quad (3.63)$$

$$\text{path 3} = \int_{t=\infty}^{t=0} d(it) e^{ik_n i(t-\beta)} [-\langle e^{iK(t-i\beta)} \Psi(\vec{r}) e^{-iK(t-i\beta)} \Psi^\dagger(\vec{r}') \rangle]. \quad (3.64)$$

Putting all paths together and using the definition of the fermionic Matsubara frequencies (Def. 3.49), i.e.  $e^{ik_n \beta} = -1$ , one gets

$$\begin{aligned} G(\vec{r}, \vec{r}'; ik_n) &= \int_{t=0}^{t=\infty} d(it) e^{ik_n it} [-\langle e^{iKt} \Psi(\vec{r}) e^{-iKt} \Psi^\dagger(\vec{r}') \rangle] \\ &+ \int_{t=0}^{t=\infty} d(it) e^{ik_n it} [-\langle e^{K\beta} e^{iKt} \Psi(\vec{r}) e^{-iKt} e^{-\beta K} \Psi^\dagger(\vec{r}') \rangle] \\ &= \int_{t=0}^{t=\infty} d(it) e^{ik_n it} [-\langle \Psi(\vec{r}, t) \Psi^\dagger(\vec{r}', 0) \rangle] \\ &+ \int_{t=0}^{t=\infty} d(it) e^{ik_n it} \left[ -\frac{\text{tr}(e^{-K\beta} e^{K\beta} e^{iKt} \Psi(\vec{r}) e^{-iKt} e^{-\beta K} \Psi^\dagger(\vec{r}'))}{\text{tr}(e^{-\beta K})} \right] \\ &= \int_{t=0}^{t=\infty} d(it) e^{ik_n it} [-\langle \Psi(\vec{r}, t) \Psi^\dagger(\vec{r}', 0) \rangle] \\ &+ \int_{t=0}^{t=\infty} d(it) e^{ik_n it} \left[ -\frac{\text{tr}(e^{-K\beta} \Psi^\dagger(\vec{r}') e^{iKt} \Psi(\vec{r}) e^{-iKt})}{\text{tr}(e^{-\beta K})} \right] \\ &= \int_{t=0}^{t=\infty} d(it) e^{ik_n it} [-\langle \Psi(\vec{r}, t) \Psi^\dagger(\vec{r}', 0) \rangle] \\ &+ \int_{t=0}^{t=\infty} d(it) e^{ik_n it} \left[ -\frac{\text{tr}(e^{-K\beta} \Psi^\dagger(\vec{r}', 0) \Psi(\vec{r}, t))}{\text{tr}(e^{-\beta K})} \right] \\ &= \int_{t=0}^{t=\infty} d(it) e^{ik_n it} [-\langle \Psi(\vec{r}, t) \Psi^\dagger(\vec{r}', 0) + \Psi^\dagger(\vec{r}', 0) \Psi(\vec{r}, t) \rangle] \\ &= -i \int_0^\infty dt e^{ik_n it} \langle \{ \Psi(\vec{r}, t), \Psi^\dagger(\vec{r}', 0) \} \rangle \quad |3.38 \\ &= \int_{-\infty}^\infty \frac{d\omega'}{2\pi} \frac{A(\vec{r}, \vec{r}'; \omega')}{ik_n - \omega'}. \end{aligned} \quad (3.65)$$

Comparing with the expression for the retarded Green's function (Eq. 3.38) we see that an analytic continuation can be performed by  $ik_n \rightarrow \omega + i\eta$  where  $\eta \leq 0$  since  $k_n \leq 0$  was assumed.

$$G^R(\vec{r}, \vec{r}'; \omega) = \lim_{ik_n \rightarrow \omega + i\eta} G(\vec{r}, \vec{r}'; ik_n). \quad (3.66)$$

### 3.4.4. Analytical continuation

The problem of finding an analytic continuation  $G^R(\vec{r}, \vec{r}'; \omega)$  from the Matsubara Green's function on discrete points  $G(\vec{r}, \vec{r}'; ik_n)$  consists in having various possible solutions. Baym and Mermin [7] were able to show that a well-defined analytic continuation exists if one considers the high frequency limits. The resulting analytic continuation is

$$G^R(\vec{r}, \vec{r}'; \omega) = \lim_{ik_n \rightarrow \omega + i\eta} G(\vec{r}, \vec{r}'; ik_n). \quad (3.67)$$

Even if this expression seems very easy it is numerically very hard to process.

Approximate methods like the Padé approximation [8],[9], the Maximum Entropy Method [10], the Stochastic analytic continuation [11] and many others try to tackle this problem.

In this work, we use the Padé approximation or the Stochastic analytic continuation depending on the quality of the output since both have sometimes unnegligible disadvantages.

#### Padé approximation

Starting point of the Padé approximation for analytic continuation is the representation of a complex function  $f : D \rightarrow D'$ , where  $D$  and  $D'$  are domains in  $\mathbb{C}$ , as a continued fraction

$$f(z) = \frac{a_1}{1 + \frac{a_2(z-z_1)}{1+\dots}}, \quad (3.68)$$

where  $a_i, z_i \in \mathbb{C} \forall i \in [1, \infty)$  and the approximation consists of determining an approximate function  $\tilde{f}$  where one determines  $a_1, \dots, a_N, N \in \mathbb{N}$ , by enforcing  $\tilde{f}(z_i) = u_i, \forall i \in [1, \dots, N]$ , for a given set of points  $u_i$  at  $z_i$ , i.e.

$$f(z) \approx \tilde{f}(z) = \frac{a_1}{1 + \frac{a_2(z-z_1)}{1+\dots+a_N(z-z_{N-1})}}. \quad (3.69)$$

As one can already imagine, this procedure is limited by the convergence of the series and the number of sampling points.

#### Stochastic analytic continuation

Different to the Padé approximation one starts the other way round with a physical spectral weight on the real axis that is correctly normalized and strictly positive. To get the corresponding complex function on the imaginary axis one has to perform a Hilbert transformation. The agreement with the input data is then checked by the squared deviation between both functions at the given points. This procedure is then repeated where the generated spectra on the real axis are treated by a Monte-Carlo approach and the spectra get finally averaged if the fit is good but not perfect. Excluding perfect fits is due to small numerical errors that might lead to unphysical features.

A small example for both kinds of analytic continuations is given in Fig. 3.3 where the spectral weight  $A(\omega)$  (Eq. 3.43) from the  $\vec{k}$ -averaged non-interacting Green's function  $G_0^R(\omega)$  (Eq. 3.41) are compared.

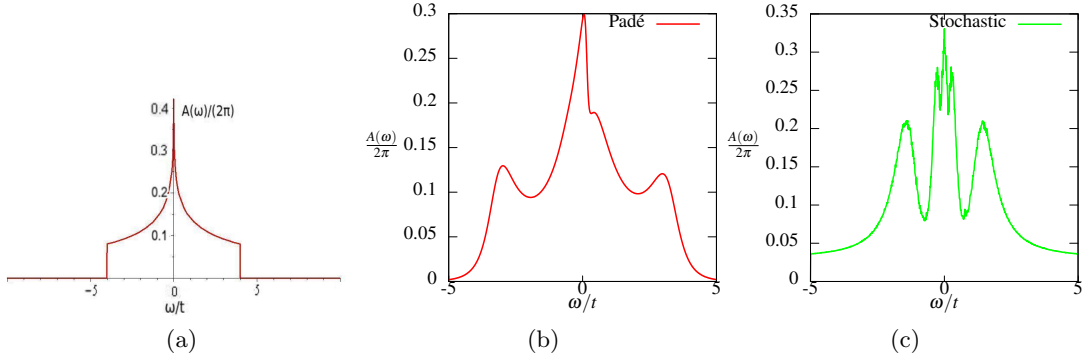


Figure 3.3: (a) The exact normalized spectral weight  $A(\omega)$  that was calculated analytically in Eq. 3.43. In (b) we show the solution of the Padé approximation that is not able to reproduce the divergencies at  $\omega/t = 0, \pm 4$  due to the polynomial expansion and has a small dip at  $\omega/t \approx 0.5$  which is a typical error of the Padé approximation. The Stochastic analytic continuation shows important deficiencies due to the divergencies but preserves the reflection symmetry more accurately. Moreover, it shows the usual noise from the Monte Carlo simulation.

### 3.5. Interacting Green's function and self-energy

#### 3.5.1. The functional derivative formalism

In 1959, P. C. Martin and J. Schwinger [12] presented a formalism that introduces artificial source fields to calculate correlation functions from functionals of these fields. Firstly, we define our source field  $\phi$  in the following way

$$\phi(1, 2) \equiv \phi_{\sigma, \sigma'}(\vec{r}, \tau; \vec{r}', \tau') \quad (3.70)$$

since we want to couple  $\Psi^\dagger(1)$  and  $\Psi(2)$  to calculate the Matsubara Green's function  $G_\phi$  that will depend on the source field.

The generating function is simply the partition function

$$\begin{aligned} Z[\phi] &\equiv \left\langle T_\tau e^{-\Psi^\dagger(\bar{1})\phi(\bar{1}, \bar{2})\Psi(\bar{2})} \right\rangle \\ &= \text{tr} \left[ e^{-\beta H} T_\tau e^{-\Psi^\dagger(\bar{1})\phi(\bar{1}, \bar{2})\Psi(\bar{2})} \right] \\ &\equiv \text{tr} \left[ e^{-\beta H} T_\tau S[\phi] \right]. \end{aligned} \quad (3.71)$$

Now, we can calculate  $G_\phi$  by the following functional derivative

$$\begin{aligned} -\frac{\delta \ln Z[\phi]}{\delta \phi(2, 1)} &= -\frac{1}{Z[\phi]} \text{tr} \left[ e^{-\beta H} T_\tau e^{-\Psi^\dagger(\bar{1})\phi(\bar{1}, \bar{2})\Psi(\bar{2})} \frac{\delta}{\delta \phi(2, 1)} \left( -\Psi^\dagger(\bar{1})\phi(\bar{1}, \bar{2})\Psi(\bar{2}) \right) \right] \\ &= -\frac{1}{Z[\phi]} \text{tr} \left[ e^{-\beta H} T_\tau e^{-\Psi^\dagger(\bar{1})\phi(\bar{1}, \bar{2})\Psi(\bar{2})} \left( -\Psi^\dagger(\bar{1})\delta(\bar{1} - 2)\Psi(\bar{2})\delta(\bar{2} - 1) \right) \right] \\ &= -\frac{1}{Z[\phi]} \text{tr} \left[ e^{-\beta H} T_\tau e^{-\Psi^\dagger(\bar{1})\phi(\bar{1}, \bar{2})\Psi(\bar{2})} \left( -\Psi^\dagger(2)\Psi(1) \right) \right] \\ &= -\frac{1}{Z[\phi]} \text{tr} \left[ e^{-\beta H} T_\tau e^{-\Psi^\dagger(\bar{1})\phi(\bar{1}, \bar{2})\Psi(\bar{2})} \Psi(1)\Psi^\dagger(2) \right] \end{aligned}$$

$$\begin{aligned}
 &= -\frac{\langle T_\tau S[\phi] \Psi(1) \Psi^\dagger(2) \rangle}{\langle T_\tau S[\phi] \rangle} \\
 &\equiv -\left\langle T_\tau \Psi(1) \Psi^\dagger(2) \right\rangle_\phi \\
 &\equiv G(1, 2)_\phi.
 \end{aligned} \tag{3.72}$$

In the limit  $\phi \rightarrow 0$  one recovers the previous Matsubara Green's function (Def. 3.45) since  $e^0 = \mathbb{I}$ . At this point, we will derive a compute order derivative that will be needed later,

$$\begin{aligned}
 \frac{\delta G(1, 2)_\phi}{\delta \phi(3, 4)} &= \frac{\langle T_\tau S[\phi] \Psi(1) \Psi^\dagger(2) \Psi^\dagger(3) \Psi(4) \rangle}{\langle T_\tau S[\phi] \rangle} - \frac{\langle T_\tau S[\phi] \Psi(1) \Psi^\dagger(2) \rangle \langle T_\tau S[\phi] \Psi^\dagger(3) \Psi(4) \rangle}{\langle T_\tau S[\phi] \rangle^2} \\
 &= \langle T_\tau \Psi(1) \Psi^\dagger(2) \Psi^\dagger(3) \Psi(4) \rangle_\phi + G(1, 2)_\phi G(4, 3)_\phi.
 \end{aligned} \tag{3.73}$$

The next step is evaluating the equation of motion for the generalized Green's function  $G_\phi$ .

At this point the form of the Hamiltonian plays a key role and we will use the Hubbard model from Eq. 2.1 where we sum over all  $i, j$ . Later, one can put the matrix elements  $t_{ij}$  to zero that do not connect neighboring sites.

To do this, one has to calculate the following terms that will appear later:

$$\begin{aligned}
 \frac{\partial c_{k,\sigma}(\tau)}{\partial \tau} &= [H, c_{k,\sigma}] \\
 &= \sum_{ij,\sigma'} [t_{ij} c_{i,\sigma'}^\dagger c_{j,\sigma'}, c_{k,\sigma}] + U \sum_i [c_{i,\uparrow}^\dagger c_{i,\uparrow} c_{i,\downarrow}^\dagger c_{i,\downarrow}, c_{k,\sigma}] - \mu \sum_i [n_i, c_{k,\sigma}].
 \end{aligned} \tag{3.74}$$

Using

$$[AB, C] = A\{B, C\} - B\{A, C\} \tag{3.75}$$

$$[AB, C] = [A, C]B + A[B, C] \tag{3.76}$$

one can continue

$$\begin{aligned}
 \frac{\partial c_{k,\sigma}(\tau)}{\partial \tau} &= \sum_{ij,\sigma'} t_{ij} \left( c_{i,\sigma'}^\dagger \{c_{j,\sigma'}, c_{k,\sigma}\} - c_{j,\sigma'} \{c_{i,\sigma'}^\dagger, c_{k,\sigma}\} \right) \\
 &\quad + U \sum_i ([n_{i,\uparrow}, c_{k,\sigma}] n_{i,\downarrow} + n_{i,\uparrow} [n_{i,\downarrow}, c_{k,\sigma}]) \\
 &\quad + \mu c_{k,\sigma} \\
 &= -\sum_j t_{kj} c_{j\sigma} - U c_{k\sigma} \delta_{\sigma,\uparrow} n_{k,\downarrow} - U n_{k\uparrow} c_{k\sigma} \delta_{\sigma,\downarrow} + \mu c_{k,\sigma} \\
 &= -\sum_j t_{kj} c_{j\sigma} - U n_{k,-\sigma} c_{k\sigma} + \mu c_{k,\sigma}
 \end{aligned} \tag{3.77}$$

and finally calculate from Eq. 3.72

$$\begin{aligned}
 \frac{\partial G(1, 2)}{\partial \tau_1} &= \sum_j t_{1j} G(\vec{r}_j - \vec{r}_2; \tau_1 - \tau_2)_\phi + U \left\langle T_\tau c_{-\sigma}^\dagger(1^+) c_{-\sigma}(1) c_\sigma(1) c_\sigma^\dagger(2) \right\rangle_\phi + \mu G(1, 2)_\phi \\
 &\quad - \delta(1 - 2) \\
 &\quad - \phi(1, \bar{2}) G(\bar{2}, 2)_\phi,
 \end{aligned} \tag{3.78}$$

where the first line originates from Eq. 3.77, the second from the time derivative of  $\Theta(\tau_1 - \tau_2)$  and  $\Theta(\tau_2 - \tau_1)$  - implicitly hidden in the time ordering operator - and the last line from  $S[\phi]$  since the integral in the exponential has to be also time ordered: In this case the integral will split into  $\int_0^\beta = \int_0^{\tau_1} + \int_{\tau_1}^\beta$ . The appearing superscript  $+$  is just an aid to the reader that the operators are already in the right time order, i.e. every  $+$  is an additional infinitesimal positive shift in imaginary time. Furthermore, one defines

$$G_0^{-1}(1, 2)_\phi \equiv - \sum_j \left[ \delta(\vec{r}_j - \vec{r}_2) \delta(\tau_1 - \tau_2) \left( \left( \frac{\partial}{\partial \tau_1} - \mu \right) \delta_{j,1} - t_{1j} \right) \right] \quad (3.79)$$

that consequently gives

$$G_0^{-1}(1, \bar{2})_\phi G(\bar{2}, 2)_\phi = - \left[ \sum_j \left( \left( \frac{\partial}{\partial \tau_1} - \mu \right) \delta_{j,1} - t_{1j} \right) \right] G(\vec{r}_j - \vec{r}_2, \tau_1 - \tau_2)_\phi. \quad (3.80)$$

Now, we are able to rearrange the equation of motion for the Green's function  $G(1, 2)_\phi$  (Eq. 3.78) and get

$$\begin{aligned} (G_0^{-1}(1, \bar{2})_\phi - \phi(1, \bar{2})) G(\bar{2}, 2)_\phi &= \delta(1 - 2) \\ &- U \left\langle T_\tau c_{-\sigma}^\dagger(1^+) c_{-\sigma}(1) c_\sigma(1) c_\sigma^\dagger(2) \right\rangle_\phi. \end{aligned} \quad (3.81)$$

Noticing the  $\delta$ -function on the right-hand side it is not very difficult to recover the Dyson equation

$$G^{-1}(1, 2)_\phi = G_0^{-1}(1, 2)_\phi - \phi(1, 2) - \Sigma(1, 2)_\phi \quad | * G(\bar{2}, 2)_\phi \quad (3.82)$$

$$\delta(1 - 2) = (G_0^{-1}(1, \bar{2})_\phi - \phi(1, \bar{2}) - \Sigma(1, \bar{2})_\phi) G(\bar{2}, 2)_\phi \quad (3.83)$$

$$\stackrel{3.81}{\implies} \Sigma(1, \bar{2})_\phi G(\bar{2}, 2)_\phi = -U \left\langle T_\tau c_{-\sigma}^\dagger(1^+) c_{-\sigma}(1) c_\sigma(1) c_\sigma^\dagger(2) \right\rangle_\phi \quad | 3.73 \quad (3.84)$$

$$\Sigma_\sigma(1, \bar{2})_\phi G_\sigma(\bar{2}, 2)_\phi = -U \left[ \frac{\delta G_\sigma(1, 2)_\phi}{\delta \phi_{-\sigma}(1^+, 1)} - G_{-\sigma}(1, 1^+)_\phi G_\sigma(1, 2)_\phi \right]. \quad (3.85)$$

Since we have a lot of integrations and summations to perform in the following, we will introduce the following matrix notation

$$AB \equiv A(1, \bar{2})B(\bar{2}, 2) \quad (3.86)$$

$$A \wedge B \equiv A(1, 2)B(3, 4) \quad (3.87)$$

One finds a different way of expressing  $\frac{\delta G}{\delta \phi}$  by starting from the simple equation

$$\delta(1 - 2) = G_\sigma(1, \bar{2})G_\sigma^{-1}(\bar{2}, 2) \quad \left| \frac{\delta}{\delta \phi_{\sigma'}(3, 4)} \right. \quad (3.88)$$

$$0 = \frac{\delta G_\sigma}{\delta \phi_{\sigma'}} G_\sigma^{-1} + G_\sigma \frac{\delta G_\sigma^{-1}}{\delta \phi_{\sigma'}} \quad (3.89)$$

$$\frac{\delta G_\sigma}{\delta \phi_{\sigma'}} = -G_\sigma \frac{\delta G_\sigma^{-1}}{\delta \phi_{\sigma'}} G_\sigma \quad | 3.82 \quad (3.90)$$

$$= -G_\sigma \frac{\delta G_{0,\sigma}^{-1}}{\delta \phi_{\sigma'}} G_\sigma + G_\sigma \frac{\delta \phi_\sigma}{\delta \phi_{\sigma'}} G_\sigma + G_\sigma \frac{\delta \Sigma_\sigma}{\delta \phi_{\sigma'}} G_\sigma$$

$$= G_\sigma \wedge G_\sigma \delta_{\sigma,\sigma'} + G_\sigma \frac{\delta \Sigma_\sigma}{\delta \phi_{\sigma'}} G_\sigma. \quad (3.91)$$

A Legendre transformation of  $\ln(Z[\phi])$  (Eq. 3.71) gives the so-called Luttinger-Ward functional  $\Phi[G]$  that is a functional of  $G$  [13]. It was shown [14] that perturbation theory in the not strongly interacting regime converges and since this is the domain of TPSC we will use the Luttinger-Ward functional  $\Phi[G]$ .

The Legendre transformation allows us to express the self-energy  $\Sigma$  as a functional of  $G$  and one can use the chain rule to rewrite 3.91

$$\frac{\delta G_\sigma}{\delta \phi_{\sigma'}} = G_\sigma \wedge G_\sigma \delta_{\sigma,\sigma'} + G_\sigma \left[ \frac{\delta \Sigma_\sigma}{\delta G_\sigma} \frac{\delta G_\sigma}{\delta \phi_{\sigma'}} \right] G_\sigma \quad (3.92)$$

$$\begin{aligned} \frac{\delta G_\sigma(1, 2)_\phi}{\delta \phi_{\sigma'}(3, 4)} &= G_\sigma(1, 3)_\phi G_\sigma(4, 2)_\phi \delta_{\sigma,\sigma'} \\ &+ G_\sigma(1, \bar{5})_\phi \left[ \frac{\delta \Sigma_\sigma(\bar{5}, \bar{6})_\phi}{\delta G_\sigma(\bar{7}, \bar{8})_\phi} \frac{\delta G_\sigma(\bar{7}, \bar{8})_\phi}{\delta \phi_{\sigma'}(3, 4)} \right] G_\sigma(\bar{6}, 2)_\phi. \end{aligned} \quad (3.93)$$

So far, we found an equation for the self-energy that is consistent with the Dyson equation and bears no approximations so far.

The next section shows how to introduce generalized susceptibilities and connect them with the self-energy.

### 3.5.2. Spin and charge susceptibilities

The spin  $S^z(1)$  and charge  $n(1)$  are defined as

$$S^z(1) \equiv n_\uparrow(1) - n_\downarrow(1) \quad (3.94)$$

$$n(1) \equiv n_\uparrow(1) + n_\downarrow(1). \quad (3.95)$$

Those can be identified in the functional derivative of  $G_\phi$  given in Eq. 3.73 as

$$\begin{aligned} -\frac{\delta G_\sigma(1, 1^+)_\phi}{\delta \phi_{\sigma'}(2^+, 2)} &= -\langle T_\tau \Psi_\sigma(1) \Psi_\sigma^\dagger(1^+) \Psi_{\sigma'}^\dagger(2^+) \Psi_{\sigma'}(2) \rangle_\phi - G_\sigma(1, 1^+)_\phi G_{\sigma'}(2, 2^+)_\phi \\ &= \langle T_\tau \Psi_\sigma^\dagger(1^+) \Psi_\sigma(1) \Psi_{\sigma'}^\dagger(2^+) \Psi_{\sigma'}(2) \rangle_\phi - G_\sigma(1, 1^+)_\phi G_{\sigma'}(2, 2^+)_\phi \\ &= \langle T_\tau n_\sigma(1) n_{\sigma'}(2) \rangle_\phi - \langle n_\sigma(1) \rangle_\phi \langle n_{\sigma'}(2) \rangle_\phi \end{aligned} \quad (3.96)$$

Remembering the ideas of Sec. 3.1 we define the charge susceptibility  $\chi_{ch}$

$$\boxed{\chi_{ch}(1, 2)_\phi \equiv \langle T_\tau n(1) n(2) \rangle_\phi - \langle n(1) \rangle_\phi \langle n(2) \rangle_\phi} \quad (3.97)$$

and already see

$$\chi_{ch}(1, 2)_\phi = -\sum_{\sigma, \sigma'} \frac{\delta G_\sigma(1, 1^+)_\phi}{\delta \phi_{\sigma'}(2^+, 2)}, \quad (3.98)$$

when we sum all spin up and spin down terms and use the definition of the charge  $n(1)$ . In the case of the spin susceptibility  $\chi_{sp}$  we are dealing with terms like

$$(n_\uparrow(1) - n_\downarrow(1))(n_\uparrow(2) - n_\downarrow(2)) \quad (3.99)$$

and have therefore negative signs when different spins are multiplied. Similarly, we define the spin susceptibility

$$\boxed{\chi_{sp}(1, 2)_\phi \equiv \langle T_\tau S^z(1) S^z(2) \rangle_\phi - \langle S^z(1) \rangle_\phi \langle S^z(2) \rangle_\phi}, \quad (3.100)$$

where

$$\chi_{sp} = - \sum_{\sigma, \sigma'} \sigma * \sigma' * \frac{\delta G_\sigma(1, 1^+)_\phi}{\delta \phi_{\sigma'}(2^+, 2)}. \quad (3.101)$$

Since the Hubbard Hamiltonian (Eq. 2.1) is spin-rotational invariant we can calculate

$$\begin{aligned} \chi_{ch} &= - \sum_{\sigma, \sigma'} \frac{\delta G_\sigma}{\delta \phi_{\sigma'}} \quad |3.92 \\ &= - \sum_{\sigma, \sigma'} \left( G_\sigma \wedge G_\sigma \delta_{\sigma, \sigma'} + G_\sigma \left[ \frac{\delta \Sigma_\sigma}{\delta G_{\bar{\sigma}}} \frac{\delta G_{\bar{\sigma}}}{\delta \phi_{\sigma'}} \right] G_\sigma \right) \\ &= -2G \wedge G - G \left[ \sum_{\sigma, \sigma''} \frac{\delta \Sigma_\sigma}{\delta G_{\sigma''}} \sum_{\sigma'} \frac{\delta G_{\sigma''}}{\delta \phi_{\sigma'}} \right] G \\ &= -2G \wedge G - G \left[ \sum_{\sigma} \frac{\delta \Sigma_\sigma}{\delta G} \sum_{\sigma', \sigma''} \frac{\delta G_{\sigma''}}{\delta \phi_{\sigma'}} \right] G \\ &= -2G \wedge G + G \left[ \sum_{\sigma} \frac{\delta \Sigma_\sigma}{\delta G} \chi_{ch} \right] G \\ &\equiv -2G \wedge G + G [U_{ch} \chi_{ch}] G. \end{aligned} \quad (3.102)$$

The function  $U_{ch}$  is called *irreducible charge vertex* and will be analyzed later. To compute  $\chi_{sp}$  we need the following consideration where one again uses spin rotational invariance

$$\begin{aligned} \sum_{\sigma} \sigma * \sigma' * \frac{\delta \Sigma_\sigma}{\delta G_{\sigma'}} &= \sigma' * \left( \frac{\delta \Sigma_\uparrow}{\delta G_{\sigma'}} - \frac{\delta \Sigma_\downarrow}{\delta G_{\sigma'}} \right) \\ &= \begin{cases} \left( \frac{\delta \Sigma_\uparrow}{\delta G_\uparrow} - \frac{\delta \Sigma_\downarrow}{\delta G_\uparrow} \right), & \text{for } \sigma' = 1 \\ \left( \frac{\delta \Sigma_\downarrow}{\delta G_\downarrow} - \frac{\delta \Sigma_\uparrow}{\delta G_\downarrow} \right), & \text{for } \sigma' = -1 \end{cases} \\ &= \left( \frac{\delta \Sigma_\uparrow}{\delta G_\uparrow} - \frac{\delta \Sigma_\downarrow}{\delta G_\uparrow} \right) \end{aligned} \quad (3.103)$$

and therefore

$$\begin{aligned} \chi_{sp} &= - \sum_{\sigma, \sigma'} \sigma * \sigma' \frac{\delta G_\sigma}{\delta \phi_{\sigma'}} \quad |3.92 \\ &= -2G \wedge G - G \left[ \sum_{\sigma, \sigma''} \sigma * 1 * \frac{\delta \Sigma_\sigma}{\delta G_{\sigma''}} \sum_{\sigma'} \frac{\delta G_{\sigma''}}{\delta \phi_{\sigma'}} * \sigma' \right] G \end{aligned}$$

$$\begin{aligned}
 &= -2G \wedge G - G \left[ \sum_{\sigma, \sigma''} \sigma * (\sigma'')^2 * \frac{\delta \Sigma_{\sigma}}{\delta G_{\sigma''}} \sum_{\sigma'} \frac{\delta G_{\sigma''}}{\delta \phi_{\sigma'}} * \sigma' \right] G \\
 &= -2G \wedge G - G \left[ \sum_{\sigma''} \sum_{\sigma} \left( \sigma * \frac{\delta \Sigma_{\sigma}}{\delta G_{\sigma''}} * \sigma'' \right) \sum_{\sigma'} \sigma'' * \frac{\delta G_{\sigma''}}{\delta \phi_{\sigma'}} * \sigma' \right] G \quad |3.103 \\
 &= -2G \wedge G - G \left[ \left( \frac{\delta \Sigma_{\uparrow}}{\delta G_{\uparrow}} - \frac{\delta \Sigma_{\downarrow}}{\delta G_{\uparrow}} \right) \sum_{\sigma', \sigma''} \sigma'' * \frac{\delta G_{\sigma''}}{\delta \phi_{\sigma'}} * \sigma' \right] G \\
 &= -2G \wedge G - G \left[ \left( \frac{\delta \Sigma_{\uparrow}}{\delta G_{\uparrow}} - \frac{\delta \Sigma_{\downarrow}}{\delta G_{\uparrow}} \right) \chi_{sp} \right] G \\
 &\equiv -2G \wedge G - G [U_{sp} \chi_{sp}] G. \quad (3.104)
 \end{aligned}$$

Similarly,  $U_{sp}$  is called *irreducible spin vertex*.

Up to this point we have only used symmetries, the form of the Hamiltonian and limited ourselves to weak and intermediate interaction strengths. Nevertheless, it is very hard to continue now and approximations will be needed to find physically relevant solutions.

But what was presented so far is all we need to derive RPA and afterwards TPSC.

## 4. Two-Particle Self-Consistent approach and Random Phase Approximation

### 4.1. Sum rules

The starting point for TPSC in this thesis will be two sum rules which can be directly derived from the simplest form of Pauli principle ( $\langle n_\sigma^2 \rangle = \langle n_\sigma \rangle$ ) taking advantage of paramagnetism  $\langle n_\downarrow \rangle = \langle n_\uparrow \rangle = \langle n \rangle / 2$ :

$$\begin{aligned} \langle S^z(0^+)S^z(0) \rangle - \langle S^z(0) \rangle \langle S^z(0) \rangle &= \langle (n_\uparrow - n_\downarrow)^2 \rangle - 0 \\ &= \langle n_\uparrow^2 \rangle + \langle n_\downarrow^2 \rangle - 2\langle n_\uparrow n_\downarrow \rangle \\ &\stackrel{Pauli}{=} n - 2\langle n_\uparrow n_\downarrow \rangle \end{aligned} \quad (4.1)$$

$$\begin{aligned} \langle \rho(0^+)\rho(0) \rangle - n^2 &= \langle (n_\uparrow + n_\downarrow)^2 \rangle - n^2 \\ &= \langle n_\uparrow^2 \rangle + \langle n_\downarrow^2 \rangle + 2\langle n_\uparrow n_\downarrow \rangle - n^2 \\ &\stackrel{Pauli}{=} n + 2\langle n_\uparrow n_\downarrow \rangle - n^2. \end{aligned} \quad (4.2)$$

Having a close look on the left-hand side of the equations and making use of translational invariance we find sums over the spin susceptibility  $\chi_{sp}(0, 0^+)$  (Eq. 3.104) and the charge susceptibility,  $\chi_{ch}(0, 0^+)$  (Eq. 3.102):

$$\begin{aligned} \langle S^z(0^+)S^z(0) \rangle - \langle S^z(0) \rangle \langle S^z(0) \rangle &= \chi_{sp}(0, 0^+) \\ &= \frac{1}{N} \sum_{\vec{q}} e^{i\vec{q}\cdot\vec{0}} \chi_{sp}(\vec{q}, 0^+) \\ &= \frac{T}{N} \sum_{\vec{q}, iq_n} e^{iq_n \cdot 0^+} \chi_{sp}(\vec{q}, iq_n). \end{aligned} \quad (4.3)$$

$$\stackrel{4.1}{\Rightarrow} \frac{T}{N} \sum_{\vec{q}, iq_n} \chi_{sp}(\vec{q}, iq_n) = n - 2\langle n_\uparrow n_\downarrow \rangle \quad : \text{ local spin sum rule} \quad (4.4)$$

$$\langle \rho(0^+)\rho(0) \rangle - n^2 = \chi_{ch}(0, 0^+) \quad (4.5)$$

$$\stackrel{4.2}{\Rightarrow} \frac{T}{N} \sum_{\vec{q}, iq_n} \chi_{ch}(\vec{q}, iq_n) = n + 2\langle n_\uparrow n_\downarrow \rangle - n^2 \quad : \text{ local charge sum rule} \quad (4.6)$$

As can be seen from the derivation of the two sum rules these equations are strict and serve in this work as direct representation of the Pauli principle. Thereupon, they will play a crucial role in the self-consistency of TPSC.

### 4.2. The Random Phase Approximation (RPA)

In 1953 [15], Bohm and Pines published a new method to treat the Coulomb interaction of a dense electron gas.

The key ideas became known as Random Phase Approximation (RPA) that are applied in this chapter to the Hubbard Hamiltonian. To derive the RPA susceptibilities we start from the defining equation for the self-energy (Eq. 3.85) and use the Hartree-Fock approximation, i.e.

$$\Sigma_\sigma(1, \bar{2})_\phi G_\sigma(\bar{2}, 2)_\phi = -U \left[ \frac{\delta G_\sigma(1, 2)_\phi}{\delta \phi_{-\sigma}(1^+, 1)} - G_{-\sigma}(1, 1^+)_\phi G_\sigma(1, 2)_\phi \right]$$

$$\approx UG_{-\sigma}(1, 1^+)_{\phi}G_{\sigma}(1, 2)_{\phi} \quad | * (G_{\sigma}(\bar{2}, 2))^{-1} \quad (4.7)$$

$$\Sigma_{\sigma}(1, 2)_{\phi} = UG_{-\sigma}(1, 1^+)_{\phi}\delta(1 - 2). \quad (4.8)$$

Using the above equations one can calculate the functional derivations of the self-energy

$$\frac{\delta\Sigma_{\sigma}(1, 2)_{\phi}}{\delta G_{-\sigma}(3, 4)_{\phi}} = U\delta(1 - 2)\delta(3 - 1)\delta(4 - 2) \quad (4.9)$$

$$\frac{\delta\Sigma_{\sigma}(1, 2)_{\phi}}{\delta G_{\sigma}(3, 4)_{\phi}} = 0 \quad (4.10)$$

that can be used to calculate the irreducible vertices (Eq. 3.104, 3.102) and since the self-energy is merely a constant we can replace the Green's function  $G$  by the non-interacting Green's function  $G_0$  and get finally

$$\begin{aligned} \chi_{ch}^{RPA}(1, 2) &= 2\chi_0(1, 2) - U\chi_0(1, \bar{3})\chi_{ch}^{RPA}(\bar{3}, 2) \\ &= \frac{2\chi_0(1, 2)}{1 + U\chi_0(1, 2)} \end{aligned} \quad (4.11)$$

$$\xrightarrow{trans.inv.} \chi_{ch}^{RPA}(\vec{q}, iq_n) = \frac{2\chi_0(\vec{q}, iq_n)}{1 + U\chi_0(\vec{q}, iq_n)} \quad (4.12)$$

$$\begin{aligned} \chi_{sp}^{RPA}(1, 2) &= 2\chi_0(1, 2) + U\chi_0(1, \bar{3})\chi_{sp}^{RPA}(\bar{3}, 2) \\ &= \frac{2\chi_0(1, 2)}{1 - U\chi_0(1, 2)} \end{aligned} \quad (4.13)$$

$$\xrightarrow{trans.inv.} \chi_{sp}^{RPA}(\vec{q}, iq_n) = \frac{2\chi_0(\vec{q}, iq_n)}{1 - U\chi_0(\vec{q}, iq_n)}, \quad (4.14)$$

where we have defined the irreducible susceptibility

$$\chi_0(1, 2) \equiv -G_0(1, 2)G_0(2, 1), \quad (4.15)$$

$$\text{the Lindhard function} \quad (4.16)$$

$$\chi_0(\vec{q}, iq_n) = -\frac{1}{N\beta} \sum_{\vec{k}, ik_m} G_0(\vec{k}; ik_m)G_0(\vec{k} + \vec{q}; ik_m + iq_n) \quad (4.17)$$

$$= -\frac{1}{N} \sum_{\vec{k}} \frac{f(\xi_{\vec{k}}) - f(\xi_{\vec{k} + \vec{q}})}{iq_n - [\xi_{\vec{k} + \vec{q}} - \xi_{\vec{k}}]}. \quad (4.18)$$

and bosonic Matsubara frequencies

$$q_n = 2\pi nT. \quad (4.19)$$

Note that the irreducible vertices  $U_{sp}$  and  $U_{ch}$  are mere constants equal to  $U$ .

#### 4.2.1. Disadvantages of RPA

In this section we show two disadvantages of RPA that can serve as a motivation for TPSC.

##### (1) Violation of the Pauli principle

Adding the local spin sum rule (Eq. 4.4) and the local charge sum rule (Eq. 4.6) one

gets

$$\frac{T}{N} \sum_{\vec{q}, iq_n} (\chi_{sp}(\vec{q}, iq_n) + \chi_{ch}(\vec{q}, iq_n)) = 2n - n^2 \quad (4.20)$$

that can be expanded for small interactions  $U\chi_0$ :

$$\begin{aligned} & \frac{T}{N} \sum_{\vec{q}, iq_n} \left( \frac{2\chi_0(\vec{q}, iq_n)}{1 - U\chi_0(\vec{q}, iq_n)} + \frac{2\chi_0(\vec{q}, iq_n)}{1 + U\chi_0(\vec{q}, iq_n)} \right) \\ & \approx \frac{T}{N} \sum_{\vec{q}, iq_n} [2\chi_0(\vec{q}, iq_n)(1 + U\chi_0(\vec{q}, iq_n) + (U\chi_0(\vec{q}, iq_n))^2) + \\ & \quad + 2\chi_0(\vec{q}, iq_n)(1 - U\chi_0(\vec{q}, iq_n) + (U\chi_0(\vec{q}, iq_n))^2)] \\ & = \frac{T}{N} \sum_{\vec{q}, iq_n} \left( 2\chi_0(2 + 2(U\chi_0(\vec{q}, iq_n))^2) \right). \end{aligned} \quad (4.21)$$

Since the Lindhard-function is positive and real there is no way that the term  $\sim U^2$  can vanish.

But the above sum rule is also valid for the non-interacting case, i.e.  $U = 0$ , and violates therefore the Pauli principle with an  $\sim U^2$  growing error. Moreover, the situation gets worse when  $U = 1/\max_{\vec{q}, iq_n} \{\chi_0(\vec{q}, iq_n)\}$  and one hits the divergence of the spin susceptibility  $\chi_{sp}$  (Eq. 4.14). The result of the sum rule will not work and the numerical calculation gives random numbers (Fig. 4.4).

## (2) Phase transtion in 2D and Mermin-Wagner theorem

As was discussed in (1) the spin susceptibility can diverge and become negative ( $U \geq 1/\max_{\vec{q}, iq_n} \{\chi_0(\vec{q}, iq_n)\}$ ). Hence, the paramagnetic ground state is not stable anymore and leads to a phase transition (even in 2D) which is prohibited by the Mermin-Wagner theorem.

### 4.2.2. Starting point: $\text{tr}(\Sigma \mathbf{G})$

To obtain the equations of TPSC one starts from the universal equation for the self-energy  $\Sigma_\sigma(1, 2)_\phi$  (Eq. 3.85):

$$\Sigma_\sigma(1, \bar{2})_\phi G_\sigma(\bar{2}, 2)_\phi = -U \left[ \frac{\delta G_\sigma(1, 2)_\phi}{\delta \phi_{-\sigma}(1^+, 1)} - G_{-\sigma}(1, 1^+)_\phi G_\sigma(1, 2)_\phi \right] \quad | * G_\sigma^{-1}(\bar{2}, 2)_\phi \quad (4.22)$$

$$\begin{aligned} \Sigma_\sigma(1, 2)_\phi & = U G_{-\sigma}(1, 1^+)_\phi \delta(1 - 2) + U \frac{\delta G_\sigma(1, \bar{2})_\phi}{\delta \phi_{-\sigma}(1^+, 1)} G_\sigma^{-1}(\bar{2}, 2)_\phi \\ & = U n_{-\sigma} \delta(1 - 2) + U \frac{\delta G_\sigma(1, \bar{2})_\phi}{\delta \phi_{-\sigma}(1^+, 1)} G_\sigma^{-1}(\bar{2}, 2)_\phi. \end{aligned} \quad (4.23)$$

In contrast to the section about spin and charge susceptibilities (Sec. 3.5.2) where it was possible to draw connections between the spin susceptibility  $\chi_{sp}$ , the charge susceptibility  $\chi_{ch}$  and  $\frac{\delta G_\sigma(1, 1^+)_\phi}{\delta \phi_{\sigma'}(2^+, 2)}$  we are now dealing with  $\frac{\delta G_\sigma(1, 2)_\phi}{\delta \phi_{\sigma'}(1^+, 1)}$ .

So, it is necessary to introduce the generalized three-point susceptibilities

$$\chi_{\sigma,\sigma'}(1, 3; 2)_\phi \equiv -\frac{\delta G_\sigma(1, 3)}{\delta \phi_{\sigma'}(2^+, 2)}. \quad (4.24)$$

Nevertheless, one can repeat the same steps as in Sec. 3.5.2, i.e. using the functional derivative of the Green's function (Eq. 3.73) to evaluate the functional derivative of the self-energy and gets

$$\begin{aligned} \chi_{\sigma,\sigma'}(1, 3; 2)_\phi &= -G_\sigma(1, 2)_\phi G_\sigma(2, 3)_\phi \delta_{\sigma,\sigma'} \\ &+ G_\sigma(1, \bar{2})_\phi U_{ir,\sigma\bar{\sigma}}(\bar{2}, \bar{3}; \bar{4}, \bar{5}) \chi_{\bar{\sigma},\sigma'}(\bar{4}, \bar{5}; 2)_\phi G_\sigma(\bar{3}, 3)_\phi. \end{aligned} \quad (4.25)$$

Differently, one deals now with a generalized *irreducible vertex*  $U_{ir,\sigma\sigma'}$  that is defined as before but allows all combination of spins  $\sigma\sigma'$ :

$$U_{ir,\sigma\sigma'} \equiv \frac{\delta \Sigma_\sigma(1, 2)_\phi}{\delta G_{\sigma'}(3, 4)_\phi}. \quad (4.26)$$

In the second step one supposes spin-rotational invariance to decouple into symmetric and antisymmetric parts that correspond to the charge and spin susceptibility, respectively.

The final result has got exactly the same structure as before but more indices

$$\chi_{sp} \equiv 2(\chi_{\uparrow\uparrow} - \chi_{\downarrow\uparrow}) \quad (4.27)$$

$$U_{sp} \equiv U_{ir,\uparrow\uparrow} - U_{ir,\downarrow\uparrow} \quad (4.28)$$

$$\begin{aligned} \chi_{sp}(1, 3; 2)_\phi &= -2G(1, 2)_\phi G(2, 3)_\phi \\ &- G(1, \bar{2})_\phi [U_{sp}(\bar{2}, \bar{3}; \bar{4}, \bar{5}) \chi_{sp}(\bar{4}, \bar{5}; 2)_\phi] G(\bar{3}, 3)_\phi \end{aligned} \quad (4.29)$$

$$\chi_{ch} \equiv 2(\chi_{\uparrow\uparrow} + \chi_{\downarrow\uparrow}) \quad (4.30)$$

$$U_{ch} \equiv U_{ir,\uparrow\uparrow} + U_{ir,\downarrow\uparrow} \quad (4.31)$$

$$\begin{aligned} \chi_{ch}(1, 3; 2)_\phi &= -2G(1, 2)_\phi G(2, 3)_\phi \\ &+ G(1, \bar{2})_\phi [U_{ch}(\bar{2}, \bar{3}; \bar{4}, \bar{5}) \chi_{ch}(\bar{4}, \bar{5}; 2)_\phi] G(\bar{3}, 3)_\phi. \end{aligned} \quad (4.32)$$

Resuming the last equation for the self-energy  $\Sigma$  (Eq. 4.23) one calculates

$$\Sigma_\sigma(1, 2)_\phi = -Un_{-\sigma}\delta(1-2) + U \frac{\delta G_\sigma(1, \bar{2})_\phi}{\delta \phi_{-\sigma}(1^+, 1)} G_\sigma^{-1}(\bar{2}, 2)_\phi \quad |4.24$$

$$= Un_{-\sigma}\delta(1-2) + U \chi_{\sigma-\sigma}(1, \bar{2}; 1) G_\sigma^{-1}(\bar{2}, 2)_\phi \quad |4.25$$

$$\begin{aligned} &= Un_{-\sigma}\delta(1-2) \\ &+ U [G_\sigma(1, \bar{2})_\phi U_{ir,\sigma\bar{\sigma}}(\bar{2}, \bar{3}; \bar{4}, \bar{5}) \chi_{\bar{\sigma},-\sigma}(\bar{4}, \bar{5}; 1)_\phi G_\sigma(\bar{3}, \bar{2})_\phi] G_\sigma^{-1}(\bar{2}, 2)_\phi \\ &= Un_{-\sigma}\delta(1-2) + U [G_\sigma(1, \bar{2})_\phi U_{ir,\sigma\bar{\sigma}}(\bar{2}, 2; \bar{4}, \bar{5}) \chi_{\bar{\sigma},-\sigma}(\bar{4}, \bar{5}; 1)_\phi] \quad |4.32 \end{aligned}$$

$$\begin{aligned} &= Un_{-\sigma}\delta(1-2) \\ &+ \frac{U}{4} G_\sigma(1, \bar{2})_\phi [U_{sp}(\bar{2}, 2; \bar{4}, \bar{5}) \chi_{sp}(\bar{4}, \bar{5}; 1) + U_{ch}(\bar{2}, 2; \bar{4}, \bar{5}) \chi_{ch}(\bar{4}, \bar{5}; 1)]. \quad (4.33) \end{aligned}$$

Central idea of TPSC is to average over all higher order correlations instead of taking them fully into account.

Mathematically, this is accomplished by parametrizing the Luttinger-Ward functional

$\Phi[G]$  by two constants (!)  $U_{\sigma-\sigma}$  and  $U_{\sigma\sigma}$ , i.e.

$$\Phi[G] = 0.5 [G_{\bar{\sigma}}(\bar{1}, 1^+) U_{\bar{\sigma}\bar{\sigma}} G_{\bar{\sigma}}(\bar{1}, 1^+) + G_{\bar{\sigma}}(\bar{1}, 1^+) U_{\bar{\sigma}-\sigma} G_{-\sigma}(\bar{1}, 1^+)]. \quad (4.34)$$

From this the irreducible vertices become

$$\begin{aligned} U_{ir,\sigma\sigma'}(1, 2; 3, 4) &= \frac{\delta\Sigma_{\sigma}(1, 2)}{\delta G_{\sigma'}(3, 4)} \\ &= \frac{\delta^2\Phi[G]}{\delta G_{\sigma}(2, 1)\delta G_{\sigma'}(3, 4)} \\ &= \delta(1-4)\delta(2-3)\delta(3^+-4)U_{\sigma\sigma'}. \end{aligned} \quad (4.35)$$

Inserting this result into the self-energy expression (Eq. 4.33) and the susceptibilities (Eq. 4.32) and taking in both cases the non-interacting Green's function  $G_0$  to be consistent regarding the level of approximation one gets

$$\chi_{sp}(\vec{q}, iq_n) = \frac{2\chi_0(\vec{q}, iq_n)}{1 - U_{sp}\chi_0(\vec{q}, iq_n)} \quad (4.36)$$

$$\chi_{ch}(\vec{q}, iq_n) = \frac{2\chi_0(\vec{q}, iq_n)}{1 + U_{ch}\chi_0(\vec{q}, iq_n)} \quad (4.37)$$

$$\begin{aligned} \Sigma_{\sigma}(\vec{k}, ik_n) &= Un_{-\sigma} \\ &+ \frac{TU}{N4} \sum_{\vec{q}, iq_m} [U_{sp}\chi_{sp}(\vec{q}, iq_m) + U_{ch}\chi_{ch}(\vec{q}, iq_m)] G_{0,\sigma}(\vec{k} + \vec{q}, ik_{n+m}). \end{aligned} \quad (4.38)$$

But the TPSC-approximation creates an ambiguity in the calculation of the self-energy because the full irreducible vertex  $U_{ir,\sigma\sigma'}$  can be divided into a parallel-spin- (longitudinal) and an antiparallel-spin- (transversal) channel [16] that gives

$$\Sigma_{\sigma}^{trans}(\vec{k}, ik_n) = Un_{-\sigma} + \frac{TU}{2N} \sum_{\vec{q}, iq_m} [U_{sp}\chi_{sp}(\vec{q}, iq_m)] G_{0,\sigma}(\vec{k} + \vec{q}, ik_{n+m}). \quad (4.39)$$

Averaging over both channels is expected to give a better self-energy since it preserves crossing-symmetry and one obtains finally

$$\begin{aligned} \Sigma_{\sigma}(\vec{k}, ik_n) &= Un_{-\sigma} \\ &+ \frac{TU}{N8} \sum_{\vec{q}, iq_m} [3U_{sp}\chi_{sp}(\vec{q}, iq_m) + U_{ch}\chi_{ch}(\vec{q}, iq_m)] G_{0,\sigma}(\vec{k} + \vec{q}, ik_{n+m}). \end{aligned} \quad (4.40)$$

### 4.2.3. Correlation lengths

Strong antiferromagnetic correlations are supposed to drive superconductivity and suppress spectral weight  $A(\vec{k}, \omega)$  at  $\omega = 0$  in the 2D Hubbard model [17, 18, 19] and therefore it is natural to introduce the antiferromagnetic correlation length

$$\xi \equiv \xi_0 \sqrt{\frac{U_{sp}}{\frac{1}{\chi_0(\vec{Q}, iq_0)} - U_{sp}}}, \quad (4.41)$$

$$\text{where: } \xi_0 \equiv \sqrt{-\frac{1}{2\chi_0(Q)} \frac{\partial^2 \chi_0(\vec{q}, iq_0)}{\partial q_x^2} \Big|_{\vec{q}=\vec{Q}}}. \quad (4.42)$$

where  $\vec{Q}$  is defined as  $\chi(\vec{Q}, iq_0) = \max_{\vec{q}}(\chi_0(\vec{q}, iq_0))$  following [1, 20, 21]. Moreover, one calls the region where  $\xi$  grows exponentially as a function of the inverse temperature  $1/T$  and surpasses the thermal de Broglie wave length

$$\xi_{th} \equiv \frac{\langle v_F \rangle_{FS}}{\pi T}, \quad (4.43)$$

- the average  $\langle \rangle_{FS}$  is taken over the Fermi surface - the *classical renormalized regime* and the temperature associated with this crossover is denoted  $T_x$  (Fig. 4.1).

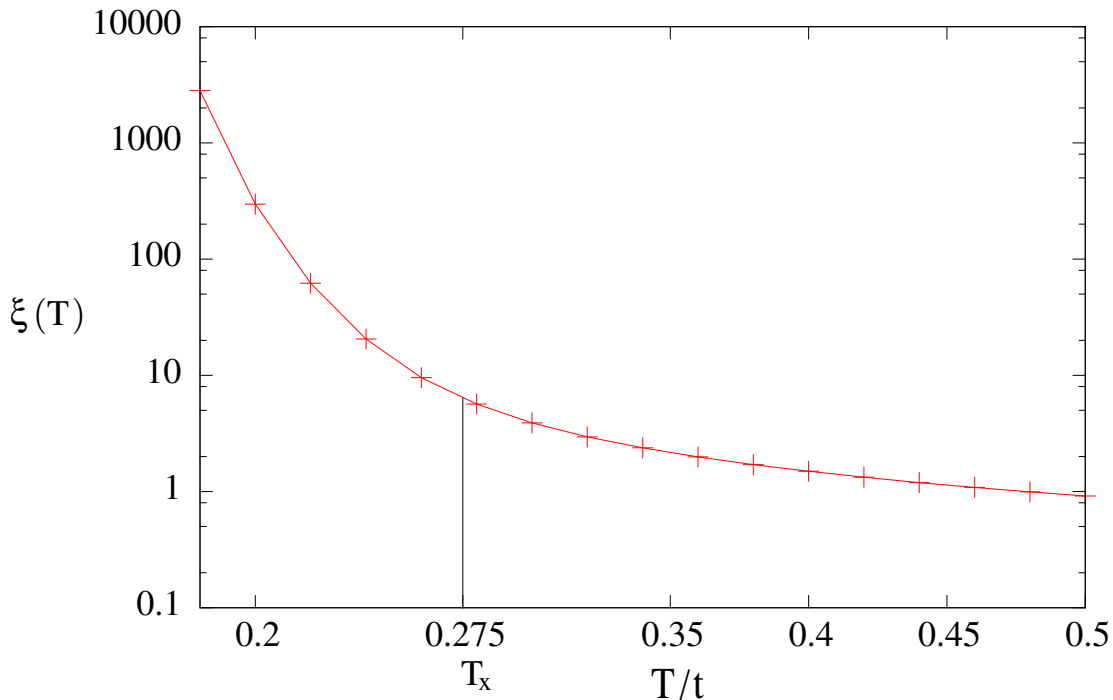


Figure 4.1: Growing antiferromagnetic correlation length  $\xi$  at low temperatures. The classical renormalized starts at  $T \approx 0.275eV$  for the square lattice,  $t' = 0$ ,  $U/t = 6$  and  $n = 1$ .

For practical calculations we take a rough estimate for  $\xi$  that is denoted by

$$\tilde{\xi} \equiv \max_{\vec{q}, n} \left( \frac{\chi_{sp}(\vec{q}, iq_n)}{\chi_0(\vec{q}, iq_n)} \right) \quad (4.44)$$

and check whether  $\tilde{\xi} = 200$  [22]. If this is the case, we have a look at  $\xi(T)$  to confirm that it is indeed shows the expected behaviour.

### 4.3. Two-particle properties and self-consistency equations

To determine  $U_{sp}$  and  $U_{ch}$  we will use the sum rules Eq.4.4 and 4.6. Since these depend on the two-particle correlator  $\langle n_{\uparrow} n_{\downarrow} \rangle$  another equation is needed to solve the set of equations.

The simplest way to tackle this problem is to make an approximative guess:  $U_{sp}$  describes the effective interaction in the singular spin channel, so one might renormalize

the Hubbard interaction by the probability to find two electrons on one site  $P_{\uparrow\downarrow}$ , which reproduces the Kanamori-Brueckner screening, i.e.

$$U_{sp} \approx P_{\uparrow\downarrow} U \quad P_{\uparrow\downarrow} = \frac{\langle n_{\uparrow} n_{\downarrow} \rangle}{\langle n_{\uparrow} \rangle \langle n_{\downarrow} \rangle}. \quad (4.45)$$

This ansatz is motivated by the work of Singwi *et al.* [23]. If  $n > 1$  one can do particle-hole transformation to keep the probabilistic picture of the approximation and the particle-hole symmetry.

Unfortunately, the ansatz fails inside the classical renormalized regime, i.e.  $T < T_x$ , since the Lindhard function  $\chi_0$  grows with decreasing temperature and from the local spin sum rule (Eq.4.4) we can see that the double occupancy  $\langle n_{\uparrow} n_{\downarrow} \rangle$  will go to zero as can be seen in Fig. 4.2.

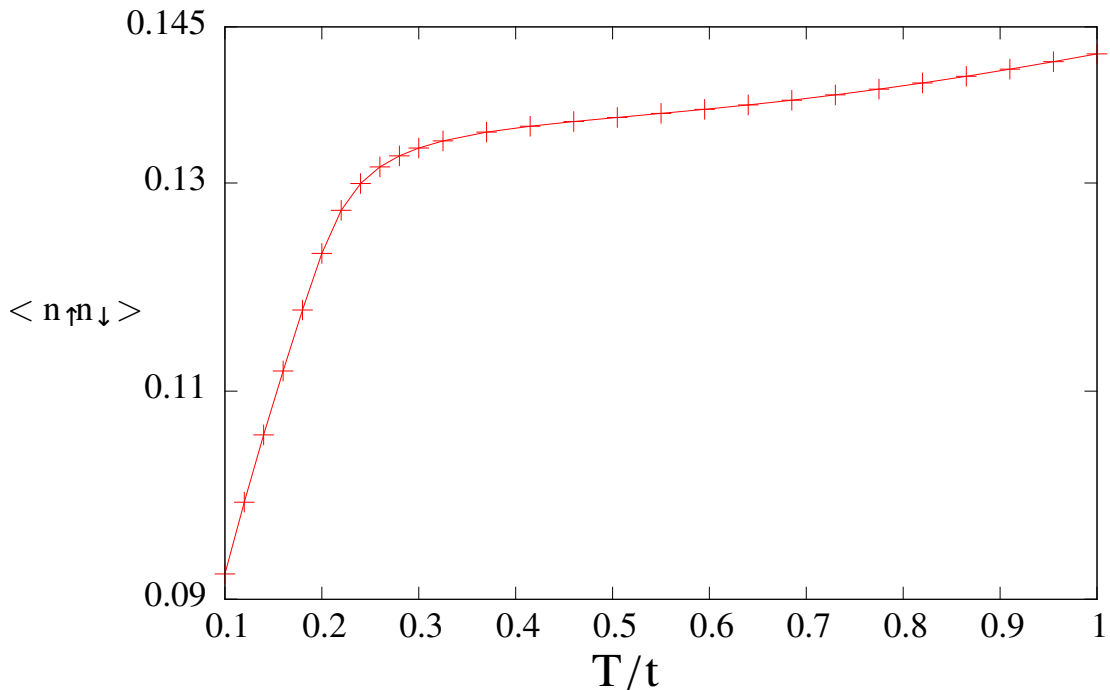


Figure 4.2: The double occupancy  $\langle n_{\uparrow} n_{\downarrow} \rangle$  - obtained from the ansatz Eq. 4.45 - decreases fast at low temperatures  $T < T_x$  due to the growing non-interacting susceptibility  $\chi_0$  that enters the local spin sum rule (Eq. 4.4). To avoid these unphysical effects one can use the double occupancy obtained at  $T = T_x$  since it does not change drastically for  $T \lesssim T_x$  [24]. The calculations were performed for the square lattice with  $t' = 0$ ,  $n = 1$  and  $U/t = 4$ .

As proposed by Vilk and Tremblay [1] one might use the double occupancy at  $T = T_x$  and make advantage of the small changes in the regime  $T \lesssim T_x$  [24].

The name Two-Particle Self-Consistent theory is rooted in the fact that it enforces two-particle properties like the Pauli principle.

Thereupon, it does not violate the Mermin-Wagner theorem.

Proof by contradiction:

$$\begin{aligned} \frac{T}{N} \sum_{\vec{q}, iq_n} \chi_{sp}(\vec{q}, iq_n) &= n - 2\langle n_\uparrow n_\downarrow \rangle & |4.36, 4.45 \\ \frac{T}{N} \sum_{\vec{q}, iq_n} \frac{2\chi_0(\vec{q}, iq_n)}{1 - U \frac{\langle n_\uparrow n_\downarrow \rangle}{\langle n_\uparrow \rangle \langle n_\downarrow \rangle} \chi_0(\vec{q}, iq_n)} &= n - 2\langle n_\uparrow n_\downarrow \rangle. \end{aligned} \quad (4.46)$$

A phase transition at finite temperature means a divergence in the spin susceptibility, i.e.

$$1 - U \frac{\langle n_\uparrow n_\downarrow \rangle}{\langle n_\uparrow \rangle \langle n_\downarrow \rangle} \chi_0(\vec{q}, iq_n) = 0 \quad (4.47)$$

$$\begin{aligned} \langle n_\uparrow n_\downarrow \rangle &= \frac{\langle n_\uparrow \rangle \langle n_\downarrow \rangle}{U \chi_0(\vec{q}, iq_n)} > 0 \\ \langle n_\uparrow n_\downarrow \rangle &> 0. \end{aligned} \quad (4.48)$$

The left-hand side of Eq. 4.46 diverges towards  $+\infty$  only when  $\langle n_\uparrow n_\downarrow \rangle > 0$  but the right-hand side can only go to  $+\infty$  when  $\langle n_\uparrow n_\downarrow \rangle \rightarrow -\infty$ .

□

To see that the Kanamori-Brueckner screening is properly included in the ansatz for the effective spin vertex (Eq. 4.45) one has to consider the spin susceptibility  $\chi_{sp}$  far away from the phase transition, i.e. in Eq. 4.36 it shows a small denominator.

Proof:

Away from phase transition  $\chi_{sp}$  given in Eq. 4.36 can be expanded in linear order of U and takes the form

$$\chi_{sp}(q) \approx 2\chi_0(q)(1 + U_{sp}\chi_0(q)). \quad (4.49)$$

This expression can now be inserted in the spin sum rule (Eq. 4.4) and solved for  $\langle n_\uparrow n_\downarrow \rangle$ :

$$n - 2\langle n_\uparrow n_\downarrow \rangle \stackrel{4.45}{\approx} \frac{T}{N} \sum_q 2\chi_0(q) \left( 1 + U \frac{\langle n_\uparrow n_\downarrow \rangle}{\langle n_\uparrow \rangle \langle n_\downarrow \rangle} \chi_0(q) \right). \quad (4.50)$$

Since the charge sum rule (Eq. 4.6) is valid for all values of U (especially for U=0) it can be used to calculate the first sum,

$$n - 2\langle n_\uparrow n_\downarrow \rangle = n + 2\langle n_\uparrow n_\downarrow \rangle - n^2 + \frac{2U\langle n_\uparrow n_\downarrow \rangle}{\langle n_\uparrow \rangle \langle n_\downarrow \rangle} \frac{T}{N} \sum_q \chi_0(q)^2 \quad (4.51)$$

$$n^2 = \langle n_\uparrow n_\downarrow \rangle \left( 4 + \frac{2U}{\langle n_\uparrow \rangle \langle n_\downarrow \rangle} \frac{T}{N} \sum_q \chi_0(q)^2 \right). \quad (4.52)$$

In the non-magnetic case one can simplify as follows:

$$P_{\uparrow\downarrow} = \frac{\langle n_\uparrow n_\downarrow \rangle}{n^2/4} \approx \frac{1}{1 + \frac{U}{2n^2} \frac{T}{N} \sum_q \chi_0(q)^2}. \quad (4.53)$$

From this equation the Kanamori-Brueckner screening of  $U_{sp}$  can be seen in the TPSC

ansatz Eq. 4.45:

$$U_{sp} = P_{\uparrow\downarrow} U \approx \frac{1}{\frac{1}{U} + \frac{1}{2n^2} \frac{T}{N} \sum_q \chi_0(q)^2}$$

$$\xrightarrow{U \rightarrow \infty} \frac{1}{\frac{1}{2n^2} \frac{T}{N} \sum_q \chi_0(q)^2}. \quad (4.54)$$

□

This saturation value is of the order of the inverse bandwidth [25] which is related to the maximum energy to form a node in the two-body wave function on the same site. This node is energetically more favorable than the on-site repulsion and leads to an effective screening. Meanwhile, it could be expected that  $U_{ch}$  shows some divergence at large  $U/t$  which announces the Mott insulator transition (Fig. 4.3).

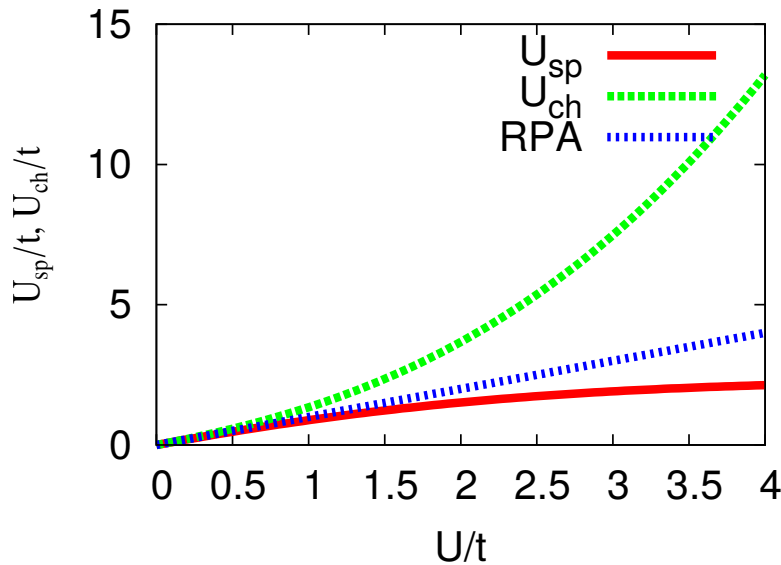


Figure 4.3: The irreducible spin vertex  $U_{sp}$  shows a convergence due to Kanamori-Brueckner screening. Differently, the irreducible charge vertex  $U_{ch}$  exhibits a divergence that is related to the Mott insulator transition. The calculations are done at  $T/t=0.3$ ,  $n=1$  and  $t'=0$ .

By construction both irreducible vertices  $U_{sp}$  and  $U_{ch}$  do not violate the local spin and charge sum rules (Eq. 4.4 and Eq. 4.6) while RPA does (Sec. 4.2.1). At a temperature dependent critical value of  $U/t$  the denominator in  $\chi_{sp}^{RPA}$  (Eq. 4.14) goes to zero and one gets numerically arbitrary values for the sum rules (Fig. 4.4).

Finally, the TPSC ansatz has to be applied to the single-particle self-energy (Eq. 4.33) and gives together with the Dyson equation a set of equations:

$$\Sigma_{\sigma}(k) = U n_{-\sigma} + \frac{U T}{8 N} \sum_q [3U_{sp}\chi_{sp}(q) + U_{ch}\chi_{ch}(q)] G_{0,\sigma}(k+q) \quad (4.55)$$

$$G(k) = G_0(k) + G_0(k)\Sigma(k)G(k). \quad (4.56)$$

The procedure for calculating this particle-hole-symmetric self-energy consists of the following steps:

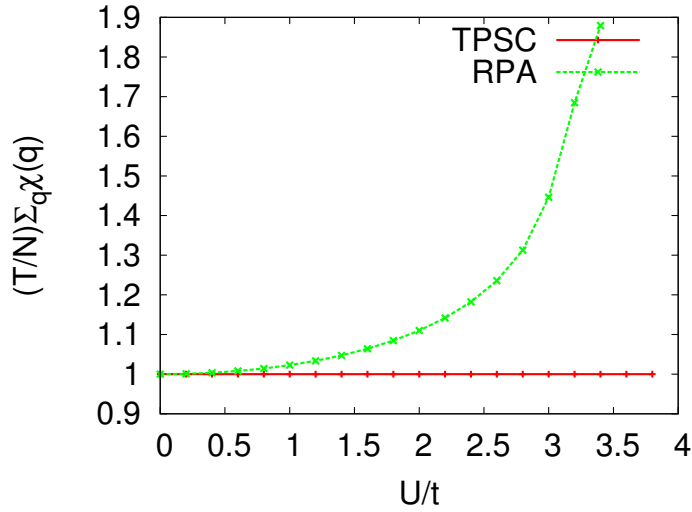


Figure 4.4: Adding up the local spin and charge sum rules (4.4 and 4.6) yields a constant in TPSC over the whole range of  $U/t$  while the result obtained by RPA grows first quadratically and crosses a divergence at  $U/t \approx 3.4$  that gives numerically random numbers that depend on the resolution if the calculation would be carried on. The temperature was set to  $T/t=0.5$  at half filling within the square lattice.

1. Starting from the bare Green's function  $G_0(k)$  one calculates the self-energy from the TPSC approximation (Eq. 4.55).
2. Next, one has to update the chemical potential  $\mu$  from Eq. 3.58.

To sum up, the set of self-consistent equations is given in the first box:

$$\begin{aligned}
 \chi_{sp}(q) &= \frac{2\chi_0(q)}{1 - U_{sp}\chi_0(q)} \\
 \chi_{ch}(q) &= \frac{2\chi_0(q)}{1 + U_{ch}\chi_0(q)} \\
 \frac{T}{N} \sum_q \chi_{sp}(q) &= n - 2\langle n_\uparrow n_\downarrow \rangle \\
 \frac{T}{N} \sum_q \chi_{ch}(q) &= n + 2\langle n_\uparrow n_\downarrow \rangle - n^2 \\
 U_{sp} &= U \frac{\langle n_\uparrow n_\downarrow \rangle}{\langle n_\uparrow \rangle \langle n_\downarrow \rangle},
 \end{aligned} \tag{4.57}$$

while the self-energy is evaluated as a single-shot quantity to keep the level of approximation

$$\begin{aligned}
 \Sigma_\sigma(k) &= U n_{-\sigma} + \frac{U T}{8 N} \sum_q [3U_{sp}\chi_{sp}(q) + U_{ch}\chi_{ch}(q)] G_{0,\sigma}(k+q) \\
 G(k) &= G_0(k) + G_0(k)\Sigma(k)G(k).
 \end{aligned} \tag{4.58}$$

### 4.3.1. Internal checks

The most important internal check that is available for TPSC comes from inserting the expression for  $\frac{\delta G}{\delta \phi}$  (Eq. 3.96) into the expression for  $tr(\Sigma G)$  (Eq. 3.85):

$$\boxed{\frac{T}{N} \sum_k \Sigma_\sigma(k) G_{0,\sigma}(k) = U \langle n_\uparrow n_\downarrow \rangle} \quad (4.59)$$

Keeping in mind that being consistent at every step of TPSC means taking  $G_{0,\sigma}$  instead of the full Green's function  $G_\sigma$  in Eq. 4.59.

This equation serves as one of many internal integrational resolution checks since this equation has to be always satisfied.

Any deviation between left-hand side and right-hand side above 3% stops the program and gives an error message with an advise to increase accuracy, i.e. Matsubara frequencies and/or  $\vec{k}$ -points.

On the other hand, this equation is in general valid for the full Green's function  $G_\sigma$  and therefore the difference between  $tr(\Sigma G)$  and  $tr(\Sigma G_0)$  gives an error estimation for TPSC.

In the case where the deviation is more than  $\sim 15\%$  one should be careful and interpret the data, if any, qualitatively.

Other important internal checks are the monotonuous decrease with increasing Matsubara frequencies of  $\chi_0(\vec{k}, iq_n)$ ,  $\chi_{sp}(\vec{k}, iq_n)$ ,  $\chi_{ch}(\vec{k}, iq_n)$ ,  $G(\vec{k}, iq_n)$ ,  $\text{Im}(\Sigma(\vec{k}, iq_n))$  and  $\text{Re}(\Sigma_\sigma(\vec{k}, iq_n)) - U n_{-\sigma}$  for all given  $\vec{k}$ . Problems that might occur are discussed in App. A and it is shown there how to fix them.

## 4.4. The Fluctuation Exchange approximation (FLEX)

Other self-consistent approaches like the Fluctuation Exchange approximation (FLEX) violate the Pauli principle but respect conservation laws. The procedure is similar to TPSC and consists of taking some subset of skeleton diagrams that build a Luttinger-Ward functional [26].

Again, one has to perform functional derivatives to get a self-energy that is self-consistent with the subset of diagrams in the Luttinger-Ward functional. In the end, FLEX yields a self-energy

$$\Sigma(k) = U n_{-\sigma} + \frac{UT}{4N} \sum_q [(3U \tilde{\chi}_{sp}^{RPA}(q) - 2U \tilde{\chi}_0(q)) - U \tilde{\chi}_{ch}^{RPA}(q)] G_\sigma(k+q), \quad (4.60)$$

where the superscript  $\sim$  signals that for the calculation one has to take the dressed Green's function  $G$ .

Since the diagrams used in FLEX do not contain all exchange diagrams it violates the Pauli principle [27].

Moreover, there is no internal mechanism to limit the value of  $\langle n_\uparrow n_\downarrow \rangle$  and even the equation for  $tr(\Sigma G)$  (Eq. 4.59) is not fulfilled if the correlator  $\langle n_\uparrow n_\downarrow \rangle$  is calculated from the susceptibilities via sum rules.

---

## 5. Superconductivity

### 5.1. The linearized Eliashberg equation

Strong antiferromagnetic correlations might be the driving mechanism that induces the creation of Cooper pairs in unconventional superconductors. In this work, we will study superconductivity within the Eliashberg theory that leads to the following equation for the superconducting gap function  $\Delta(\vec{k}, ik_n)$ :

$$\begin{aligned}\lambda\Delta(\vec{k}, ik_n) &= -\frac{1}{2} \sum_{\vec{k}', ik_m} V(\vec{k} - \vec{k}', ik_n - ik_m) G(-\vec{k}', -ik_m) \Delta(\vec{k}', ik_m) G(\vec{k}', ik_m) \\ &\equiv M * \Delta\end{aligned}\tag{5.1}$$

$$V(\vec{q}, iq_n) \equiv U + \frac{3}{2} U_{sp} \chi_{sp}(\vec{q}, iq_n) U - \frac{1}{2} U_{ch} \chi_{ch}(\vec{q}, iq_n) U,\tag{5.2}$$

where  $V$  is the pairing potential in the singlet case and  $\lambda$  is the largest positive eigenvalue of the equation. Superconductivity is reached when  $\lambda = 1$ . Usually, one is interested in the even frequency gap function, i.e.

$$\Delta(ik_n) = \Delta(-ik_n)\tag{5.3}$$

and since we limit ourselves to the singlet case we have inversion symmetry,

$$\Delta(\vec{k}, ik_n) = \Delta(-\vec{k}, -ik_n).\tag{5.4}$$

Numerically, we can simplify the calculations by choosing  $\Delta$  to be real.

Secondly, one determines the largest eigenvalue by application of the power method:

1) Starting with a random gap function  $\Delta_0(\vec{k}, ik_n)$  one calculates the right-hand side of the linearized Eliashberg equation 5.1. It makes calculations much faster to start with an already symmetric function and a Matsubara-decreasing function like

$$\Delta_0(\vec{k}, ik_n) = \frac{\cos(k_x) - \cos(k_y)}{k_n^2}\tag{5.5}$$

but it is always recommended to start with a random gap as a preliminary test. The resulting gap is called  $\tilde{\Delta}_1(\vec{k}, ik_n)$

2) We calculate

$$\lambda_0 = \max_{\vec{k}, ik_n} [\tilde{\Delta}_1(\vec{k}, ik_n)]\tag{5.6}$$

and normalize

$$\Delta_1 = \tilde{\Delta}_1 / \lambda_0.\tag{5.7}$$

3) We reiterate the procedure with  $\Delta_i$  and  $\lambda_{i-1}$  to get  $\Delta_{i+1}$  and  $\lambda_i$ ,  $i \in \mathbb{N}$ , until both do not change anymore within some tolerance.

Experience taught us that the converged eigenvalue  $\tilde{\lambda}$  is in general negative but this is fine since the power method provides the eigenvalue with the largest absolute value.

In that case one has to continue with the following:

4) We redo all steps 1) to 3) but subtract after every evaluation of the linearized

Eliashberg equation (Eq. 5.1) the term  $\tilde{\lambda}\Delta_{i-1}$ , i.e.

$$\tilde{\Delta}_i = M * \Delta_{i-1} - \tilde{\lambda}\Delta_{i-1} \quad (5.8)$$

that again has to be normalized by the maximal entry and so on and so forth.

5) When  $\Delta$  and  $\lambda$  are converged one has to do the transformation

$$\lambda \rightarrow \lambda + \tilde{\lambda} \quad (5.9)$$

to get the maximal eigenvalue for the initial problem.

## 5.2. Symmetry of the gap function

Since we have limited ourselves to singlet pairs of electrons it is now possible to expand the gap function in spherical harmonics with even angular momentum  $l$ . The two important cases for this work are the solutions with angular momentum  $l = 0, 2$  that are called *s*- and *d*-wave, respectively.

The s-wave solution is just constant in  $\vec{k}$ -space and known from the phonon-coupling in the BCS theory.

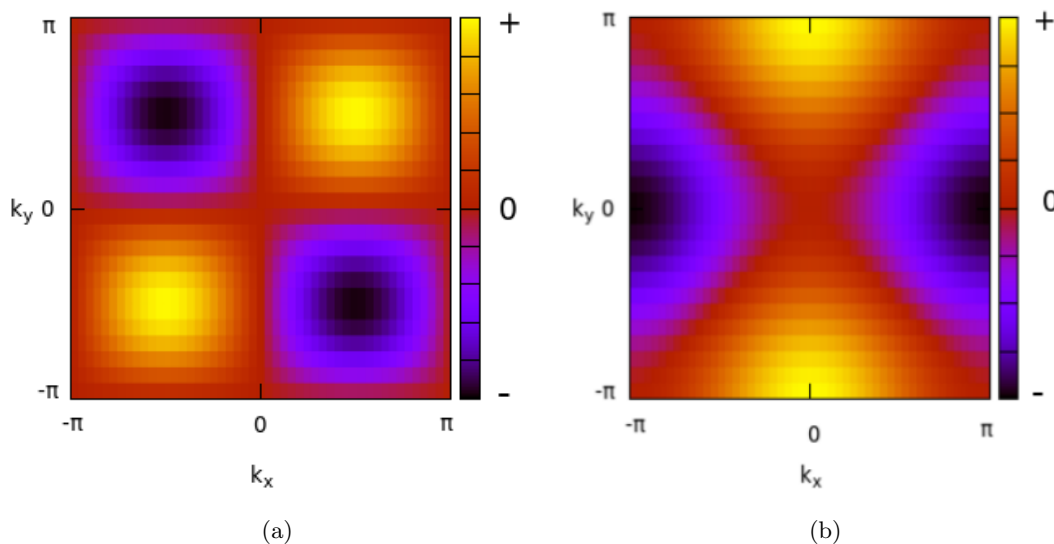


Figure 5.1: (a)  $d_{xy}$ -symmetry of the gap function shows nodes along the reciprocal lattice vectors. (b)  $d_{x^2-y^2}$ -symmetric gap functions show nodes along the diagonals of the first Brillouin zone.

In contrast to this, the d-wave solution (Fig. 5.1) is often encountered in high-temperature superconductors like cuprates or organic charge transfer salts.

## 6. Numerical results for the square and triangular lattice

Implementing the TPSC equations of 4.57, 4.58 one is able to study a variety of observables. In this work we will concentrate on the pseudogap physics and the d-wave superconductivity for the square lattice and the triangular lattice within the single-orbital Hubbard model.

### 6.1. Square lattice - Cuprates

As described in Sec. 4.2.3 the antiferromagnetic correlation length is a quantity that measures the antiferromagnetic correlations and leads to the pseudogap physics that is believed to be crucial for the understanding of the superconductivity in cuprates. Therefore, the first calculations are dedicated to the suppression of spectral weight at  $\omega = 0$  and the calculation of the cross-over temperature  $T_x$ .

#### 6.1.1. Pseudogap and crossover temperature $T_x$

First, we will compare TPSC with other theories that are valid for the treated regime of the Hubbard model.

Vilk and Tremblay [1] already found good agreement with Quantum Monte Carlo simulations (QMC) but we present comparisons with determinantal quantum Monte Carlo simulations [28] that show the development of the pseudogap with decreasing temperature.

DQMC calculations show that a very small pseudogap is already visible at  $T/t=0.28$  but becomes distinct at  $T/t=0.2$  which is a behavior that can be reproduced by TPSC (Fig. 6.1).

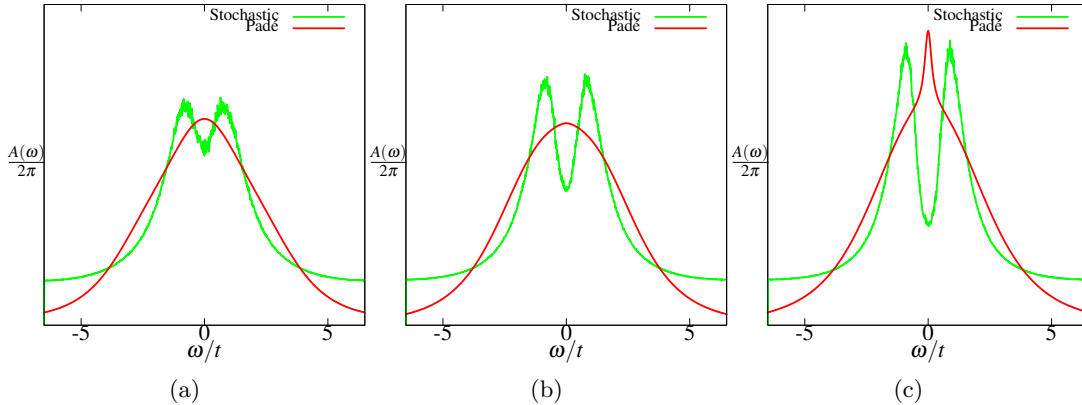


Figure 6.1: Spectral weight in the Hubbard square lattice system for  $U/t = 4$ ,  $n = 1$  and (a)  $T/t = 0.28$ , (b)  $T/t = 0.2$  and (c)  $T/t = 0.18$ . The suppression of spectral weight at  $\omega = 0$  due to growing antiferromagnetic correlations becomes visible when the analytical continuation is carried out with the Stochastic analytic continuation method while the Padé approximation is not able to resolve the gap and gives even a peak at low temperatures as shown in panel (c).

The antiferromagnetic correlations that start to grow exponentially [29, 30] below the crossover temperature  $T_x$  (Fig. 4.1) lead to a suppression of spectral weight at

$\omega = 0$  and in other theories that are valid for even stronger correlations to a Mott-metal-insulator transition at even lower temperatures [31].

Next, one can check whether the crossover temperature  $T_x$  shows the correct dependence on the filling  $n$  (Fig. 2.3). Since the TPSC equations are particle-hole symmetric we show the calculations only for the hole-doped case (Fig. 6.2).

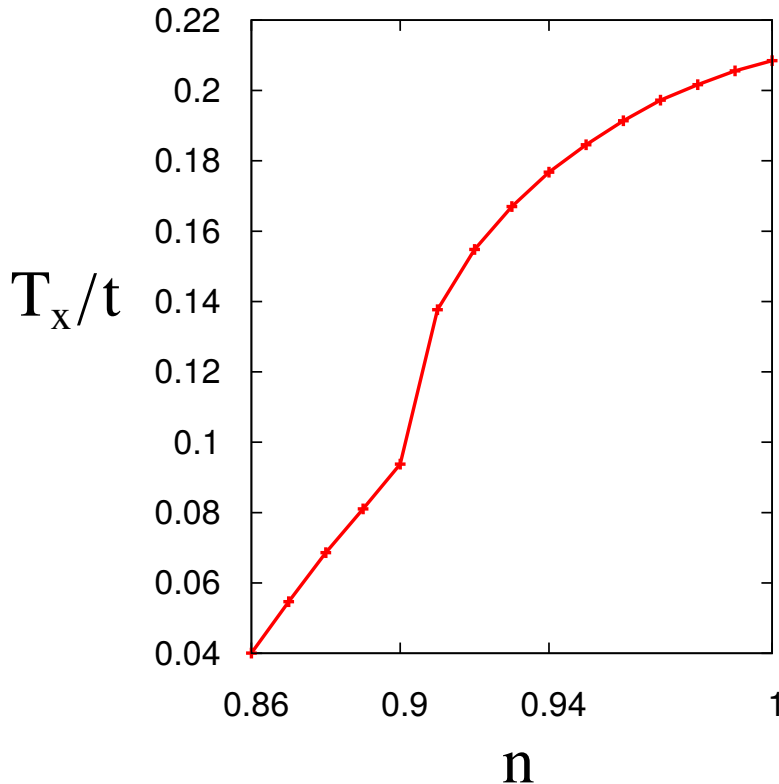


Figure 6.2: Dependence of the crossover temperature  $T_x$  on the filling  $n$  for  $U/t = 4$ . The pseudogap crossover is in qualitative agreement with the experimental results (Fig. 2.3) and Monte Carlo simulations [32] for the cuprate systems. The small kink at  $n = 0.9$  appears because the wavevector of the non-interacting susceptibility  $\chi_0$  is not commensurate for  $n \leq 0.9$ .

So far, there is no satisfactory explanation for the pseudogap phase but many attempts bring it into relation with the pre-forming of Cooper pairs or hidden orders like charge-, spin-density-waves and/or electron-nematic order [33, 34].

Bringing in the results of B. Kyung *et al.* [35] who also performed TPSC calculation for the same parameters one even gets the qualitatively right position of the superconducting dome below the pseudogap.

### 6.1.2. Superconductivity

An important characteristic of the cuprate phase diagram is the superconducting dome that can be reproduced within TPSC by estimation of the superconducting transition temperature  $T_c$  using the Kosterlitz-Thouless-criterion [35]. Nevertheless, one does not have to calculate  $T_c$  to see the dome-like shape since the largest eigenvalue of the linearized Eliashberg equation  $\lambda$  grows exponentially with temperature (Fig. 6.3). Hence, one can already see the tendencies of  $T_c$  if  $\lambda \approx 1$  for given parameters.

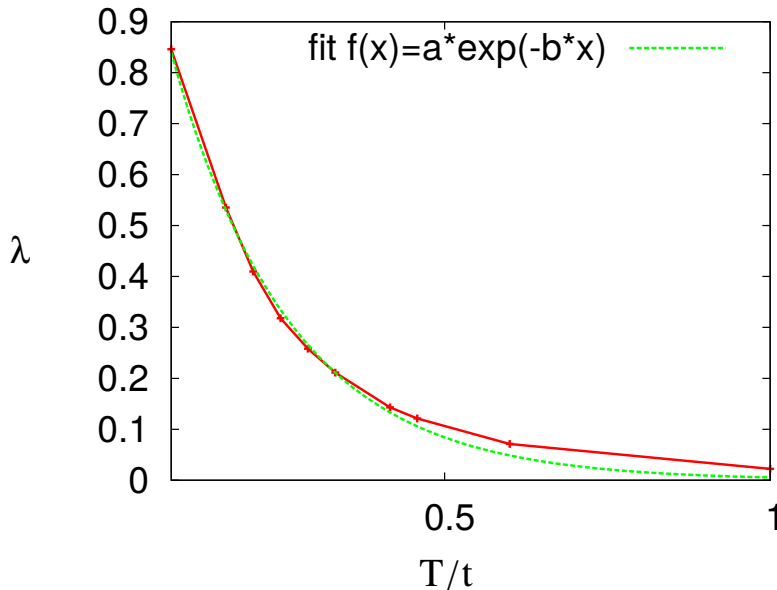


Figure 6.3: Temperature dependence of the largest eigenvalue of the linearized Eliashberg equation  $\lambda$  for the square lattice with  $U/t = 6$  and  $n = 1.125$ . The typical exponential growth is due to the exponentially increasing correlations in the pairing potential  $V$  in Eq. 5.2. The green line shows a fit of the numerical data to the function  $f(x) = a \cdot e^{-bx}$  where  $a$  and  $b$  are fitting parameters.

Therefore, the dome-like shape of the phase diagram becomes visible within the  $\lambda(n)$ -plot (Fig. 6.4) and even the maximum value of  $T_c$  is near the value obtained from the Kosterlitz-Thouless-criterion  $T_c/t(n = 1.125, U/t = 6) \approx 0.725$  although the peak of the dome is slightly shifted.

The dome-like shape might be induced by the decreasing antiferromagnetic correlations that are represented approximately by  $\tilde{\xi}$  (Fig. 6.4). Near half-filling one is confronted with large correlations that lead to a highly developed pseudogap and therefore to a large suppression of spectral weight at the Fermi surface which might, in result, hinder superconductivity (Fig. 6.5).

Having a closer look at the superconducting gap function (Fig. 6.6) and the linearized Eliashberg equation 5.1 we see that the form of  $\Delta(\vec{k}, ik_0)$  is mainly developed by the shape of the Fermi surface and the peak position of the Lindhard function  $\chi_0(\vec{q}, 0)$  that is also the same for the spin susceptibility  $\chi_{sp}(\vec{q}, 0)$  and the charge susceptibility  $\chi_{ch}(\vec{q}, 0)$ .

As another example we extended the model to diagonal hopping  $t'$  and chose  $t'/t > 1$  which shifts the nesting vector from  $(\pi, \pi)$  to  $(0, \pi - c)$  where  $c$  is a constant in  $[0, \pi)$ . This shift of the wavevector leads to a change of the gap symmetry, namely from  $d_{x^2-y^2}$  to  $d_{xy}$ . An explanation of this behavior can be seen from the linearized Eliashberg equation 5.1 since scattering at nesting vectors that are located near  $\vec{k} - \vec{k}' \approx (\pm\pi, \pm\pi)$ ,  $(\mp\pi, \pm\pi)$  for  $d_{x^2-y^2}$ -symmetry and  $\vec{k} - \vec{k}' \approx (\pm\pi, 0)$ ,  $(0, \pm\pi)$  for  $d_{xy}$ -symmetry yields the largest contributions to the  $\vec{k}'$ -integration [22]. Those results can be clearly seen in Fig. 6.7.

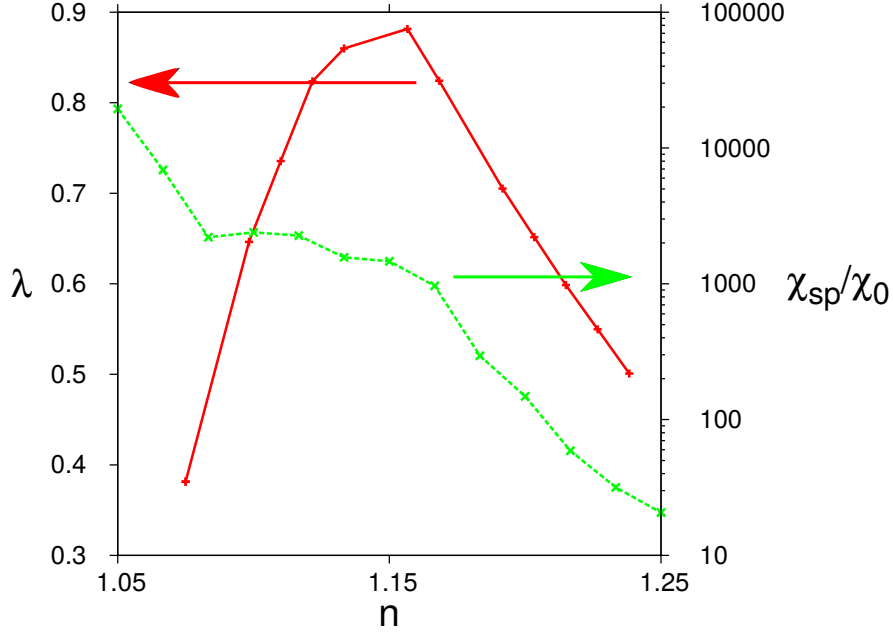


Figure 6.4: Filling dependence of the largest eigenvalue of the linearized Eliashberg equation  $\lambda$  (red line) for the square lattice with  $U/t = 6$  and  $T/t = 0.08$ . Near half-filling the antiferromagnetic fluctuations are very strong causing a large suppression of spectral weight near the Fermi surface and a decrease in  $T_c$ . On the other hand, the same fluctuations away from half-filling are less pronounced and lead to the dome-like shape of  $\lambda$ . The green line shows  $\tilde{\xi} = \max \frac{\chi_{sp}}{\chi_0}$  that can be interpreted as a measure of the antiferromagnetic correlations (Sec. 4.2.3).

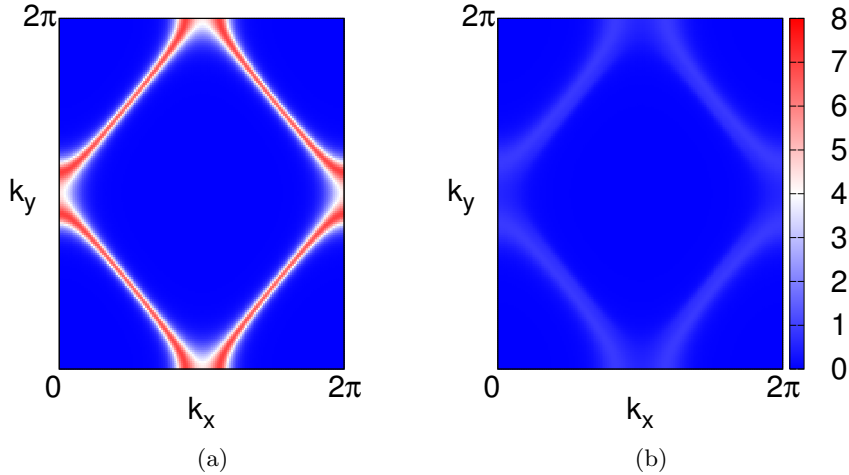


Figure 6.5: Fermi surface of the (a) non-interacting and (b) interacting square lattice system with  $U/t = 6$ ,  $T/t = 0.06$  and  $n = 1.075$  obtained from linear fitting of the imaginary part of  $G(\vec{k}, i\omega_n) \forall \vec{k}$  to obtain the values at  $\omega = i\omega_n = 0$ . Introducing a Hubbard repulsion  $U$  to the system leads to a suppression of spectral weight that is especially important at  $(0, \pi), (\pi, 0), (2\pi, \pi)$  and  $(\pi, 2\pi)$  because the superconducting gap has its maximum values at these points (Fig. 6.6).

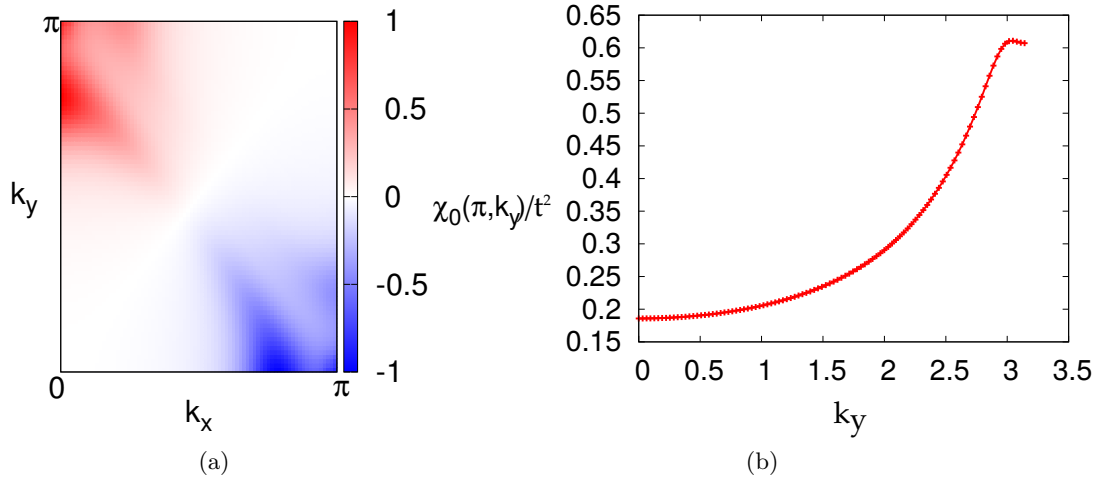


Figure 6.6: (a) The superconducting gap function  $\Delta(\vec{k}, i\omega_0)$  shows  $d_{x^2-y^2}$ -symmetry (therefore only the domain  $[0, \pi] \times [0, \pi]$  is depicted) for the square lattice and  $U/t = 6$ ,  $n = 1.075$  and  $T/t = 0.06$ . The form of the gap function has two main sources: Firstly, the shape of the Fermi surface (Fig. 6.5) and secondly the peak position of the Lindhard function  $\chi_0(\vec{q}, 0)$  at approximately  $(\pi, 3)$  as can be seen in (b).

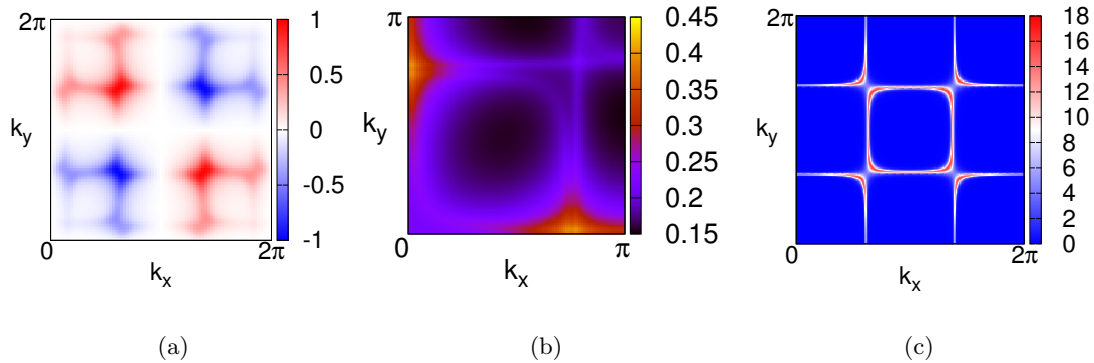


Figure 6.7: Results for the square lattice with  $t'/t = 1.375$  and  $U/t = 4$  at half-filling and  $T/t = 0.026$ . (a) The superconducting gap function  $\Delta(\vec{k}, i\omega_0)$  has  $d_{xy}$ -symmetry since the nesting vectors are found in the vicinity of  $(0, \pm\pi)$  as for the non-interacting susceptibility  $\chi_0(\vec{q}, 0)$  that is shown in (b). The Fermi surface for the non-interacting case (c) shows us the same wave vectors when connecting occupied states and influences the shape of (a).

## 6.2. Triangular lattice - Organic charge transfer salts

material	$t$ [meV]	$t'$ [meV]	$U$ [meV]	$T_x$ [K]
$\kappa$ -(ET) <sub>2</sub> Ag(CF <sub>3</sub> ) <sub>4</sub> (TCE)	67.7	30.4	336	181
$\kappa$ -(ET) <sub>2</sub> I <sub>3</sub>	75.35	26.1	360	183
$\kappa$ -(ET) <sub>2</sub> Ag(CN) <sub>2</sub> I·H <sub>2</sub> O	63.8	30.2	370	185
$\kappa$ - $\alpha'_1$ -(ET) <sub>2</sub> Ag(CF <sub>3</sub> ) <sub>4</sub> (TCE)	66.45	32.9	332	182
$\kappa$ -(ET) <sub>2</sub> Cu(NCS) <sub>2</sub>	59.75	41.2	380	45
$\kappa$ - $\alpha'_2$ -(ET) <sub>2</sub> Ag(CF <sub>3</sub> ) <sub>4</sub> (TCE)	67.35	33.35	330	178
$\kappa$ -(ET) <sub>2</sub> Cu[N(CN) <sub>2</sub> ](CN)	58.65	39.25	350	43
$\kappa$ -(ET) <sub>2</sub> Cu[N(CN) <sub>2</sub> ]Br	65.9	30	354	185

Table 1: Model parameters and calculated crossover temperatures  $T_x$  for several organic charge transfer salts.

As a second lattice geometry we consider the anisotropic triangular lattice that can be described by a next nearest neighbor tight binding model.

A widely used example are organic charge transfer salts  $\kappa$ -(BEDT-TTF)<sub>2</sub>X within the dimer model, where X stands for the anions separating the conducting layers and BEDT-TTF is commonly abbreviated as ET. Assuming the dimers as the tight-binding sites the model parameters  $t$ ,  $t'$  and the on-site interactions  $U$  (Tab. 1) can be derived from geometrical relations from the molecule model [6], whose parameters in turn are obtained by the projective Wannier function method. As the validity of the dimer model is very controversially discussed we will use the trends of the experimental data of the critical temperatures  $T_c$  as a benchmark for the quality of its approximations.

material	$T_c$ (TPSC) [K]	$T_c$ [36, 37, 38, 39] [K]
$\kappa$ -(ET) <sub>2</sub> Ag(CF <sub>3</sub> ) <sub>4</sub> (TCE)	30.17	2.6
$\kappa$ -(ET) <sub>2</sub> I <sub>3</sub>	29.01	3.6
$\kappa$ -(ET) <sub>2</sub> Ag(CN) <sub>2</sub> I·H <sub>2</sub> O	31.91	5.0
$\kappa$ - $\alpha'_1$ -(ET) <sub>2</sub> Ag(CF <sub>3</sub> ) <sub>4</sub> (TCE)	25.53	9.5
$\kappa$ -(ET) <sub>2</sub> Cu(NCS) <sub>2</sub>	5.8	10.4
$\kappa$ - $\alpha'_2$ -(ET) <sub>2</sub> Ag(CF <sub>3</sub> ) <sub>4</sub> (TCE)	23.21	11.1
$\kappa$ -(ET) <sub>2</sub> Cu[N(CN) <sub>2</sub> ](CN)	6.6	11.2
$\kappa$ -(ET) <sub>2</sub> Cu[N(CN) <sub>2</sub> ]Br	32.49	11.6

Table 2: Comparison of the calculated and experimental critical temperatures  $T_c$  for several organic charge transfer salts.

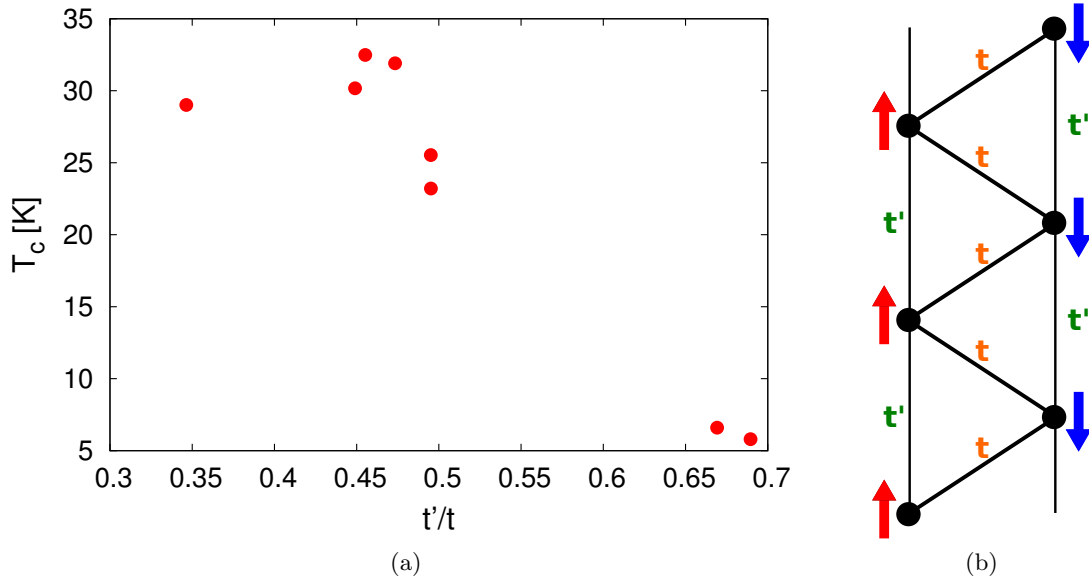


Figure 6.8: (a) Dependence of the critical temperature  $T_c$  (from Tab. 2) on the ratio  $t'/t$ . (b) A small  $t'/t$  ratio allows antiferromagnetic ordering since there is no frustration, while at large  $t'/t$  ratios antiferromagnetic spin fluctuations are highly suppressed.

### 6.2.1. Pseudogap and superconductivity

First, we examine whether a pseudogap appears in the organic charge transfer salts by using the criterion that the antiferromagnetic correlation length  $\xi$  grows exponentially and is larger than the thermal de Broglie wave length (Sec. 3.1).

In contrast to the square lattice systems we will not use an approximate value by stating a condition on  $\xi$  (Eq. 4.44) because the model parameters show only small differences for each system that can not be properly resolved otherwise. A table with all crossover temperatures calculated from the above condition is given in Tab. 1. The values of  $T_x$  are all of the same order of magnitude except for  $\kappa$ -(ET) $_2$ Cu(NCS) $_2$  and  $\kappa$ -(ET) $_2$ Cu[N(CN) $_2$ ](CN) that both have a large  $t'/t$ -ratio that suppresses antiferromagnetic correlations and hinders also superconductivity (Fig. 6.8).

Comparing the calculated results for the critical temperature  $T_c$  for superconductivity in Tab. 2 one already sees that the pseudogap should be detected in every studied compound since  $T_x > T_c$ .

As expected the calculated values for  $T_c$  from TPSC show large deviations from the experimental results. This has several reasons and the most important one is that the dimer model has been found to be an inappropriate description for the organic charge transfer salts. Especially, when focussing on the discordant values we see that the results highly depend on the ratio  $t'/t$  (Fig. 6.8). This can be understood as a large  $t'$  coupling suppresses a  $d_{x^2-y^2}$  gap function. Since this reduction of the critical temperatures is not present in experimental observation this is already a strong hint that further extensions with more degrees of freedom for the calculations are necessary.

Moreover, the values for the Hubbard repulsion  $U$  are derived from the rather crude approximation  $U = 2t_1$ , where  $t_1$  is the hopping amplitude between two molecules of the dimer. As it is very difficult to obtain more accurate values for  $U$  in the dimer model the extension to a molecule model where the tight-binding sites are located at

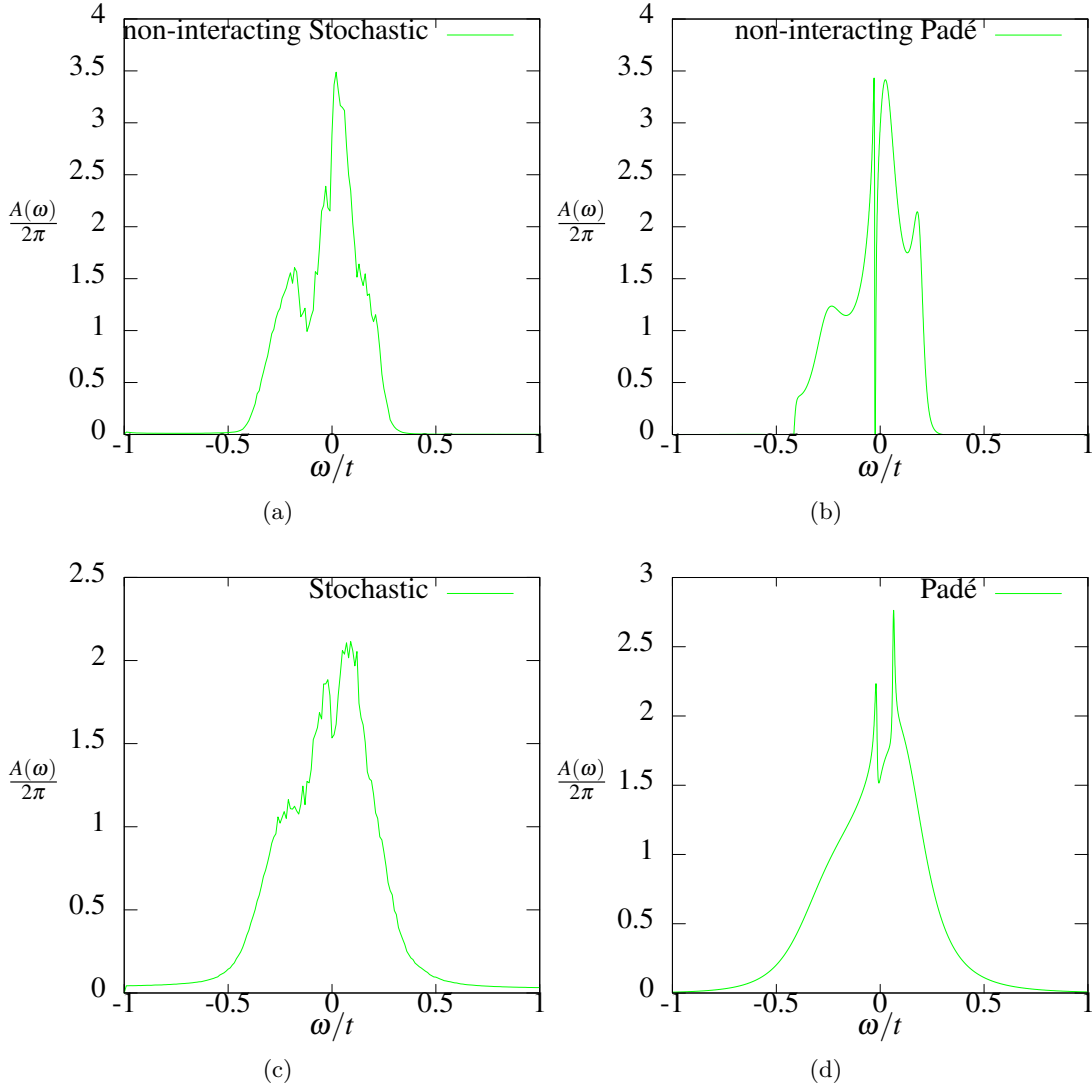


Figure 6.9: Spectral weight of  $\kappa$ -(ET<sub>2</sub>)I<sub>3</sub> at  $T = 41.78 K$  in the noninteracting  $U = 0$  (a-b) and interacting (c-d) case. For nonzero interactions a small pseudogap is already visible at  $\omega = 0$ .

the centers of each ET molecule allows a more systematic approach. Since the shape of the ET molecules can be considered as independent of its crystal environment it is justified to use the same Hubbard repulsion for every material.

As an example for the form of the pseudogap Fig. 6.9 (c-d) shows the spectral weight for  $\kappa$ -(ET<sub>2</sub>)I<sub>3</sub> at  $T = 41.78 K$  and for comparison Fig. 6.9 (a-b) shows the same for the non-interacting system. The pseudogap is just beginning to evolve and is visible in both methods for analytical continuation.

All systems studied within the dimer model reveal  $d_{x^2-y^2}$ -symmetry of the gap function as shown exemplarily in Fig. 6.10.

### 6.2.2. Comparisons to other theories

Since the results for the anisotropic triangular lattice exhibit large deficiencies compared to the experimental results it seems reasonable to compare to other theories in

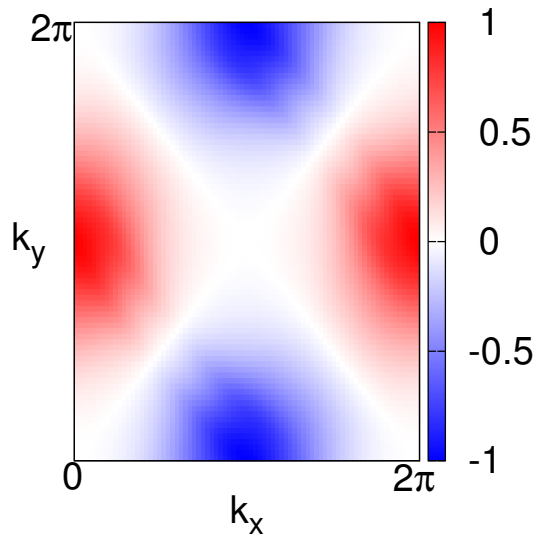


Figure 6.10: Superconducting gap function  $\Delta(\vec{k}, i\omega_0)$  for the  $\kappa$ -(ET) $_2$ Cu[N(CN) $_2$ ]Br system at  $T = 32.96$  K. The system reveals  $d_{x^2-y^2}$ -symmetry in the dimer model.

order to know whether the problem is founded on the grounds of the method or the model.

First, it was shown that FLEX also finds a wide domain of superconductivity in the phase diagram and even yields the same dependency of  $T_c$  on the  $t'/t$  ratio [40]. Furthermore, it was found that quantum Monte Carlo [41] is able to detect an enhancement of pairing correlations for superconducting order parameters. Nevertheless, within the variational Monte Carlo approaches it is still not clear whether a superconducting domain is present or not [42, 43] since the results depend on the chosen ansatz for the wave function.

So far, it is controversial whether superconductivity is inherent property of the anisotropic triangular lattice or not and at least it is not an exception that TPSC yields a superconducting phase.

The most important point is still the wrong trend in the calculated critical temperatures (Tab. 2) that motivates us to take a closer look to the molecule model for organic charge transfer salts as explained in the outlook.

## 7. Summary and Outlook

In this work we have reviewed the TPSC approach to spin fluctuation mediated superconductivity. We have followed the derivation of the key equations that in contrast to the widely used random phase approximation obey the sum rules, which represent the simplest form of the Pauli principle. Furthermore, it is a conserving approximation as it can be constructed from a Luttinger-Ward functional like the fluctuation exchange approximation, which suffers from the disadvantage that it violates the Mermin-Wagner theorem in contrast to TPSC. Next, we have investigated two different lattice geometries: First, we have studied square lattices that are realized f.i. in cuprates. Second, we have examined the triangular lattice geometry on the example of the organic charge transfer salts (dimer model).

In the case of the square lattices we were able to reproduce the suppression of spectral weight at  $\omega = 0$  at temperatures above the critical temperature  $T_c$ . Moreover, for the first time we investigated the pseudogap evolution using TPSC that was previously studied with determinantal quantum Monte Carlo simulations [28]. During the course of our examinations of the pseudogap phase we found that it is essential to use the Stochastic analytic continuation method as the simplistic Padé approximation yields an unphysical enhancement of spectral weight at  $\omega = 0$  at low temperatures. Furthermore, while Monte Carlo simulations [32] produce an inexplicable second kink in the crossover temperature  $T_x$  to filling diagramm, our results reveal only the physically relevant peak that can be associated to the transition from commensurate to incommensurate nesting vectors (Fig. 6.2).

Monitoring the largest eigenvalue of the linearized Eliashberg equation we were already able to estimate the shape of the superconducting region in the  $T - n$ -phase diagramm without the necessity of tedious calculations of the critical temperature  $T_c$ .

To explore the considered model further, we performed calculations for different  $t'/t$  ratios and saw that by choosing  $t'/t > 1$  the symmetry of the gap function changes from  $d_{x^2-y^2}$  to  $d_{xy}$ .

As a second case we considered triangular lattices on the example of the organic charge transfer salts within the dimer model. First, we saw that the pseudogap appears and should be observable in all considered compounds as the calculated values for the crossover temperature are always larger than the critical temperatures. The wrong trends in the calculated critical temperatures are supposedly rooted in the failure of the dimer model and the ambiguity in the choice of the Hubbard repulsion.

To summarize we have seen that using single-orbital TPSC we were able to reproduce the right pseudogap physics and the correct shape of the temperature-filling phase diagram. Nevertheless, during the study we were confronted with limitations that we can fix only partially. To be able to apply the TPSC method to more realistic cuprate band structures it was shown by Ogura *et al.* that an extension to a multi-orbital TPSC [44] is necessary to recover the dome-like shape of the critical temperature  $T_c$  in dependence of the filling [4].

For a more accurate description of the organic charge transfer salts we have seen that the dimer model is not sufficient. Therefore, it is necessary to extend our study to a molecule-based multi-site model, which has been found to yield a different gap symmetry. The averaging over the hopping paths from the molecules of one dimer to one molecule of a neighboring dimer is only legitimate if both hoppings are of a similar

---

magnitude [6]. In the case of the studied compounds (Tab. 1) this condition is not satisfied. Hence, we will take the full set of hopping parameters, which we obtain using the projective Wannier function method after a density functional calculation. So far, there is no formulation of multi-site TPSC and we are going to develop this by always sticking to the main ideas of TPSC, i.e. sum rules and self-consistency. Another possible extension would be the insertion of a nearest neighbor interaction  $V$ .

Regarding improvements of the TPSC method:

Deficiencies in the strong coupling limit are inherent problems since the ansatz for the Luttinger-Ward functional (Eq. 4.34) explicitly averages over higher order correlations and drops therefore the frequency dependency.

Nevertheless, one might be able to improve the theory and allow calculations deeper inside the classical renormalized regime by taking a different ansatz for the irreducible spin vertex  $U_{sp}$  (Eq. 4.45) that does not lead to  $\langle n_{\uparrow}n_{\downarrow} \rangle \rightarrow 0$  deep inside the pseudogap phase.

## A. Numerical issues

In this appendix we show how to perform sums over Matsubara frequencies by high-frequency expansion.

### A.1. High-frequency behaviour of $G$ and $\Sigma$

Firstly, we use the relation between the Matsubara Green's function  $G(\vec{k}, ik_n)$  and the spectral weight  $A(\vec{k}, \omega)$  (Eq. 3.65) to see the form of  $G(\vec{k}, ik_n)$  for large  $n$ :

$$\begin{aligned} G(\vec{k}, ik_n) &= \int_{-\infty}^{\infty} \frac{d\omega}{2\pi} \frac{A(\vec{k}, \omega)}{ik_n - \omega} \\ &\rightarrow \frac{1}{ik_n} \int_{-\infty}^{\infty} \frac{d\omega}{2\pi} A(\vec{k}, \omega) \quad |3.39 \\ &= \frac{1}{ik_n}. \end{aligned} \quad (\text{A.1})$$

Hence, from the Dyson equation (Eq. 4.56) follows that the self-energy should not diverge. Intuitively, we expect the spectral weight  $A(\vec{k}, \omega)$  to fall off very fast for large  $|\omega|$  which can also be proven [2] and we can expand

$$G(\vec{k}, ik_n) = \sum_{j=0}^{\infty} \frac{c_j(\vec{k})}{(ik_n)^j} = \frac{1}{ik_n} + \frac{c_1(\vec{k})}{(ik_n)^2} + O\left(\left(\frac{1}{k_n}\right)^3\right) \quad (\text{A.2})$$

$$\Sigma(\vec{k}, ik_n) = \sum_{j=0}^{\infty} \frac{d_j(\vec{k})}{(ik_n)^j}. \quad (\text{A.3})$$

### A.2. Calculation of the filling $n$ / adjusting the chemical potential $\mu$

At two steps of the self-consistency one is confronted with changes of the Green's function (Sec. 4.3) and therefore with an aberration from the correct filling.

At large Matsubara frequencies the Green's function can be expanded in terms of the Matsubara frequencies  $ik_n$  with coefficients  $c_j(\vec{k}) \in \mathbb{R}$  and shows the following asymptotic behaviour

$$\begin{aligned} G(\vec{k}, i\omega_n) &= \sum_{j=0}^{\infty} \frac{c_j(\vec{k})}{(ik_n)^j} \\ &\underset{n \gg 1}{\approx} c_0(\vec{k}) + \frac{c_1(\vec{k})}{ik_n} + \frac{c_2(\vec{k})}{(ik_n)^2} + \frac{c_3(\vec{k})}{(ik_n)^3} + \frac{c_4(\vec{k})}{(ik_n)^4}. \end{aligned} \quad (\text{A.4})$$

In case of Matsubara Green's functions (Eq. 4.56) the Fourier transformation is well defined and the function is normalized to one particle, i.e.  $c_0(\vec{k}) = 0$  and  $c_1(\vec{k}) = 1$ .

Numerically one is restricted to finite sums which means that the sum appearing in the formula for the filling  $n_{\vec{k}}$  (Eq. 3.58) has to be approximated by fitting analytically calculated tails. The number of Matsubara frequencies we want to store and use for calculations is limited to  $N_{mats}$  and the remaining ones are approximated by the high-frequency tail.

$$G(\vec{k}, \tau) = T \sum_{n=-\infty}^{\infty} G(\vec{k}, ik_n) e^{-ik_n \tau}$$

### A.3 Matsubara sums of the form $\sum_n f(n) * g(n + m)$

$$\begin{aligned}
&= T \left( \sum_{n=-N_{mats}}^{N_{mats}} G(\vec{k}, ik_n) e^{-ik_n \tau} + \sum_{n \notin [-N_{mats}, N_{mats}]} G(\vec{k}, ik_n) e^{-ik_n \tau} \right) \\
&\stackrel{A.4}{\approx} T \left[ \sum_{n=-N_{mats}}^{N_{mats}} G(\vec{k}, ik_n) e^{-ik_n \tau} \right. \\
&\quad \left. + \sum_{n \notin [-N_{mats}, N_{mats}]} \left( \frac{1}{ik_n} + \frac{c_2(\vec{k})}{(ik_n)^2} + \frac{c_3(\vec{k})}{(ik_n)^3} + \frac{c_4(\vec{k})}{(ik_n)^4} \right) e^{-ik_n \tau} \right].
\end{aligned} \tag{A.5}$$

To complete the second sum one inserts an effective zero by adding and subtracting the missing part of the sum,

$$\begin{aligned}
G(\vec{k}, \tau) &\approx T \left[ \sum_{n=-N_{mats}}^{N_{mats}} \left( G(\vec{k}, ik_n) - \left( \frac{1}{ik_n} + \frac{c_2(\vec{k})}{(ik_n)^2} + \frac{c_3(\vec{k})}{(ik_n)^3} + \frac{c_4(\vec{k})}{(ik_n)^4} \right) \right) e^{-ik_n \tau} \right. \\
&\quad \left. + \sum_{n=-\infty}^{\infty} \left( \frac{1}{ik_n} + \frac{c_2(\vec{k})}{(ik_n)^2} + \frac{c_3(\vec{k})}{(ik_n)^3} + \frac{c_4(\vec{k})}{(ik_n)^4} \right) e^{-ik_n \tau} \right].
\end{aligned} \tag{A.6}$$

The second sum can be evaluated analytically and give the following result after performing  $\lim_{\tau \rightarrow 0^-}$ :

$$n_{\vec{k}} \approx \frac{1}{2} - \frac{c_2(\vec{k})}{4T} + \frac{c_4(\vec{k})}{48T^2} + T \sum_{n=-N_{mats}}^{N_{mats}} \left( G(\vec{k}, ik_n) + \frac{c_2(\vec{k})}{k_n^2} - \frac{c_4(\vec{k})}{k_n^4} \right). \tag{A.7}$$

To get the total filling it suffices to sum over the first Brillouin zone, i.e.

$$n \approx \frac{1}{2} + \frac{1}{N} \sum_{\vec{k}} \left[ -\frac{c_2(\vec{k})}{4T} + \frac{c_4(\vec{k})}{48T^2} + T \sum_{n=-N_{mats}}^{N_{mats}} \left( G(\vec{k}, ik_n) + \frac{c_2(\vec{k})}{k_n^2} - \frac{c_4(\vec{k})}{k_n^4} \right) \right]. \tag{A.8}$$

Fixing the chemical potential to the right filling  $n_0$  is now accomplished by finding the root of the function

$$f(\mu) = n(\mu) - n_0. \tag{A.9}$$

$n(\mu)$  is the calculated filling (Eq. A.8) where  $\mu$  influences the appearing coefficients and the Matsubara Green's function  $G(\vec{k}, ik_n)$ .

The root is numerically found by using the bisection method where  $\mu \in [-U/2, U/2]$ .

### A.3. Matsubara sums of the form $\sum_n f(n) * g(n + m)$

The considerations of this sections are explained within the example of calculating the irreducible susceptibility  $\chi_0(\vec{q}, iq_n)$  (Eq. 4.17) but they can be analogously applied to the calculation of the self-energy  $\Sigma(\vec{k}, ik_n)$  (Eq. 4.55) and the superconducting gap function  $\Delta(\vec{k}, ik_n)$  (Eq. 5.1).

We start with

$$\chi_0(\vec{q}, iq_n) = -\frac{T}{N} \sum_{\vec{k}, ik_m} G_0(\vec{k}; ik_m) G_0(\vec{k} + \vec{q}; ik_n + iq_m). \quad (\text{A.10})$$

Again, one has to approximate an infinite sum over Matsubara frequencies by a finite one. But differently to the steps shown in Sec. A.2 it is important to take care of the shift while performing the analytically exact sum. The approximation will take the following form for one fixed addend  $\vec{k}$ ,

$$\begin{aligned} & -T \sum_{n=-\infty}^{\infty} G_0(\vec{k}; ik_m) G_0(\vec{k} + \vec{q}; ik_n + iq_m) \\ &= -T \sum_{n=-N_{\text{mats}}}^{N_{\text{mats}}} G_0(\vec{k}; ik_m) G_0(\vec{k} + \vec{q}; ik_n + iq_m) \\ &\quad - T \sum_{n \notin [-N_{\text{mats}}, N_{\text{mats}}]} G_0(\vec{k}; ik_m) G_0(\vec{k} + \vec{q}; ik_n + iq_m) \\ &\approx -T \sum_{n=-N_{\text{mats}}}^{N_{\text{mats}}} G_0(\vec{k}; ik_m) G_0(\vec{k} + \vec{q}; ik_n + iq_m) \\ &\quad - T \sum_{n \notin [-N_{\text{mats}}, N_{\text{mats}}]} \left( \frac{1}{ik_n} + \frac{c_1(\vec{k})}{(ik_n)^2} \right) \left( \frac{1}{ik_{n+m}} + \frac{c_1(\vec{k} + \vec{q})}{(ik_{n+m})^2} \right). \quad (\text{A.11}) \end{aligned}$$

Adding and subtracting the same terms as done before completes the second sum and leads to the following result:

$$\begin{aligned} & -T \sum_{n=-N_{\text{mats}}}^{N_{\text{mats}}} \left[ G_0(\vec{k}; ik_m) G_0(\vec{k} + \vec{q}; ik_n + iq_m) \right. \\ &\quad \left. + \left( \frac{1}{ik_n} + \frac{c_1(\vec{k})}{(ik_n)^2} \right) \left( \frac{1}{ik_{n+m}} + \frac{c_1(\vec{k} + \vec{q})}{(ik_{n+m})^2} \right) \right] \\ & -T \sum_{n=-\infty}^{\infty} \left( \frac{1}{ik_n} + \frac{c_1(\vec{k})}{(ik_n)^2} \right) \left( \frac{1}{ik_{n+m}} + \frac{c_1(\vec{k} + \vec{q})}{(ik_{n+m})^2} \right) \\ & \approx -T \sum_{n=-N_{\text{mats}}}^{N_{\text{mats}}} \left[ G_0(\vec{k}; ik_m) G_0(\vec{k} + \vec{q}; ik_n + iq_m) \right. \\ &\quad \left. + \left( \frac{1}{ik_n} + \frac{c_1(\vec{k})}{(ik_n)^2} \right) \left( \frac{1}{ik_{n+m}} + \frac{c_1(\vec{k} + \vec{q})}{(ik_{n+m})^2} \right) \right] \\ & -T \sum_{n=-\infty}^{\infty} \left( \frac{1}{ik_n} + \frac{c_1(\vec{k})}{(ik_n)^2} \right) \left( \frac{1}{ik_{n+m}} + \frac{c_1(\vec{k} + \vec{q})}{(ik_{n+m})^2} \right) \\ &= -T \sum_{n=-N_{\text{mats}}}^{N_{\text{mats}}} \left[ G_0(\vec{k}; ik_m) G_0(\vec{k} + \vec{q}; ik_n + iq_m) \right. \\ &\quad \left. + \left( \frac{1}{ik_n} + \frac{c_1(\vec{k})}{(ik_n)^2} \right) \left( \frac{1}{ik_{n+m}} + \frac{c_1(\vec{k} + \vec{q})}{(ik_{n+m})^2} \right) \right] \end{aligned}$$

$$-T \begin{cases} \frac{-1}{4T^2} + \frac{c_1(\vec{k})c_1(\vec{k}+\vec{q})}{48T^4}, & \text{for } m = 0 \\ \frac{1}{2Tq_n^2} \left\{ \frac{c_1(\vec{k})c_1(\vec{k}+\vec{q})}{T} + im\pi [c_1(\vec{k}) - c_1(\vec{k} + \vec{q})] \right\}, & \text{for } m \neq 0 \end{cases} \quad (\text{A.12})$$

These sums have to be performed for every  $\vec{q}$ -point of the mesh and every Matsubara frequency  $q_n$  where  $n \in [0, N_{mats}]$ . These calculations yield deeply nested loops that increase the computing time dramatically.

To tackle this problem it is convenient to vectorize the innermost sum over the Matsubara frequencies and to parallelize over the  $\vec{q}$ -mesh.

Finally, the shift in the second factor  $G_0(\vec{k} + \vec{q}; ik_n + iq_m)$  induces another significant problem. If one intends to store the irreducible susceptibility  $\chi_0(q)$  for the first  $N_{mats}$  frequencies it is not enough to carry out the sum only from  $-N_{mats}$  to  $N_{mats}$  since this would mean a cut-off in the summation although a non-negligible overlap is present. Fig. A.1 shows this situation schematically in the case of  $\chi_0(iq_{N_{mats}})$ .

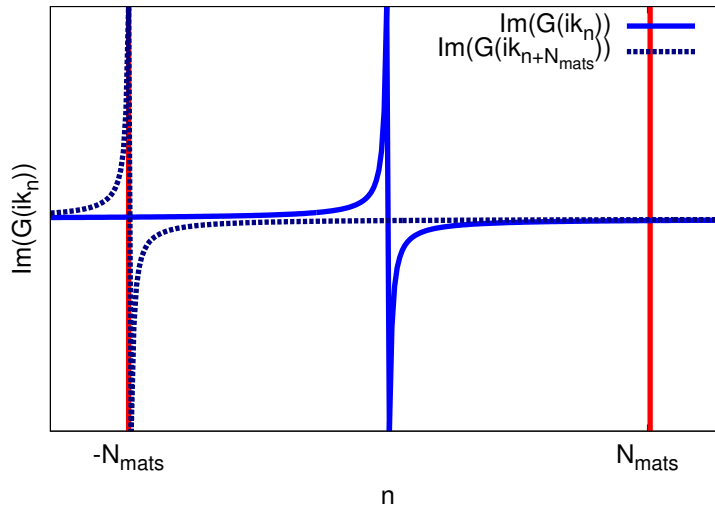


Figure A.1: Schematic overlap over the imaginary part of both Green's function  $G(ik_n)$  (solid line) and  $G(ik_{n+N_{mats}})$  (dotted line) to get  $\chi_0(iq_{N_{mats}})$ . Performing the summation only from  $-N_{mats}$  to  $N_{mats}$  would cut off an important contribution from  $n < N_{mats}$ .

This cut-off leads to a non-physical increase of the non-interacting susceptibility  $\chi_0(iq_n)$  at large Matsubara frequencies (Fig. A.2). To avoid this behavior it suffices to increase the summation domain by the number of the bosonic Matsubara frequency, i.e. for the calculation of  $\chi_0(iq_m)$  one would have to integrate  $n \in [-N_{mats} - m, N_{mats}]$ .

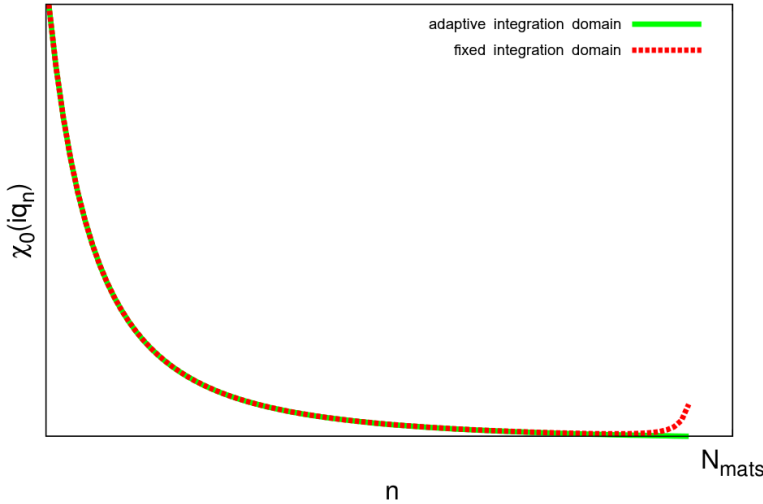


Figure A.2: Improvement of the high-frequency behavior of  $\chi_0(iq_n)$  (green line) at large Matsubara frequencies if the summation is carried out in an adaptive integration domain  $[-N_{mats} - n, N_{mats}]$  for every point of  $\chi_0(iq_n)$ . An increase for large  $n$  is not physical but a consequence of insufficient summation (red dotted line).

## B. $\vec{k}$ -integration

A few subtleties that occurred while implementing the  $\vec{k}$ -integration for TPSC shall be mentioned in this section.

- a)  $\vec{k}$ -integrations by means of the adaptive cubature procedure and the 2D-trapezoidal rule:

One of the most frequent operations within TPSC is the integration over the first Brillouin zone. In my implementation we make a difference between integrands that are available at all  $\vec{k}$ -points and at finite  $\vec{k}$ -points.

(i) adaptive cubature:

The non-interacting Green's function  $G_0(\vec{k}; ik_n)$  (Eq. 3.55) is known at all points of its domain and appears as a part of an integrand in the calculation of the initial filling  $n$  (Eq. 3.58) and of the non-interacting susceptibility  $\chi_0(\vec{q}; iq_n)$  (Eq. 4.17).

The Green's function might exhibit strong dependence of  $\vec{k}$  as shown in Fig. B.1 where it remains nearly constant in a large region and changes drastically near the Fermi surface. In this case it is reasonable to use a rare integration grid far from the kinks and to increase the density of integration points near the kinks.

The adaptive cubature applies exactly this idea and proceeds in the following way:

- 0) Divide domain into triangles and do the following steps for every triangle.
- 1) Calculate integral over the triangular region.
- 2) Divide the triangle into four triangles and integrate again over each new triangular region.
- 3) Do the four new integrals sum up to the previous one within some given tolerance  $\epsilon$ ?
  - No, repeat 2) for all four triangles.
  - Yes, the integral is converged; return value.

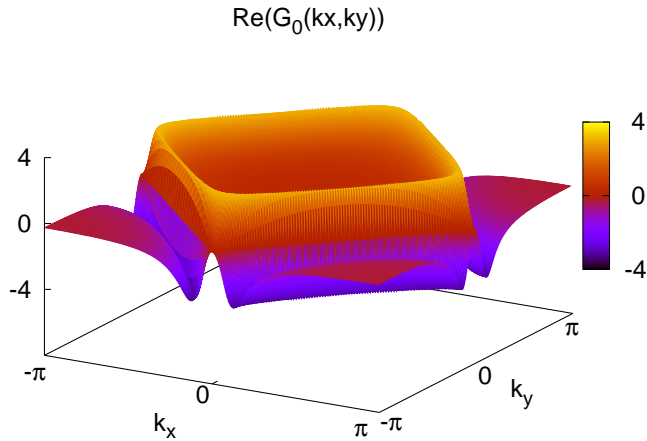


Figure B.1: Real part of the non-interacting Green's function  $G_0(kx, ky; ik_0)$  for the square lattice at  $T = 0.05\text{eV}$  and half filling. The function shows a strong dependence on  $k_x, k_y$  only near the Fermi surface and is therefore predestined for adaptive cubature.

To perform the integration over triangular regions one can take advantage of the seven-point cubature-formula [45],

$$\int_{\Delta} f(x, y) dx dy \approx |\Delta| \sum_{i=1}^7 w_i f(x_i, y_i). \quad (\text{B.1})$$

The positions of the nodes  $(x_i, y_i)$  in natural coordinates (Fig. B.2) and the weights  $w_i$  are

$x_i$	$y_i$	$w_i$
0	0	3/60
0	1	
1	0	
0.5	0	8/60
0	0.5	
0.5	0.5	
1/3	1/3	27/60

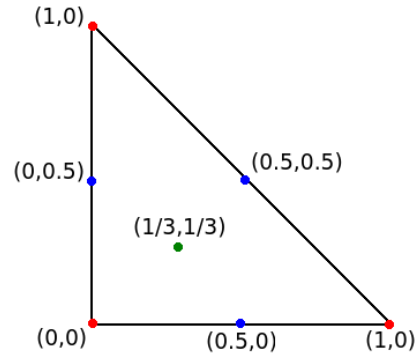


Figure B.2: Natural coordinates for the triangle and position of integration nodes. The red point at the edges will bear a weight of 3/60, the blue points in between of 8/60 and the green point in the center of 27/60.

(ii) 2D trapezoidal-rule:

In many other cases the integrand is only available at a number of positions. An easy but nevertheless reliable integration routine in this case is the 2D-trapezoidal rule. This is demonstrated – although it might be formulated more generally, we will show it only for the relevant cases of this work – for the integration of an arbitrary integrable function from some two-dimensional field  $K^2$  to an one-dimensional field  $K'$ ,  $f : K \rightarrow K'$ , that is known at  $N^2 \in \mathbb{N}$  points  $(x_i, y_j) \in K^2 \forall i, j \in \{1, \dots, N\}$  that are located homogeneously in our integration domain, a two-dimensional square  $[x_1, x_N] \times [y_1, y_N]$ . The procedure consists of the application of twice the trapezoidal rule. We define  $A := (x_N - x_1)(y_N - y_1)$  and get

$$\begin{aligned}
 \frac{1}{A} \int_{x_1}^{x_N} \int_{y_1}^{y_N} f(x, y) dx dy &\approx \frac{1}{N(y_N - y_1)} \int_{y_1}^{y_N} \left( \frac{1}{2} f(x_1, y) + \sum_{i=2}^{N-1} f(x_i, y) + \frac{1}{2} f(x_N, y) \right) dy \\
 &\approx \frac{1}{N^2} \left[ \frac{1}{4} (f(x_1, y_1) + f(x_1, y_N) + f(x_N, y_1) + f(x_N, y_N)) \right. \\
 &\quad + \frac{1}{2} \sum_{i=2}^{N-1} (f(x_1, y_i) + f(x_N, y_i) + f(x_i, y_1) + f(x_i, y_N)) \\
 &\quad \left. + \sum_{i,j=2}^{N-1} f(x_i, y_j) \right]. \tag{B.2}
 \end{aligned}$$

To ensure an efficient implementation one should rearrange the last two sums in an outer and an inner sum.

**B.1. Calculation of the Lindhard function**  $\chi_0(\vec{q}, iq_n)$

Starting-point for the calculation of the non-interacting susceptibility  $\chi_0(q)$  is equation 4.17,

$$\chi^0(\vec{q}, iq_n) = -\frac{1}{N} \sum_{\vec{k}} \frac{f(\xi_{\vec{k}}) - f(\xi_{\vec{k}+\vec{q}})}{iq_n - [\xi_{\vec{k}+\vec{q}} - \xi_{\vec{k}}]}. \quad (\text{B.3})$$

Since it might happen at  $iq_n = 0$  that  $\xi_{\vec{k}+\vec{q}} = \xi_{\vec{k}}$  and therefore also  $f(\xi_{\vec{k}+\vec{q}}) = f(\xi_{\vec{k}})$  one has to apply the rule of de l'Hospital to get correct results, i.e.

$$\frac{f(\xi_{\vec{k}}) - f(\xi_{\vec{k}+\vec{q}})}{[\xi_{\vec{k}+\vec{q}} - \xi_{\vec{k}}]} \xrightarrow{\xi_{\vec{k}+\vec{q}} \rightarrow \xi_{\vec{k}}} -\frac{1}{T} \frac{e^{\xi_{\vec{k}}/T}}{(1 + e^{\xi_{\vec{k}}/T})^2}. \quad (\text{B.4})$$

---

## References

- [1] Y.M. Vilk and A.-M.S. Tremblay. Non-perturbative many-body approach to the hubbard model and single-particle pseudogap. *J. Phys. I France*, 7(11):1309–1368, 1997.
- [2] André-Marie Tremblay. *Problème à N-corps (notes de cours)*. André-Marie Tremblay, 2014.
- [3] J. Hubbard. Electron correlations in narrow energy bands. *Proceedings of the Royal Society of London A: Mathematical, Physical and Engineering Sciences*, 276(1365):238–257, 1963.
- [4] Daisuke Ogura and Kazuhiko Kuroki. Asymmetry of superconductivity in hole- and electron-doped cuprates: Explanation within two-particle self-consistent analysis for the three-band model. *Phys. Rev. B*, 92:144511, Oct 2015.
- [5] Tohru Nakano, Naoki Momono, Migaku Oda, and Masayuki Ido. Correlation between the doping dependences of superconducting gap magnitude  $2\Delta_0$  and pseudogap temperature  $t^*$  in high- $T_c$  cuprates. *Journal of the Physical Society of Japan*, 67(8):2622–2625, 1998.
- [6] Daniel Guterding, Michaela Altmeyer, Harald O. Jeschke, and Roser Valentí. Near-degeneracy of extended  $s + d_{x^2-y^2}$  and  $d_{xy}$  order parameters in quasi-two-dimensional organic superconductors. *Phys. Rev. B*, 94:024515, Jul 2016.
- [7] Gordon Baym and N. David Mermin. Determination of thermodynamic green’s functions. *Journal of Mathematical Physics*, 2(2):232–234, 1961.
- [8] Henri Padé. Sur la représentation approchée d’une fonction par des fractions rationnelles. *Annales Scientifiques de l’École Normale Supérieure*, 1892.
- [9] Georg Frobenius. über relationen zwischen den näherungsbrüchen von potenzreihen. *Journal für die reine und angewandte Mathematik*, 1881.
- [10] E. T. Jaynes. Information theory and statistical mechanics. *Phys. Rev.*, 106:620–630, May 1957.
- [11] Anders W. Sandvik. Stochastic method for analytic continuation of quantum monte carlo data. *Phys. Rev. B*, 57:10287–10290, May 1998.
- [12] Paul C. Martin and Julian Schwinger. Theory of many-particle systems. i. *Phys. Rev.*, 115:1342–1373, Sep 1959.
- [13] J. M. Luttinger and J. C. Ward. Ground-state energy of a many-fermion system. ii. *Phys. Rev.*, 118:1417–1427, Jun 1960.
- [14] Evgeny Kozik, Michel Ferrero, and Antoine Georges. Nonexistence of the luttingerward functional and misleading convergence of skeleton diagrammatic series for hubbard-like models. *Phys. Rev. Lett.*, 114:156402, Apr 2015.
- [15] David Bohm and David Pines. A collective description of electron interactions: Iii. coulomb interactions in a degenerate electron gas. *Phys. Rev.*, 92:609–625, Nov 1953.

- [16] S. Moukouri, S. Allen, F. Lemay, B. Kyung, D. Poulin, Y. M. Vilks, and A.-M. S. Tremblay. Many-body theory versus simulations for the pseudogap in the hubbard model. *Phys. Rev. B*, 61:7887–7892, Mar 2000.
- [17] Morr D.K. Chakravarty S., Laughlin R.B. and Nayak C. *Phys. Rev. B*, 63:94503, 2001.
- [18] Chandra Varma. High-temperature superconductivity: Mind the pseudogap. *Nature*, 468:184185, 2010.
- [19] Y. Kitaoka, S. Ohsugi, K. Ishida, and K. Asayama. Antiferromagnetic spin correlation and superconductivity in  $\text{La}_2\text{SrCuO}_4$ : Cunnr study. *Physica C: Superconductivity*, 170(3):189 – 194, 1990.
- [20] Y. M. Vilks, Liang Chen, and A.-M. S. Tremblay. Theory of spin and charge fluctuations in the hubbard model. *Phys. Rev. B*, 49:13267–13270, May 1994.
- [21] Sudip Chakravarty, Bertrand I. Halperin, and David R. Nelson. Two-dimensional quantum heisenberg antiferromagnet at low temperatures. *Phys. Rev. B*, 39:2344–2371, Feb 1989.
- [22] S. R. Hassan, B. Davoudi, B. Kyung, and A.-M. S. Tremblay. Conditions for magnetically induced singlet  $d$ -wave superconductivity on the square lattice. *Phys. Rev. B*, 77:094501, Mar 2008.
- [23] S. Ichimaru. Strongly coupled plasmas: high-density classical plasmas and degenerate electron liquids. *Rev. Mod. Phys.*, 54:1017, 1982.
- [24] Ehsan Khatami and Marcos Rigol. Thermodynamics of strongly interacting fermions in two-dimensional optical lattices. *Phys. Rev. A*, 84:053611, Nov 2011.
- [25] Liang Chen, C. Bourbonnais, T. Li, and A.-M. S. Tremblay. Magnetic properties of the two-dimensional hubbard model. *Phys. Rev. Lett.*, 66:369–372, Jan 1991.
- [26] Gordon Baym. *Phys. Rev. B*, 127(1391), 1962.
- [27] P.C.E Stamp. PhD thesis, University of Sussex, 1983.
- [28] D. Rost, E. V. Gorelik, F. Assaad, and N. Blümer. Momentum-dependent pseudo-gaps in the half-filled two-dimensional hubbard model. *Phys. Rev. B*, 86:155109, Oct 2012.
- [29] Anne-Marie Daré, Y. M. Vilks, and A. M. S. Tremblay. Crossover from two- to three-dimensional critical behavior for nearly antiferromagnetic itinerant electrons. *Phys. Rev. B*, 53:14236–14251, Jun 1996.
- [30] Dominic Bergeron, Debanjan Chowdhury, Matthias Punk, Subir Sachdev, and A.-M. S. Tremblay. Breakdown of fermi liquid behavior at the  $(\pi, \pi) = 2k_F$  spin-density wave quantum-critical point: The case of electron-doped cuprates. *Phys. Rev. B*, 86:155123, Oct 2012.
- [31] Masanori Kohno. Mott transition in the two-dimensional hubbard model. *Phys. Rev. Lett.*, 108:076401, Feb 2012.
- [32] Jackson F. Master’s thesis, Université de Sherbrook.

- 
- [33] C. M. Varma. Pseudogap phase and the quantum-critical point in copper-oxide metals. *Phys. Rev. Lett.*, 83:3538–3541, Oct 1999.
- [34] Sudip Chakravarty, R. B. Laughlin, Dirk K. Morr, and Chetan Nayak. Hidden order in the cuprates. *Phys. Rev. B*, 63:094503, Jan 2001.
- [35] Bumsoo Kyung, Jean-Sébastien Landry, and A.-M. S. Tremblay. Antiferromagnetic fluctuations and  $d$ -wave superconductivity in electron-doped high-temperature superconductors. *Phys. Rev. B*, 68:174502, Nov 2003.
- [36] Takaaki Hiramatsu, Yukihiro Yoshida, Gunzi Saito, Akihiro Otsuka, Hideki Yamochi, Mitsuhiko Maesato, Yasuhiro Shimizu, Hiroshi Ito, and Hideo Kishida. Quantum spin liquid: design of a quantum spin liquid next to a superconducting state based on a dimer-type mott insulator. *J. Mater. Chem. C*, 3:1378–1388, 2015.
- [37] Kato Reizo, Kobayashi Hayao, Kobayashi Akiko, Moriyama Shinji, Nishio Yutaka, Kajita Koji, and Sasaki Wataru. A new ambient-pressure superconductor,  $-(\text{bedt-ttf})_2\text{i}_3$ . *Chemistry Letters*, 16(3):507–510, 1987.
- [38] Hatsumi Mori, Izumi Hirabayashi, Shoji Tanaka, Takehiko Mori, and Hiroo Inokuchi. A new ambient-pressure organic superconductor,  $-(\text{bedt-ttf})_2\text{ag}(\text{cn})_2\text{h}_2\text{o}$  ( $t_c=5.0$  k). *Solid State Communications*, 76(1):35 – 37, 1990.
- [39] Aravinda M. Kini, Urs Geiser, Hau H. Wang, K. Douglas Carlson, Jack M. Williams, W. K. Kwok, K. G. Vandervoort, James E. Thompson, Daniel L. Stupka, D. Jung, and Myung Hwan Whangbo. A new ambient-pressure organic superconductor,  $-(\text{et})_2\text{cu}[\text{n}(\text{cn})_2]\text{br}$ , with the highest transition temperature yet observed (inductive onset  $t_c = 11.6$  k, resistive onset = 12.5 k). *Inorganic Chemistry*, 29(14):2555–2557, 12 1990.
- [40] Hiori Kino and Hiroshi Kontani. Phase diagram of superconductivity on the anisotropic triangular lattice hubbard model: An effective model of  $-(\text{bedt-ttf})$  salts. *Journal of the Physical Society of Japan*, 67(11):3691–3694, 1998.
- [41] Kazuhiko Kuroki and Hideo Aoki. Superconductivity and spin correlation in organic conductors: A quantum monte carlo study. *Phys. Rev. B*, 60:3060–3063, Aug 1999.
- [42] Luca F. Tocchio, Hélène Feldner, Federico Becca, Roser Valentí, and Claudius Gros. Spin-liquid versus spiral-order phases in the anisotropic triangular lattice. *Phys. Rev. B*, 87:035143, Jan 2013.
- [43] Tsutomu Watanabe, Hisatoshi Yokoyama, Yukio Tanaka, and Jun ichiro Inoue. Superconductivity and a mott transition in a hubbard model on an anisotropic triangular lattice. *Journal of the Physical Society of Japan*, 75(7):074707, 2006.
- [44] Hideyuki Miyahara, Ryotaro Arita, and Hiroaki Ikeda. Development of a two-particle self-consistent method for multiorbital systems and its application to unconventional superconductors. *Phys. Rev. B*, 87:045113, Jan 2013.
- [45] Henrik Büsing. Multivariate numerische integration und anwendungen in der peridynamik. Master’s thesis, Technische Universität Berlin, 2008.